UNIVERSITY OF CALIFORNIA
RIVERSIDE

Surface Reactivity of Copper Precursors for Atomic Layer Deposition (ALD) on Metal Surfaces

A Dissertation submitted in partial satisfaction
of the requirements for the degree of

Doctor of Philosophy

in

Chemistry

by

Qiang Ma

December 2010

Dissertation Committee:

Dr. Francisco Zaera, Chairperson
Dr. Yadong Yin
Dr. Jingsong Zhang

The Dissertation of Qiang Ma is approved:

_____

_____

_____

Committee Chairperson

University of California, Riverside

ACKOWLEDGEMENTS

From a more global perspective, I would like to thank my research adviser Professor Francisco Zaera, a famous surface scientist, and more important for me, an outstanding educator. I am very grateful with him for having given me the opportunity, guidance, and assistance throughout my graduate studies. His valuable comments and discussions about my research work and results every month gave me the light of what might be the next step to continue with my work. He is always there to give me a hand whenever I encountered problem. Without his guidance and support, this research would have been impossible and I would have never made it through to the hardest parts of the climb.

Also, I would like to thank Professor Yadong Yin and Professor Jingsong Zhang for their advices on my thesis. Discussion with these two outstanding scientists is one of the most rewarded and memorial experiences of mine.

I am also grateful to my labmates: Dr. Ilkeun Lee, for being able to help me and guide me to build the RAIRS chamber; Stan Sheldon, for his help in the electronic, glass instruments and home-made equipments; Dr Min Shen, for his help in the LEIS and being my lab partner in these two years; Dr Xiangdong Qin ,for assisting in the equipment repairing and results discussion, and to all the persons that share with me the five years at our lab, and they will have a nice place in my memory as friends: Zhen, Chris, Ryan, Shinji, Xin, Huaxing, Menno, Ricardo, Byung-Chan, Manuel, Luiz,

Taeseung, Susan, Hugo, Jarod, Egor…thanks because I learned something from all of you. You made the journey of my PhD study more enjoyable and my life in UCR so colorful.

I appreciate all the help provided in all times by Linda Edwards, Barbara Outzen, Priscilliano Saavedra, Wayne Kaylor and Tina Enriquez.

Last but not least, I will like to thank all the support that was given by my family and friends. Thanks for all their warmness words.

COPYRIGHT ACKNOWLEDGMENTS

Some text and figures of this dissertation in part are reprinted from the publication listed below.

Qiang Ma, Hansheng Guo, Roy G. Gordon and Francisco Zaera, *Chemistry of Materials*. **2010**, 22, 352.

ABSTRACT OF THE DISSERTATION

Surface Reactivity of Copper Precursors for
Atomic Layer Deposition (ALD) on Metal Surfaces

by

Qiang Ma

Doctor of Philosophy, Graduate Program in Chemistry
University of California, Riverside, December 2010
Dr. Francisco Zaera, Chairperson

Acetamidinate precursors have shown great promise for atomic layer deposition (ALD) applications, but potentially deposit impurities that may degrade the quality of the films and hinder their practical applications. To help solve this problem, the uptake, the surface chemistry, and the effect of hydrogen coadsorption of copper(I)(*N*,*N'*-di-*sec*-butylacetamidinate) and *N*,*N'*-di-*sec*-butylacetamidine on different metals were characterized under ultrahigh vacuum (UHV) conditions by using a combination of X-ray photoelectron spectroscopy (XPS), low-energy ion scattering (LEIS), and temperature programmed desorption (TPD). The main objective of this research project has been to develop a better molecular-level understanding of the chemical reactions associated with ALD of copper metal films, to design and optimize the film deposition processes to be used in the microelectronics industry.

In our initial studies on a Ni (110) single crystal, a temperature window between approximately 350 and 450 K was identified for the ALD of Cu using the Cu acetamidinate precursor: lower temperatures are insufficient for activation of the dissociative adsorption, and higher temperatures lead to continuous decomposition beyond Cu monolayer saturation. Approximately three dosing cycles are required to reach full Cu monolayer saturation, the equivalent of a film growth rate of ~0.75 Å/cycle in ALD. Preadsorption of hydrogen on the surface does not modify any of this behavior because of its rapid desorption at temperatures below 350 K once the gas-phase H_2 is removed. The surface chemistry of the Cu precursor is complex, leading to the desorption of not only hydrogen but also 2-butene and small amidine (*N*-*sec*-butylacetamidine, ^{s}But–NH–C(CH_3)=NH); it seems that the amidine ligands decompose via beta-hydride elimination from one of their terminal *sec*-butyl moieties. The ligands of the copper acetamidinate precursors further decompose on Ni (110) surfaces at higher temperature, leading to the desorption of more hydrogen and leaving some carbon and nitrogen on the surface. The free hydrogenated amidine ligand is less reactive, and no *N*-*sec*-butylacetamidine is produced by its thermal activation, but the remaining chemistry follows similar temperature transitions. Similar results were also observed on a Cu (110) surface.

Other copper precursors, Cu(acac)$_2$ (copper(II) acetylacetonate) and Cu-KI5 (copper(I) (N(1(dimethylvinylsiloxy)-1- methylethano)-2-imino-4-pentanoate)) in particular, were tested as well. Details of the results from this work are discussed.

TABLE OF CONTENTS

Pages

ACKNOWLEDGEMENTS……iv

ABSTRACT……vii

TABLE OF CONTENTS……...ix

LIST OF FIGURES……xiv

CHAPTER ONE

Introduction and Overview……1

1.1. Integrated Circuit development……....1

1.2. Atomic layer deposition……...2

1.3. Copper precursors……...……4

1.4. Dissertation work……..…….....6

1.5. References……..…….....8

CHAPTER TWO

Experimental……..10

2.1. Introduction……...10

2.2. Surface Analysis Techniques……10

2.2.1. X-ray photoelectron spectroscopy (XPS)……...12

2.2.2. Low-energy ion scattering (LEIS)……..13

2.2.3. Temperature Programmed Desorption (TPD)……13

2.3. Experimental Apparatus:"Michelle"……14

2.4. Chemicals……..20

2.5. Thermal desorption particle beam mass spectrometry (TDPBMS)……22

2.6. Knudsen Cells…….23

2.7. High pressure cell for atomic layer deposition……...26

2.8. Reflection-absorption infrared spectroscopy (RAIRS)……...29

2.9. References……...34

CHAPTER THREE

Uptake of the Copper Acetamidinate ALD Precursor on Nickel Surfaces…….36

3.1. Introduction……36

3.2. Results……39

3.2.1. XPS……39

3.2.2. LEIS……47

3.2.3. Experiments with Coadsorbed Hydrogen……...54

3.3. Discussion……..59

3.4. Conclusions……71

3.5. References……..74

CHAPTER FOUR

Surface Chemistry of the Copper Acetamidinate ALD Precursor on Nickel Surfaces……76

4.1. Introduction……76

4.2. Results……77

4.2.1. XPS……77

4.2.2.TPD……..82

4.2.3. Experiments with Coadsorbed Hydrogen……...91

4.3. Discussion……..95

4.4. Conclusions……99

4.5. References……101

CHAPTER FIVE

Thermal Reactivity of the Copper Acetamidinate ALD Precursor on Copper Surfaces……..103

5.1. Introduction……..103

5.2. Results……..104

5.2.1. XPS……104

5.2.2. TPD……109

5.3. Discussion…….113

5.4. Conclusions……...114

5.5. References…….115

CHAPTER SIX

Thermal Reactivity of Acetamidine on Nickel and Copper Surfaces……116

6.1. Introduction……...116

6.2. Results……...118

6.2.1. Nickel Surface……118

6.2.2. Copper Surface……...122

6.3. Discussion…….128

6.4. Conclusions……...129

6.5. References……..131

CHAPTER SEVEN

Thermal Reactivity of Cu-KI5 on Copper Surfaces…….132

7.1. Introduction……132

7.2. Results……134

7.2.1. XPS……..134

7.2.2. TPD……..140

7.3. Summary…….143

7.4. References……...145

CHAPTER EIGHT

Thermal Reactivity of $Cu(acac)_2$ on Nickel and Copper Surfaces……...146

8.1. Introduction……146

8.2. Results……147

8.2.1. Copper Surface……147

8.2.2. Nickel Surface…….151

8.3. Discussion……..159

8.4. Conclusions……161

8.5. References……..163

CHAPTER NINE

General Conclusions and Future work…….164

9.1. General Conclusions……..164

9.2. Future work……....167

9.2.1. Studies on copper ALD……167

9.2.2. Studies on ruthenium ALD……..168

9.3. References……...170

LIST OF FIGURES

CHAPTER ONE

Figure 1.1 Scheme process of atomic layer deposition (ALD) of copper(I)-*N*,*N*'-di-*sec*-butylacetamidinate…….....5

CHAPTER TWO

Figure 2.1 A picture of the Michelle ultrahigh vacuum system used in this dissertation 11

Figure 2.2 C 1s XPS data for a Ni (110) single crystal surface before (upper line) and after (bottom line) 5-min sputtering……15

Figure 2.3 C 1s (top) and O 1s (bottom) XPS from Cu (110), dirty and after sputtering/annealing and oxidation/annealing cleaning procedures...……19

Figure 2.4 Thermal desorption particle beam mass spectrometry (TDPBMS) of copper(I)-*N*,*N*'-di-*sec*-butylacetamidinate…….24

Figure 2.5 Two kinds of home-made Knudsen cells to introduce solid copper(I)-*N*,*N*'-di-*sec*-butylacetamidinate into the ultra high vacuum chamber……...25

Figure 2.6 Cu 2p (left), Ni 2p (right) XPS data for 1000 L of copper(I)-*N*,*N*'-di-*sec*-butylacetamidinate dosed on Ni (110) surface…….…….27

Figure 2.7 C 1s (left), N 1s (right) XPS data for 1000 L of copper(I)-*N*,*N*'-di-*sec*-butylacetamidinate dosed on Ni (110) surface……..28

Figure 2.8 Schematic plot of our six-way high pressure cell with feedthroughs. Top: side view; bottom: top view……..30

Figure 2.9 Schematic plot and picture of the RAIRS system arrangement……...33

CHAPTER THREE

Figure 3.1 Molecular structure and mass spectrum of copper(I)-*N,N'*-di-*sec*-butylacetamidinate……..38

Figure 3.2 Cu $2p_{3/2}$ XPS for a Ni (110) single crystal surface dosed with 10.0 L of copper(I)-*N,N'*-di-*sec*-butylacetamidinate……40

Figure 3.3 C 1s XPS for a Ni (110) single crystal surface dosed with 10.0 L of copper(I)-*N,N'*-di-*sec*-butylacetamidinate……..41

Figure 3.4 N 1s XPS for a Ni (110) single crystal surface dosed with 10.0 L of copper(I)-*N,N'*-di-*sec*-butylacetamidinate……..42

Figure 3.5 Ni $2p_{3/2}$ XPS for a Ni (110) single crystal surface dosed with 10.0 L of copper(I)-*N,N'*-di-*sec*-butylacetamidinate…….43

Figure 3.6 Cu $2p_{3/2}$ XPS uptake for copper(I)-*N,N'*-di-*sec*-butylacetamidinate on Ni (110) at 350 (left), 400 (center) and 460 (right) K……...46

Figure 3.7 Ni $2p_{3/2}$ XPS uptake for copper(I)-*N,N'*-di-*sec*-butylacetamidinate on Ni (110) at 460 K……..48

Figure 3.8 Ne^+ LEIS data from a Ni (110) single crystal surface dosed at 90 K with copper(I)-*N,N'*-di-*sec*-butylacetamidinate as a function of exposure……...49

Figure 3.9 He^+ LEIS data from a Ni (110) single crystal surface dosed at 90 K with 10 L copper(I)-*N,N'*-di-*sec*-butylacetamidinate as a function of annealing temperature……51

Figure 3.10 Ne^+ LEIS data obtained during the deposition of copper on Ni (110) Using copper(I)-*N,N'*-di-*sec*-butylacetamidinate…….53

Figure 3.11 Cu $2p_{3/2}$ XPS uptake for copper(I)-*N,N'*-di-*sec*-butylacetamidinate on H-Saturated Ni (110) at 350 (left), 400 (center) and 460 (right) K……..…….....55

Figure 3.12 Copper uptake estimated from Cu $2p_{3/2}$ XPS experiments such as those shown in Figures 3.6 and 3.11 for copper(I)-*N,N'*-di-*sec*-butylacetamidinate on clean (as marked) and H-Saturated (as marked) Ni (110) as a function of surface temperature…56

Figure 3.13 C 1s XPS for a Ni (110) single crystal surface dosed with 30.0 L of copper(I)-*N,N'*-di-*sec*-butylacetamidinate as a function of annealing temperature (left panel, clean surface; right panel, H-Saturated surface)……..57

Figure 3.14 N 1s XPS for a Ni (110) single crystal surface dosed with 30.0 L of copper(I)-*N,N'*-di-*sec*-butylacetamidinate as a function of annealing temperature (left panel, clean surface; right panel, H-Saturated surface)…….58

Figure 3.15 H_2 (2 amu) temperature programmed desorption (TPD) traces from a Ni (110) single-crystal surface dosed with 3.0 L H_2 (bottom trace), 2.0 L di-*sec*-butylacetamidine (middle), and 20.0 L copper(I)-*N,N'*-di-*sec*-butylacetamidinate (top), all at 100 K….60

Figure 3.16 Potential energy plot for H_2 adsorption on Ni surfaces……..…69

Figure 3.17 Estimated steady-state hydrogen surface coverage on Ni (110) as a function of hydrogen pressure and surface temperature, as calculated using adsorption and desorption parameters from the literature…….….70

CHAPTER FOUR

Figure 4.1 Cu $2p_{3/2}$ and AES data from 50.0 L copper acetamidinate on clean Ni (110), after dosing at 90 K and after annealing to 150, 200, 250, 300, 400, 500, 600, 700 and 800 K……78

Figure 4.2 N 1s and C 1s data from 50.0 L copper acetamidinate on clean Ni (110), after dosing at 90 K and after annealing to 150, 200, 250, 300, 400, 500, 600, 700, and 800 K……..79

Figure 4.3 Summary of integrated XPS peaks areas from the data in Figure 4.1 and 4.2 versus surface temperature……..……83

Figure 4.4 2-butnen TPD from copper acetamidinate decomposition on clean Ni (110) surface as a function of exposure……..……84

Figure 4.5 Small amidine TPD from copper acetamidinate decomposition on clean Ni (110) surface as a function of exposure……...85

Figure 4.6 Small amidine (^{s}But–NH–C(CH_3)=NH_2) structure (top), and relative intensities for the signals for 112, 114, 154, 155 and 170 amu in the peaks at 215 and 300 K after 20 L exposure of copper acetamidinate on Ni (110) ……..…...88

Figure 4.7 114 and 170 amu TPD from 20 L of copper acetamidinate on Ni (110), and 113, 114, 170 amu TPD from 6.0 L amidine on Ni (110).……...89

Figure 4.8 TPD from 20 L of copper acetamidinate on Ni (110)…….……....90

Figure 4.9 C 1s, N 1s, Ni $2p_{3/2}$ and Cu $2p_{3/2}$ XPS from 50.0 L copper acetamidinate dosed on a Ni (110) surface previously saturated with hydrogen at 90 K as a function of temperature……..92

Figure 4.10 C 1s, N 1s, Ni $2p_{3/2}$ and Cu $2p_{3/2}$ XPS and Cu AES from 50.0 L copper acetamidinate dosed on a Ni (110), at 90 K and after annealing to the indicated temperatures…….94

Figure 4.11 56 and 58 amu TPD from 2-iodobutane dosed on Ni (110)…….…...96

CHAPTER FIVE

Figure 5.1 Cu $2p_{3/2}$ XPS and Cu AES from 50.0 L copper acetamidinate on clean Cu (110), dosed at 90 K and after annealing to the indicated temperatures……..105

Figure 5.2 C 1s and N 1s XPS from 50.0 L copper acetamidinate on clean Cu (110), dosed at 90 K and after annealing to the indicated temperatures…….....……..106

Figure 5.3 114 and 170 amu TPD from copper acetamidinate on clean Cu (110) surface versus exposure……110

Figure 5.4 56 and 58 amu TPD from copper acetamidinate on clean Cu (110) surface versus exposure……..…111

Figure 5.5 55, 56, 57 and 58 (left) and 114, 170 and 171 amu (right) TPD from 15.0 L copper acetamidinate on clean Cu (110)……..…….112

CHAPTER SIX

Figure 6.1 Molecular structure and mass spectrum of *N*,*N*′-di-*sec*-butylacetamidine……...……117

Figure 6.2 He^+ LEIS from a Ni (110) single crystal surface dosed at 90 K with *N*,*N*′-di-*sec*-butylacetamidine as a function of exposure……..……....119

Figure 6.3 C 1s, N 1s and Ni $2p_{3/2}$ XPS form 50.0 L *N*,*N*′-di-*sec*-butylacetamidine on clean Ni (110) dosed at 90 K and after annealing to the indicated temperatures…….120

Figure 6.4 56 (2-butnen) and 114 amu TPD from acetamidine on clean Ni (110) versus exposure…….123

Figure 6.5 C 1s, N 1s and Cu $2p_{3/2}$ XPS form 50.0 L *N*,*N*′-di-*sec*-butylacetamidine on clean Cu (110) dosed at 90 K and after annealing to the indicated temperatures..……124

Figure 6.6 113, 114, 155, 169 and 170 amu TPD from 20.0 L *N,N'*-di-*sec*-butylacetamidine on clean Cu (110) ……...……126

Figure 6.7 Left: 55, 56 (butene), 57 and 170 (molecule) amu TPD from10.0 L *N,N'*-di-*sec*-butylacetamidine on clean Cu (110). Right: 56 (butene) amu TPD from 6.0 L *N,N'*-di-*sec*-butylacetamidine on clean Cu (110) dosed at the indicated temperatures...…….127

CHAPTER SEVEN

Figure 7.1 Molecular structure of Cu-KI5, copper(I)(N(1(dimthylvinylsiloxy)-1-methylethano)-2-imino-4-pentanoate)…….....**.....**133

Figure 7.2 C 1s, N 1s and O 1s XPS from Cu-KI5 on clean Cu (110) dosed at 90 K versus exposure…..……..135

Figure 7.3 Cu $2p_{3/2}$ and Si 2p XPS from Cu-KI5 on clean Cu (110) dosed at 90 K versus exposure……136

Figure 7.4 C 1s, N 1s and O 1s XPS from 300 L Cu-KI5 on clean Cu (110), dosed at 90 K and after annealing to the indicated temperatures……...138

Figure 7.5 Si 2p and Cu $2p_{3/2}$ XPS from 300 L Cu-KI5 on clean Cu (110), dosed at 90 K and after annealing to the indicated temperatures……**...**139

Figure 7.6 59, 63, 73 amu TPD from Cu-KI5 on clean Cu (110) surface as a function of exposure……**...**141

Figure 7.7 59, 63, 73 amu (left panel) and 96, 97, 98, 142, 143, 144, 239, 240, 241 amu (right panel) TPD from 50 L Cu-KI5 on clean Cu (110)……..……**...**142

CHAPTER EIGHT

Figure 8.1 C 1s, O 1s and Cu $2p_{3/2}$ XPS from 100 L $Cu(acac)_2$ on clean Cu (110), dosed at 90 K and after annealing to the indicated temperatures……...……...148

Figure 8.2 2, 15, 39, 43, 85 and 100 amu (left panel) and 105, 147, 162 and 163 amu (right panel) TPD from 10 L $Cu(acac)_2$ on clean Cu (110)…….….150

Figure 8.3 Cu $2p_{3/2}$ XPS and Cu LVV AES from 100 L $Cu(acac)_2$ on clean Ni (110), dosed at 90 K and after annealing to the indicated temperatures…….....….152

Figure 8.4 C 1s, O 1s and Ni $2p_{3/2}$ XPS form 100 L $Cu(acac)_2$ on clean Ni (110), dosed at 90 K and after annealing to the indicated temperatures……..…...154

Figure 8.5 C 1s, O 1s and Ni $2p_{3/2}$ XPS form 100 L Hacac on clean Ni (110), dosed at 90 K and after annealing to the indicated temperatures……156

Figure 8.6 Left: 58, 85, 105 amu TPD from 10 L $Cu(acac)_2$ on clean Cu (110) and Right: 2, 43, 58 amu TPD from 5 L Hacac on clean Cu (110)…….158

CHAPTER ONE

Introduction and Overview

1.1. Integrated Circuit development

Electronic products have changed dramatically in recent times. For instance, laptops have become more and more powerful while they have shrunk in size. That requires for its circuits to decrease in dimensions, in order to be able to fit more electronic units in a limit space. Usually integrated circuits are arranged on a two-dimensional surface, as in a parking lot, where cars can park side by side. If the parking lot includes many stores, more cars can park in the same area. In the same way, the semiconductor industry also has a strong motivation to move from 2-D to 3-D integration, which has been proposed to be achieved by using TSV (Through-Silicon Via) approach. If multiple chips are stacked together, all layers must be connected with conductive interconnect.

To achieve high electrical conductivity, copper is considered the primary choice for most TSV interconnects. Copper is replacing aluminum as the interconnect metal in microelectronics because of its relatively low resistivity and excellent electromigration properties [1,2]. Most of the copper in these applications is electroplated, but a serious

problem arises by the extremely deep, high aspect ratio structures associated with modern TSV: How to obtain void-free fill of those complex structures [3]? Void formation during copper deposition would degrade device quality. Only if this problem is solved, modern microelectronic structures may be made smaller and smaller. Accordingly, the deposition and surface preparation and treatment of the copper films on the complex structures of TSV are becoming increasingly critical steps in the manufacturing of interconnect [4,5].

In the current technology, physical vapor deposition methods are used to deposit these layers. However, it is difficult to sputter completely conformal and uniform copper film into the increasingly narrow trenches in modern interconnects [6,7]. To solve this problem, atomic layer deposition (ALD), a modified version of chemical vapor deposition (CVD) methods, is being considered.

1.2. Atomic layer deposition

Atomic layer deposition (ALD, also called atomic layer epitaxy, a method introduced by T. Suntola in Finland) is a technique which can assemble thin films atom by atom with exact control over their composition and structure [8]. During ALD, a vapor reacts with a surface until a monolayer has been chemisorbed. The reaction then stops, so the process is called "self-limiting". A second vapor then reacts with this surface in a second

self-limiting reaction, thus depositing a second layer of atoms onto the first. The second reaction must change the surface to a state in which it is ready to react with the first reactant. That means the two half cycles of the ALD are complementary [9]. The cycle of reactions can be repeated to build up a film atomic layer by atomic layer.

ALD offers a number of remarkable capabilities in addition to the control of stoichiometry at an atomic level. The thickness of a film can be controlled by the number of reaction cycles. Also, ALD avoids the problem caused by the nonuniform distribution of vapors or temperature in the reaction zone. Uniformly thin films can be easily deposited over large areas and complex substrates, even inside of very narrow holes [10]. The silicon semiconductor industry is currently devoting a large amount of research to ALD as a promising method for the production of the very thin films needed in microelectronics [11].

However, despite the wide applications and the many advantages of ALD, the mechanistic details of many ALD processes remain unclear, in particular in connection with how the decomposition of the r precursors can be achieved to deposit clean films. The key to solving this issue is to advance the understanding of ALD processes at a molecular level.

1.3. Copper precursors

One limitation of ALD is the availability of appropriate precursors. Finding effective ALD precursors is difficult because they must meet several very stringent requirements: (1) sufficient volatility; (2) sufficient thermal stability; (3) high but self-limited reactivity with surfaces prepared by a complementary reactant and also with suitably prepared substrates; (4) saturation thickness independent of the flux of molecules to the surfaces; (5) saturated surface suitable for reaction with a complementary precursor [12]. Some copper compounds have been developed for Cu CVD processes, including carboxylates, oxalates, and acetonates [13-15], but only a few have ever been tested for ALD [7,9,16-20] and those have proven to lead to films with high resistivity and poor growth. Fortunately, some copper precursors recently synthesized by Dr. Gordon [1,12] and Dr. Park [21] have shown great promise. ALD processes using such precursors have been shown to produce thin, completely continuous and highly conductive copper films conformably inside very narrow holes with aspect ratios of over 40:1 [22]. One ALD process proposed using copper(I)- *N,N'*-di-*sec*-butylacetamidinate is shown in Figure 1.1.

In our research, we chose one of the most promising copper precursor, copper(I)-*N,N'*-di-*sec*-butyl acetamidinate, to investigate the surface chemistry of ALD processes. Although Gordon *et al* reported the deposition of Cu and CuN film on different substrates

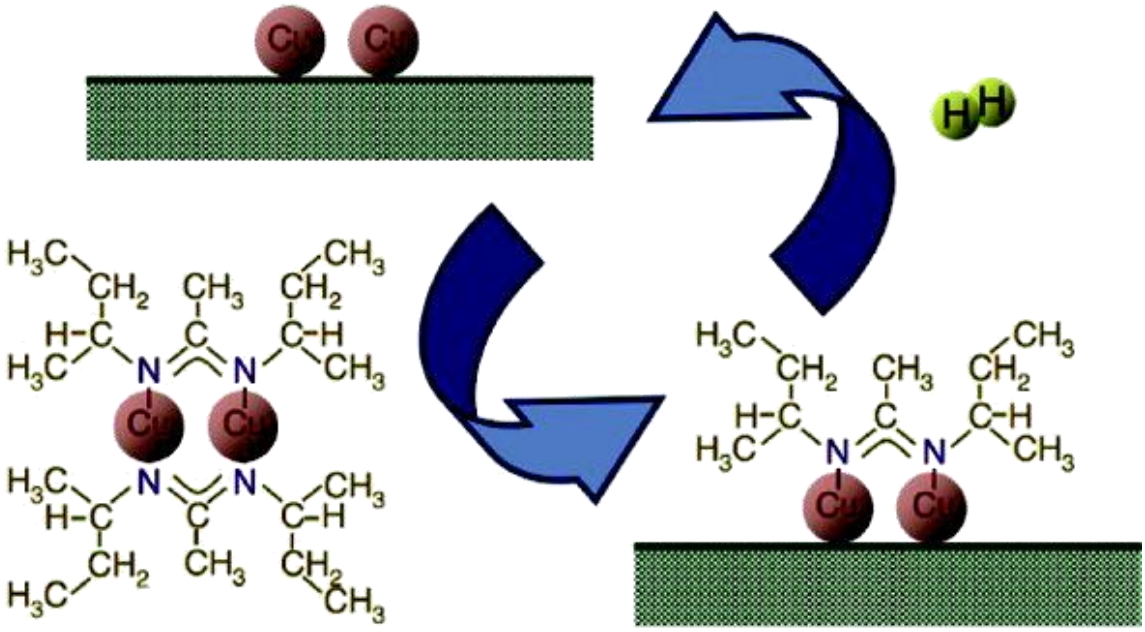

Figure 1.1 Scheme process of atomic layer deposition (ALD) of copper(I)-*N*,*N'*-di-*sec*-butylacetamidinate.

using this precursor [2,22], no details of its surface chemistry, specially the way the amidine ligand elimination occurs, was provided. It is important to note that the amidine side reactions are likely to determine the purity of the growing copper films. Our work includes, but is not limited ,to this precursor, and focuses on the use of *in situ* surface science techniques in order to better understand the key criteria for the selection of optimum organometallic ligands in copper ALD precursors. Other copper compounds, includes Cu-KI5 and $Cu(acac)_2$, were also probed.

1.4. Dissertation work

The work described in this dissertation has been divided into 9 chapters: after an introduction and overview of the different projects carried out (Chapter 1), a discussion of the experimental procedures that were used is given in Chapter 2, including description of the materials, experimental apparatus and surface analysis techniques employed. Chapter 3 describes the uptake of the copper acetamidinate ALD precursors on Ni (110) surfaces. In Chapter 4, the surface chemistry of copper acetamidinate on Ni (110) surfaces is described; butane and a small amidine were identified as key products. Chapter 5 describes the thermal reactivity of copper acetamidinate on Cu (110) surfaces. Chapter 6 describes the thermal reactivity of acetamidine, the hydrogenated ligand in the copper acetamidinate, on Ni (110) and Cu (110) surfaces. Chapter 7 investigates the

thermal reactivity of one new copper(I) precursor, Cu-KI5, on Cu (110) surfaces. Chapter 8 studies the surface reactivity of another copper(II) precursor, $Cu(acac)_2$ on both Ni (110) and Cu (110) surfaces. Finally, some general conclusions and proposed future work are given in Chapter 9. Most of the results shown on Chapter 3 were published in an article that appeared in *Chemistry of Materials*, 2010, *22*, 352 (copyright by American Chemical Society).

1.5. References

[1] Z. Li, S. T. Barry, R. G. Gordon, *Inorganic Chemistry*. **2005**, *44*, 1728.

[2] Z. Li, A. Rahtu, R. G. Gordon, *Journal of the Electrochemical Society*. **2006**, *153*, C787.

[3] Z. Li, R. G. Gordon, D. B. Farmer, Y. Lin, J. Vlassak, *Electrochemical and Solid-State Letters*. **2005**, *8*, G182.

[4] K. F. Jensen, *Adv. Chem. Ser.* **1995**, *245*, 297.

[5] M. Schumacher, P. K. Baumann, T. Seidel, *Chem. Vapor Dep.* **2006**, *12*, 99.

[6] A. Niskanen, A. Rahtu, T. Sajavaara, K. Arstila, M. Ritala, M. Leskelä, *Journal of the Electrochemical Society*. **2005**, *152*, G25.

[7] M. Leskelä, M. Ritala, *Angewandte Chemie, International Edition*. **2003**, *42*, 5548.

[8] D. Hausmann, J. Becker, S. Wang, R. G. Gordon, *Science.* **2002**, *298*, 402.

[9] B. S. Lim, A. Rahtu, R. G. Gordon, *Nature Materials.* **2003**, *2*, 749.

[10] A. E. Braun, *Semiconductor International.* **2001**, *24*, 52.

[11] A. I. Kingon, J. –P. Maria, S. K. Streiffer, *Nature.* **2000**, *406*, 1032.

[12] B. S. Lim, A. Rahtu, J. –S. Park, R. G. Gordon, *Inorganic Chemistry.* **2003**, *42*, 7951.

[13] M. Joulaud, C. Angekort, P. Doppelt, T. Mourier, D. Mayer, *Microelectron. Eng.* **2002**, *64*, 107.

[14] J. Teichgräber, S. Dechert, F. J. Meyer, *Organomet. Chem.* **2005**, *690*, 5255.

[15] A. Grodzicki, I. Lakomska, P. Piszczek, I. Szymanska, E. Szzyk, *Coord. Chem. Rev.* **2005**, *249*, 2232.

[16] P. Martensson, J. O. Carlsson, J. *Electrochem. Soc.* **1998**, *145*, 2926.

[17] R. Solanki, B. Pathangey, *Electrochem. Solid State Lett*. **2000**, *3*, 479.

[18] J. Huo, R. Solanki, J. McAndrew, *J. Mater. Res.* **2002**, *17*, 2394.

[19] A. Johansson, T. Torndahl, L. M. Ottosson,M. Boman, J. O. Carlsson, *Mater. Sci. Eng.*, **C 2003**, *23*, 823.

[20] A. U. Mane, S. A. Shivashankar, *J. Cryst. Growth*, **2005**, *275*, e1253.

[21] K. –H. Park, A. Z. Bradley, J. S. Thompson, W. J. Marshall, *Inorganic Chemistry*. **2006**, *45*, 8480.

[22] Z. Li, R. G. Gordon, *Chemical Vapor Deposition*. **2006**, *12*, 435.

CHAPTER TWO

Experimental

2.1. Introduction

All the experiments discussed in this dissertation were carried out inside an ultrahigh vacuum (UHV) chamber equipped with X-ray photoelectron spectroscopy (XPS), low-energy ion scattering (LEIS) and Temperature Programmed Desorption (TPD) techniques in order to investigate the surface chemistry of copper precursors and relative chemicals on Ni (110) and Cu (110) single crystal surfaces under different experimental conditions. Figure 2.1 shows a picture taken of this system, which we have affectionately named Michelle. A more detailed description of these techniques is presented below.

2.2. Surface Analysis Techniques

Since 1970's, many modern surface-sensitive techniques, such as X-ray photoelectron spectroscopy (XPS), low-energy ion scattering (LEIS), temperature programmed desorption (TPD), reflection adsorption infrared spectroscopy (RAIRS), Auger electron spectroscopy (AES), Low energy electron diffraction (LEED), high-resolution electron energy loss spectroscopy (HREEL), electron stimulated desorption ion angular

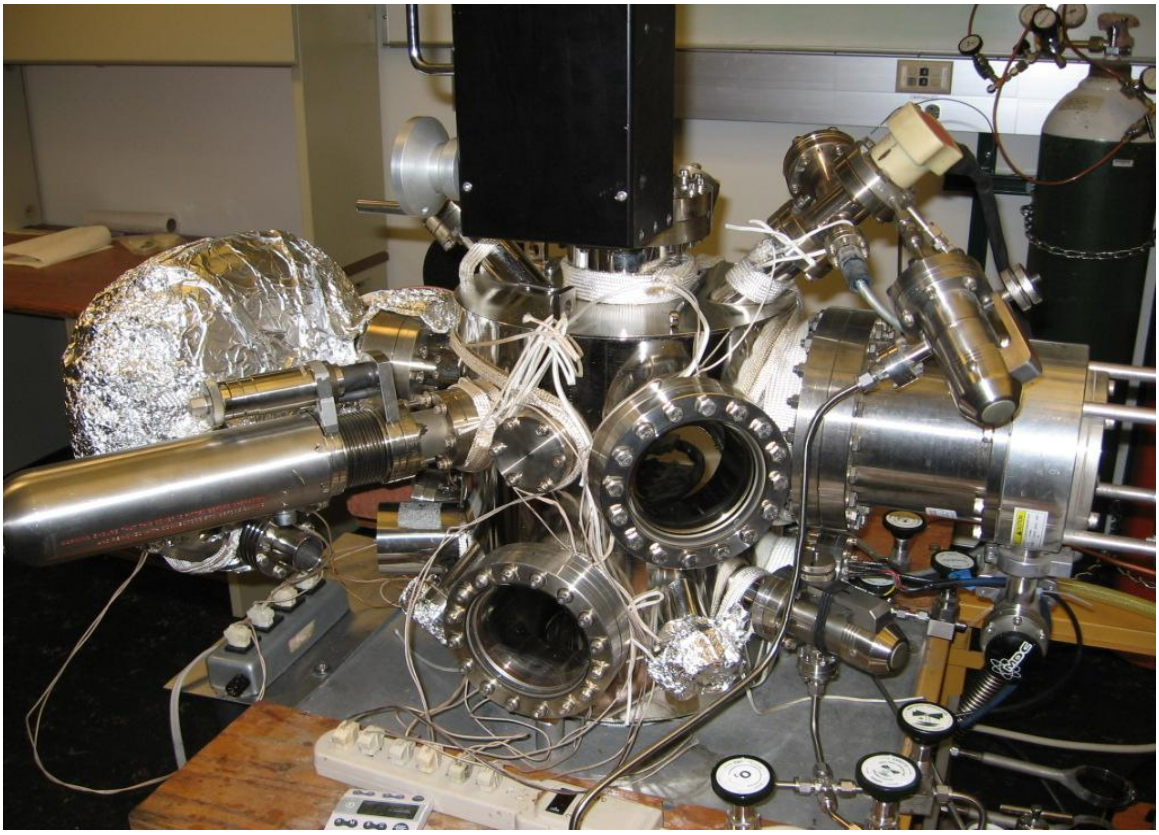

Figure 2.1 A picture of the Michelle ultrahigh vacuum system used in this dissertation.

distributions (ESDIAD), and more recently scanning tunneling microscopy (STM) and sum frequency generation (SFG), have been employed to probe various surface phenomena in order to provide molecular-level insights for chemical reaction [1-3]. Typically, such studies have been performed on single-crystal samples and under ultrahigh vacuum (UHV) condition, hence atomically clean surfaces can be obtained and modified for various purposes. Then different surface reactions can be studied and surface intermediate can be characterized, ultimately to provide corroborative information on the mechanisms of the reactions involved in industrial processes. Below we discuss the first three techniques listed, since those were the ones predominantly used in our studies.

2.2.1. X-ray photoelectron spectroscopy (XPS)

X-ray photoelectron spectroscopy (XPS) is a well known technique used to examine composition and electronic structure of elements in thin film (~5 nm) layer structures [4]. Usually an aluminum and/or magnesium anode is employed as the X-ray source. The X-rays generated in this way approach the surface and excite photoelectrons, which are then detected by a hemispherical electron energy analyzer. The XPS spectra obtained exhibit peaks at different binding energies. The XPS peak position is decided by the identity and chemical environments of the surface elements, while the peak intensity is

related to, even though not exactly proportional to, the surface concentration of these elements or of one element in a particular oxidation state. A free software name ‘XPS PEAK 4.1’ (Raymund W. M. Kwok, Chinese University of Hong Kong) was used in our work to deconvolution the XPS peaks with different binding energies.

2.2.2. Low-energy ion scattering (LEIS)

Low-energy ion scattering (LEIS) was first proposed for elemental identification by Smith in 1967 [5]. It provides mass-selected signals and structure information about the nuclear positions of atoms on surfaces in real space [6]. More detailed information on this technique is available in multiple reviews [6]. For our project, LEIS is used to tell us not only the composition of the film, but also the nature of the very topmost layer. LEIS was therefore a powerful tool to calibrate the exposures required for the buildup of a monolayer coverage of the adsorbed copper acetamidinate [7].

2.2.3. Temperature programmed desorption (TPD)

TPD, sometimes called TDS (Thermal Desorption Spectroscopy), is an excellent technique to identify the desorbing products from any reaction that happens on the surface [2]. Most of the TPD experiments are carried out on single crystal surfaces, and performed under UHV conditions. In a typical TPD experiment, specific amounts of

chemicals are dosed onto the solid surface at low temperatures, and that surface is then heated rapidly while the desorbing species are monitored by using mass spectrometry [8,9]. For the simplest case of an adsorbate in which the activation energy of desorption is constant as a function of coverage, a single desorption peak is obtained. By using the so-called Redhead method [10], information about the activation energy of desorption of the adsorbates can be drawn from the TPD data. In addition, after proper deconvolution of the TPD data obtained for several selected masses, the different gas-phase products can be identified.

2.3. Experimental Apparatus: "Michelle"

All the experiments were performed in an ultra-high-vacuum (UHV) chamber described elsewhere [11-13]. This system is pumped by a molecular turbo pump, operated at a base pressure of approximately 1 x 10^{-10} torr, and equipped with a UTI 100C quadruple mass spectrometer (QMS) for TPD, a dual-anode X-ray source and a concentric hemispherical analyzer (VG 100AX) for XPS and LEIS spectroscopy, an Al Kα/Mg Kα dual anode X-ray source for XPS, and a Kratos rasterable mini-beam rare-gas ion sputtering gun for sample cleaning and LEIS. Figure 2.2 displayed typical XPS data for the C 1s photoelectrons from a Ni (110) single crystal surface before (upper line) and after (bottom line) 5-min sputtering. The difference between the two is obvious: carbon is

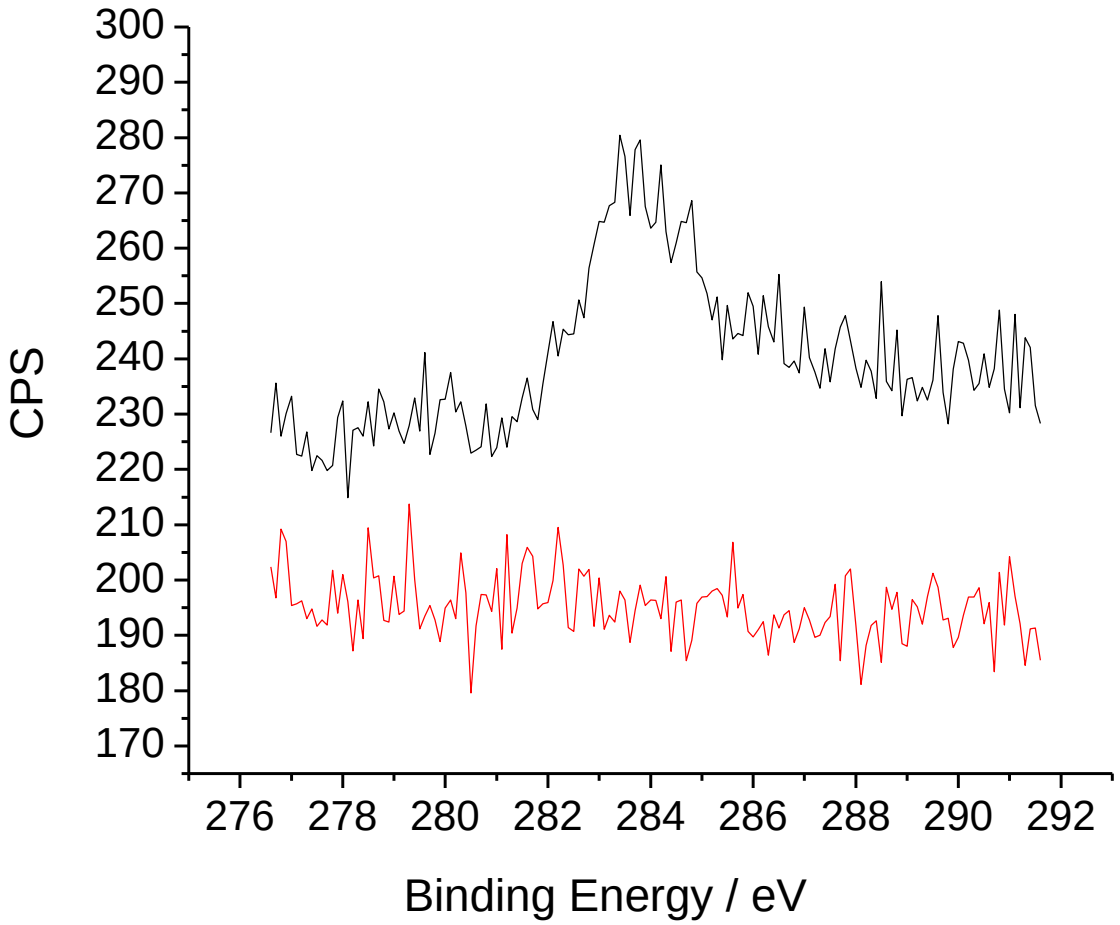

Figure 2.2 C 1s XPS data for a Ni (110) single crystal surface before (upper line) and after (bottom line) 5-min sputtering.

removed by sputtering. The XPS data reported here were taken by using an Al Kα X-ray source ($h\nu$ = 1486.6 e V), recorded in 0.1 eV increments. An electron-energy-analyzer pass energy of 50 eV was used, which in our system corresponds to an analyzer resolution of 0.6 eV and a total resolution of approximately 1.0 eV once the natural width of the Al Kα line is taken into consideration. The binding energies in the XPS data were calibrated by referring to signals from pure copper metal [14]. Most of the LEIS studies were carried out by using Ne^+ ions to better discriminate between copper and nickel surface atoms, but He^+ was also used in some instances to identify lighter elements such as carbon, nitrogen and oxygen. An incident energy of 2,000 eV was used in the experiments reported below. The instrumentation for TPD, XPS and LEIS are interfaced to a personal computer for data acquisition and processing. The mass spectrometer was retrofitted with an extendable nose cone with a 5.0 mm diameter aperture for the selective detection of species desorbing from the front surface in the TPD experiments. To minimize the possible decomposition of the adsorbates induced by stray electrons from the ionizer of the ion gauge or the mass spectrometer [15], a grounded grid was set in front of the ion gauge and the crystal was biased with a -100 V potential. Up to 15 different masses could be monitored in a single TPD run, all using the same sensitive factor. The mass spectrometer needed to be calibrated from time to time to ensure its resolution and accuracy. The TPD traces are reported in arbitrary units, but scaling bars

are provided in most figures to allow for relative comparisons of the different signal intensities.

Two single-crystal samples were used as substrates in this dissertation: Ni (110) and Cu (110). The Ni (110) single crystal sample, 10 mm in diameter and 1 mm in thickness, was cut and polished by standard procedures. Nickel was chosen as a convenient representative of the later transition metals used as diffusion barriers for copper; typical barriers are made out of metal nitrides, but those interfere with the nitrogen signals of the copper acetamidinate precursor in XPS experiments [13]. The Ni (110) crystal was spot-welded to two molybdenum wires suspended on the ends of two copper posts directly connected via vacuum feedthroughs to a liquid nitrogen reservoir. Cooling was accomplished by using liquid nitrogen contact directly with the copper wires of feedthroughs, and resistive heating was used to reach any desired temperature between 90 and 1100 K. The sample temperature was measured using a K-type thermocouple spot-welded to the edge of the crystal, and a homemade temperature controller was used to provide linear temperature ramps or maintain the crystal to within 0.5 K of the specified temperatures. The heating rate for all TPD measurements was set to 10 K/s. Normally, the Ni (110) crystal was cleaned by repeated cycles of Ar+ ion sputtering (2 x 10^{-7} torr Ar, @ room temperature, 5 min) and annealing (1100 K) until the surface was

deemed clean and well ordered by XPS and TPD experiments with hydrogen and CO [12]. Ni (110) surfaces with extensive amount of contaminants could be cleaned by oxidation/annealing (5 x 10^{-7} torr O_2, @800 K, 10 min) and reduction /annealing (5 x 10^{-7} torr H_2, @900 K, 10 min) procedures to get rid of carbon and oxide.

The Cu (110) single crystal sample, 10 mm in diameter and 2 mm in thickness, was polished to a mirror finish before use [16,17]. 0.015-inch tungsten wire was used to directly mount the Cu (110) crystal on the sample holder by wedging those into grooves cut in the sides of the sample. The lowest temperature possible with this setup was around 90 K. A K-type thermocouple was inserted into a hole located on the side of the crystal for temperature measurement [16]. Normally, the Cu (110) crystal was cleaned by repeated cycles of Ar+ ion sputtering (2 x 10^{-7} torr Ar, @ room temperature, 5 min) and annealing (1000 K) until the surface was deemed clean and well ordered by XPS. Strong carbon and oxygen signals were typically observed in the XPS spectra initially, as shown in Figure 2.3. That surface was cleaned by several cycles of sputtering and annealing for about 8 hours each time, and oxygen treatment at 800 K for several more hours to remove the carbon (Figure 2.3, top panel), and hydrogen, also at 800 K, was introduced for several hours to remove the oxygen (Figure 2.3, bottom panel).

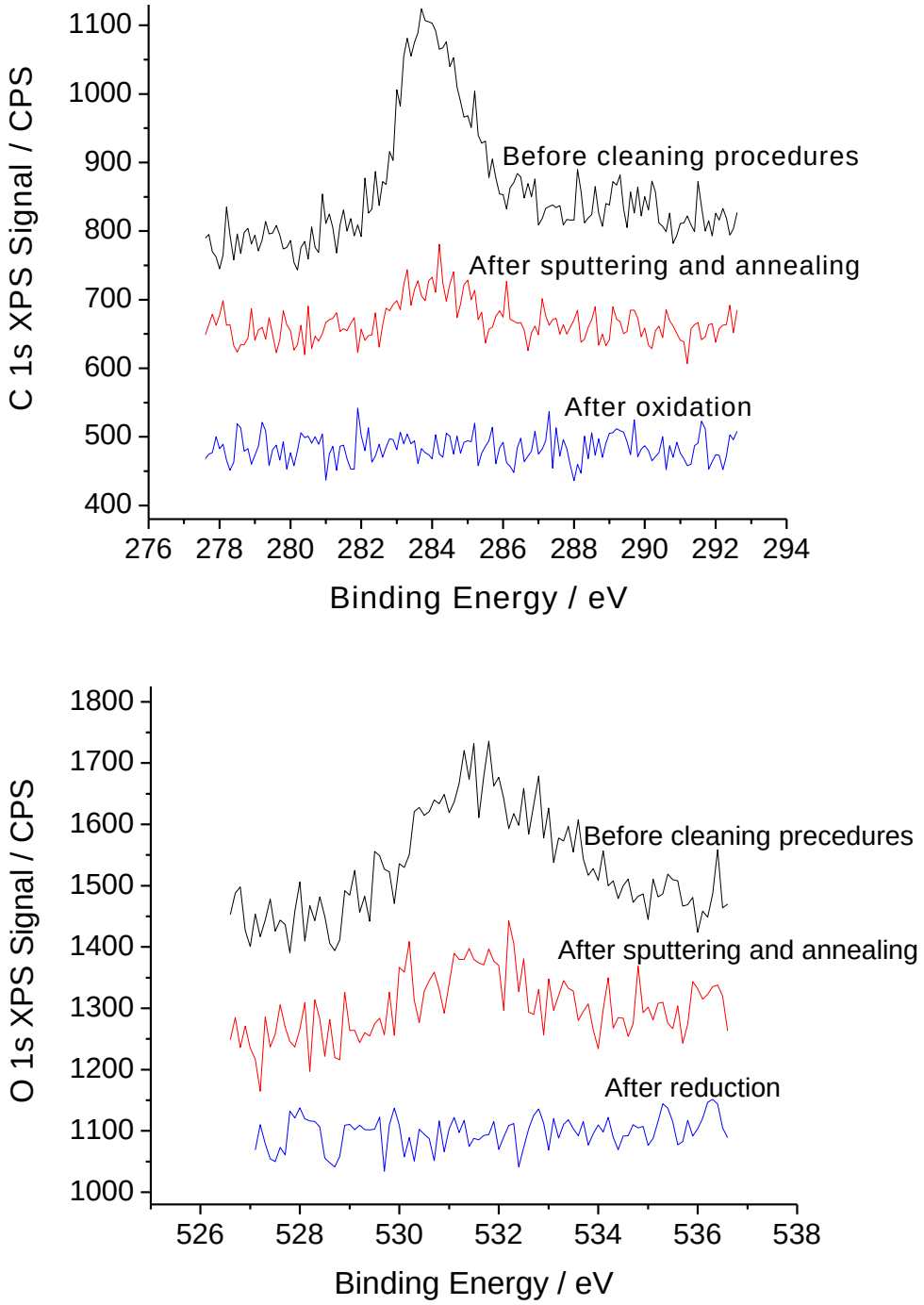

Figure 2.3 C 1s (top) and O 1s (bottom) XPS from Cu (110), dirty and after sputtering/annealing and oxidation/annealing cleaning procedures.

2.4. Chemicals

The copper(I)-*N,N'*-di-*sec*-butylacetamidinate and *N,N'*-di-*sec*-butylacetamidine were provide by Professor R. G. Gordon of Harvard University. The copper(I)-*N,N'*-di-*sec*-butylacetamidinate precursor was synthesized by reaction of *N,N'*-di-*sec*-butylacetamidine with methyl-lithium and then with CuCl; the free acetamidine was prepared by reaction of acetonitrile with *sec*-butylamine. Details of the synthesis and full characterization of them are provided elsewhere [18-20]. The melting point of the copper(I)-*N,N'*-di-*sec*- butylacetamidinate is 77 ℃, the vapor pressure is 0.1 torr at 85 ℃ and 0.23 torr at 95 ℃, it is a yellow-brown color solid at room temperature. The *N,N'*-di-*sec*- butylacetamidine is light yellow color liquid at room temperature, at 58℃ the vapor pressure is 5 torr, the density is 0.85 g/cm^3.

The Cu-KI5 ($C_{12}H_{22}O_2NSiCu$, MW= 303.5 g/mol) was provided by Dr. John Norman of Air Products Inc. Details of this chemical are provided elsewhere [21]. The experiments with Cu-KI5 were a little tricky to perform, because the compound is very air and water sensitive, it changes to green color in 5 minutes while exposed in air. The original Cu-KI5 sample, which was of yellow-brown color, was heated to 65 ℃, and then pumped out while cooling down to room temperature, several cycles were necessary. Then it was continuously pumped overnight at room temperature, after which it was ready to use.

While dosing, all the tubes and valves in the gas manifold were heated to temperature above 65 ℃. The melting point of Cu-KI5 is 63 ℃, its vapor pressure 0.1 torr at 100 ℃. The pure Cu-KI5 is colorless.

The $Cu(acac)_2$ ($Cu(CH_3COCHCOCH_3)_2$, MW= 261.77 g/mol) is blue powder bought from Sigma-Aldrich. At 78 ℃ the vapor pressure (it sublimes) is 0.05 torr. It's an air and moisture-stable solid. Hacac ($CH_3COCH_2COCH_3$, MW= 100.12 g/mol), also known as 2,4-pentanedione, is a precursor to acetylacetonate (acac), a common bidentate ligand. It is a colorless liquid bought from Sigma-Aldrich. Its melting point is -23 ℃ and its boiling point 140 ℃. The vapor pressure is 6 torr at 20 ℃. A salt-water bath was used to cool down the Hacac below 0 ℃ doing dosing to minimize dosing impurities.

All gases were purchased from Liquid Carbonic (Research Purity, >99.995%), and used without further treatment. Dosing of the sample was done by backfilling of the chamber using appropriate leak valves; in the case of the copper acetamidinate precursor, the gas lines behind the valve were heated at 330 K in order to minimize condensation (65 ℃ for Cu-KI5, 100 ℃ for $Cu(acac)_2$). The pressure in the main UHV chamber was measured using a nude ion gauge. Chemicals doses are reported in Langmuirs (1 L = 1 x 10^{-6} torr **s**), uncorrected for differences in ion gauge sensitivities. All exposures were performed at the

constant surface temperatures indicated in the corresponding figures. All the chemical purities were checked *in situ* prior each experiment by using the mass spectrometer in the UHV chamber.

2.5. Thermal desorption particle beam mass spectrometry (TDPBMS)

At the very beginning of this project, we need to check the integrity of the copper(I)-*N*,*N'*-di-*sec*-butylacetamidinate introduced into the ultrahigh vacuum chamber. Since the melting point of the precursor is 77 ℃, it is a solid at room temperature, and to introduce it into the chamber as a vapor, it needs to be heated. Unfortunately, this heating also has the potential to decompose the copper precursor. This could not be easily checked with our QMS, which has an upper limit of 300 amu: the molecular weight of the copper precursor is 464 amu.

To check on the success of the introduction of the copper precursor into the ultrahigh vacuum chamber, many tests were carried out. One of them relied on the use of the thermal desorption particle beam mass spectrometry (TDPBMS) instrument available in Dr Ziemann group. The details of this method can be found elsewhere [22]. The copper acetamidinate was put in one stainless steel tube heated outside with heating tape. As the sample temperature was increased to around 100 ℃, some signals at high masses were

observed. In Figure 2.4, for instance, a 464 amu peak, due to molecular copper acetamidinate is clearly displayed. This was our first solid evidence that the copper acetamidinate could be introduced into the ultrahigh vacuum chamber by heating it up to 100 ℃.

2.6. Knudsen Cells

As a alter nature, the dosing of copper(I)-*N,N'*-di-*sec*-butylacetamidinate precursor was tried directly inside the UHV chamber by using a home-made Knudsen cell. Two types of Knudsen cells were made to introduce the copper acetamidinate into the ultra high vacuum chamber, both shown in Figure 2.5. One has an integrated shutter to shut off the vapor beam pathway (the left cell in the figure), the other a cooling tube to cool down the cell with liquid nitrogen (the cell on the right).

The UHV chamber was open, copper acetamidinate was put in the Knudsen cell, the chamber pumped for 68 hours, and moderate baking at less than 70 ℃ was done for about 20 hours, until reaching a base pressure of 9.7E-10 torr. In one test, 1000 L copper acetamidinate was dosed on the Ni (110) surface at 90 K using the Knudsen cell, then XPS for Cu, Ni, N and C were acquired.

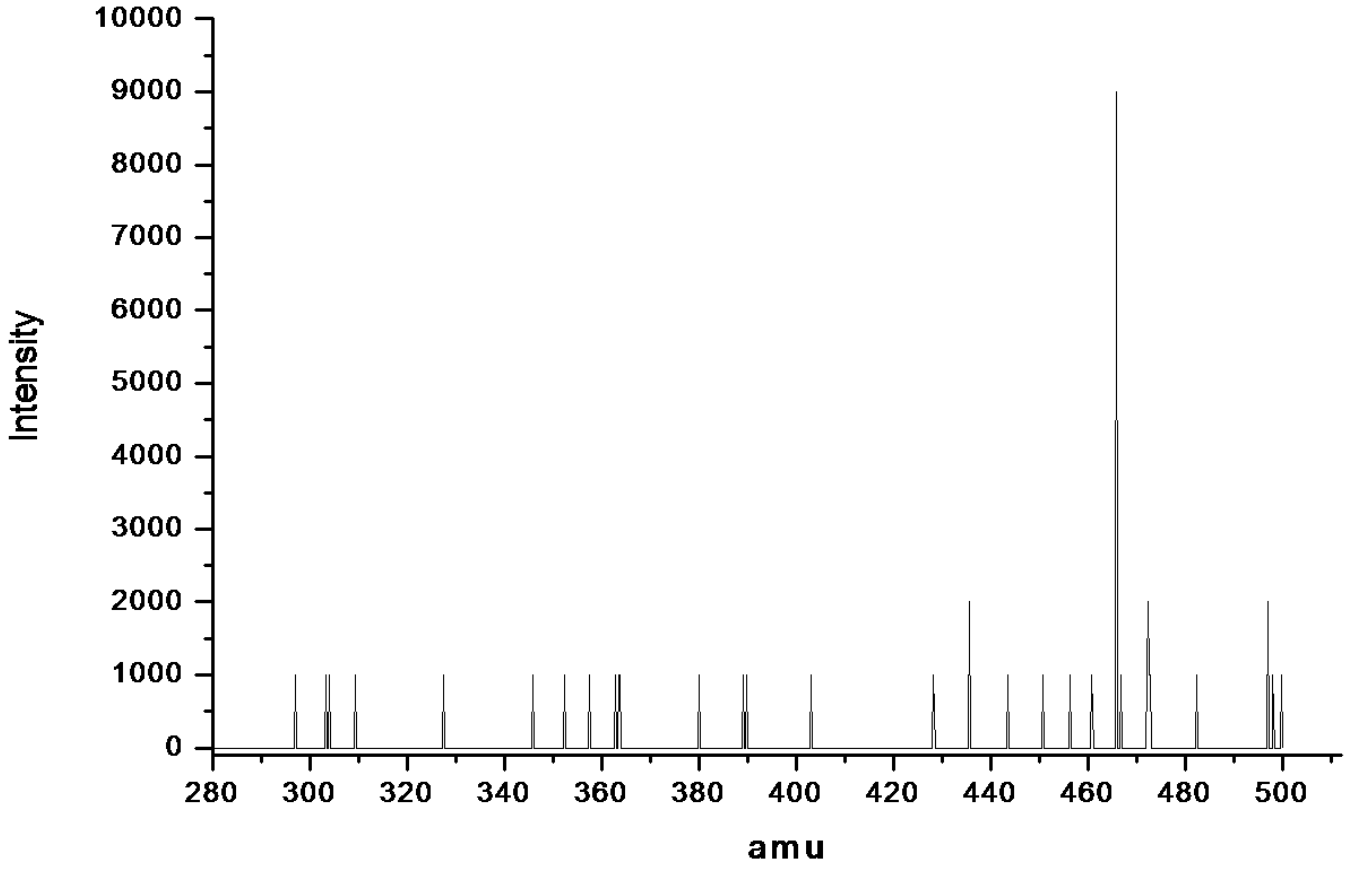

Figure 2.4 Thermal desorption particle beam mass spectrometry (TDPBMS) of copper(I)-*N,N'*-di-*sec*-butylacetamidinate.

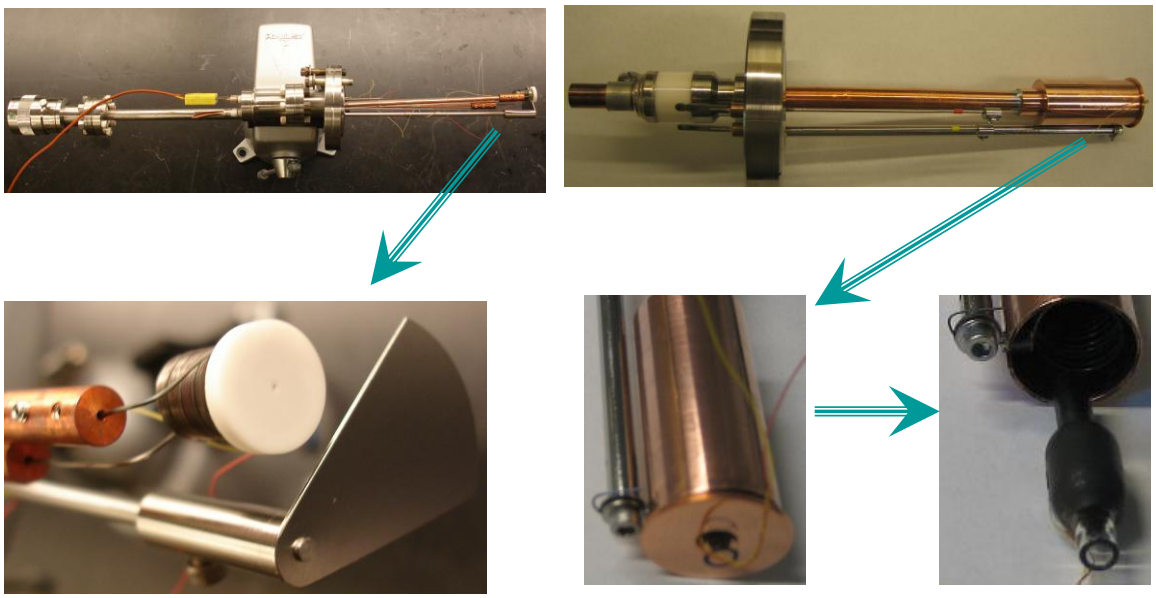

Figure 2.5 Two kinds of home-made Knudsen cells to introduce solid copper(I)-*N,N'*-di-*sec*-butylacetamidinate into the ultra high vacuum chamber.

The XPS of Cu $2p_{1/2}$ and $2p_{3/2}$, C 1s, N 1s, Ni $2p_{1/2}$ and $2p_{3/2}$ peaks first were acquired at 100 K. Then the Ni (110) surface was annealed to different temperatures, and XPS data acquired, as shown in Figures 2.6 and 2.7. For all four elements, the peaks positions and intensities showed some changes while increasing surface temperature, indicating that some chemistry takes place during the temperature range studies. The dose used in this example is quite large, and the adsorption on the surface amounts to much more than a monolayer, so most of the changes observed correspond not to adsorption, but to condensation. Nevertheless, this set of XPS data was a milestone in the project, proving that we would DIRECTLY observe some copper acetamidinate adsorbed on the Ni (110) surface and also the information of a copper film on the surface after heating to high temperatures.

2.7. The high pressure cell for atomic layer deposition

As described before, all the experiments of this dissertation were carried out under ultrahigh vacuum. On the other hand, most of the atomic layer deposition processes are performed in the millitorr to torr pressure range. To bridge this experimental gap, a high pressure cell was added to the main chamber with windows for *in-situ.* Reflection-absorption infrared spectroscopy (RAIRS) studies. This will allow for the identification of adsorbates, a determination of their concentration, and the

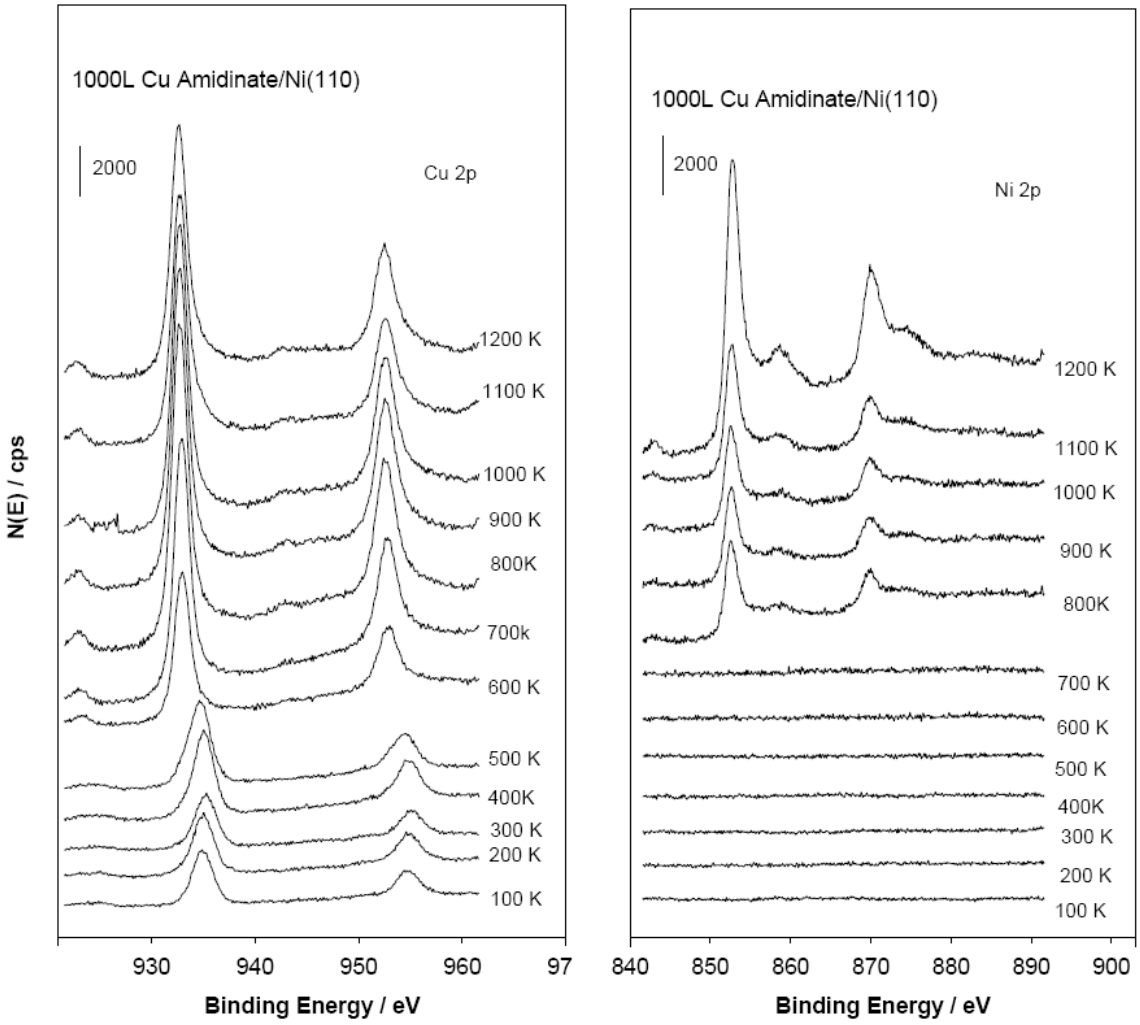

Figure 2.6 Cu 2p (left), Ni 2p (right) XPS data for 1000 L of copper(I)-*N,N'*-di-*sec*-butylacetamidinate dosed on Ni (110) surface.

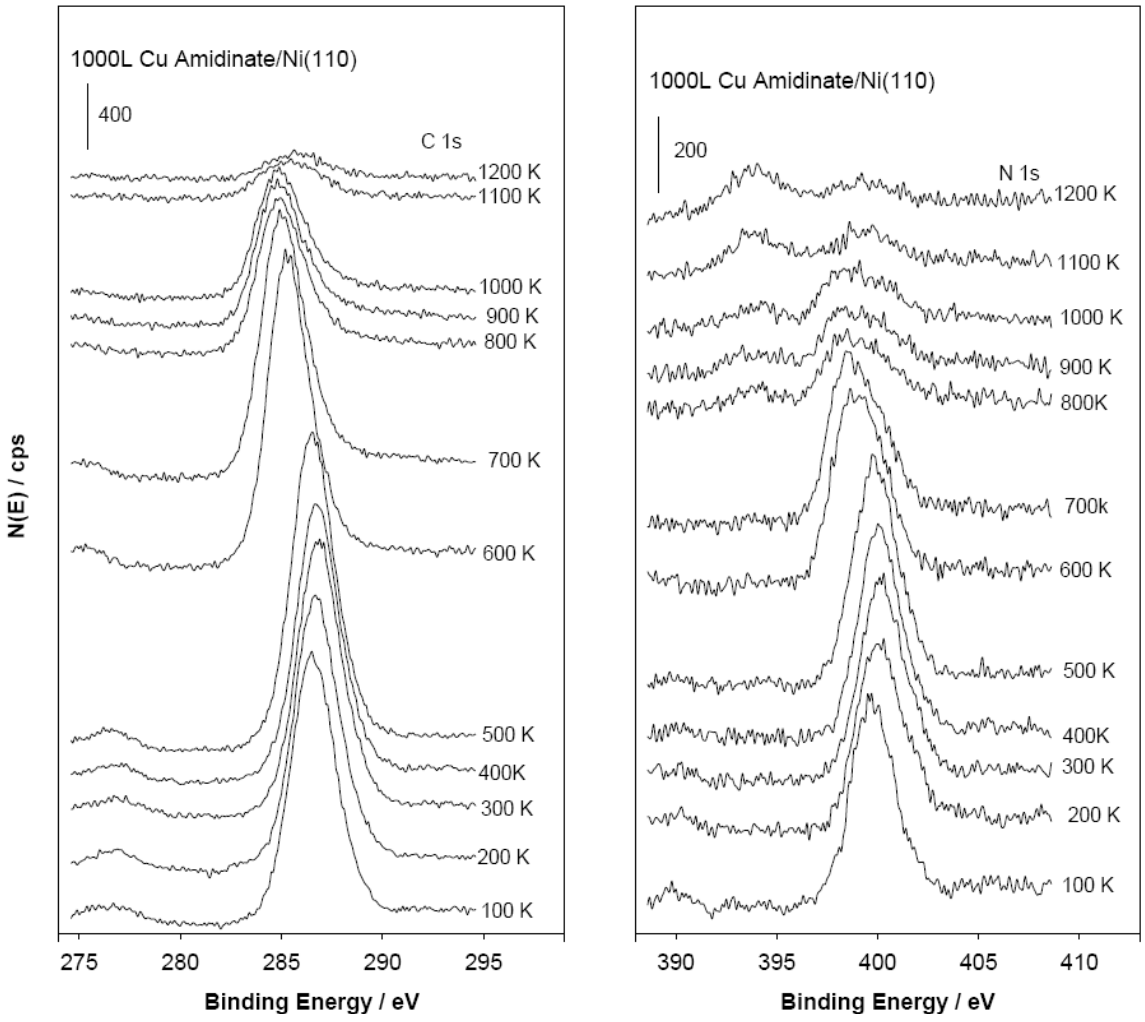

Figure 2.7 C 1s (left), N 1s (right) XPS data for 1000 L of copper(I)-*N,N'*-di-*sec*-butylacetamidinate dosed on Ni (110) surface.

characterization of the active sites under relative high pressure conditions *in-situ* will be described in detail next.

The high pressure (HP) cell consists of a six-way cross cylindrical cell, made out of stainless steel (shown in Figure 2.8, with feedthroughs). It is connected with the main chamber by a 2.75" flange with a Viton O-ring inside. Two NaCl windows are pressed by means of Viton O-rings and bolts. In order to close the HP cell, the manipulator can be used to manually transfer the sample down from the main chamber to the high pressure cell through the O-ring between them. The guide tube comes in close contact with the O-ring, making a seal and separating the two chambers. The high pressure side is pumped by means of a PFEIFFER TPU170 turbo molecular pump, used to reach low pressures prior to opening the high pressure cell to the main UHV vacuum, so a sudden increase in pressure can be avoided. The pressure inside the HP cell is measured with a KJL-6000MC thermocouple gauge. With this set up the ultrahigh vacuum chamber retains a pressure of $1x10^{-7}$ torr while the high pressure cell is open to air. The cell is now operational, but was not used for any of the experiments reported here.

2.8. Reflection-absorption infrared spectroscopy (RAIRS)

Infrared (IR) absorption spectroscopy is one of the techniques used to measure

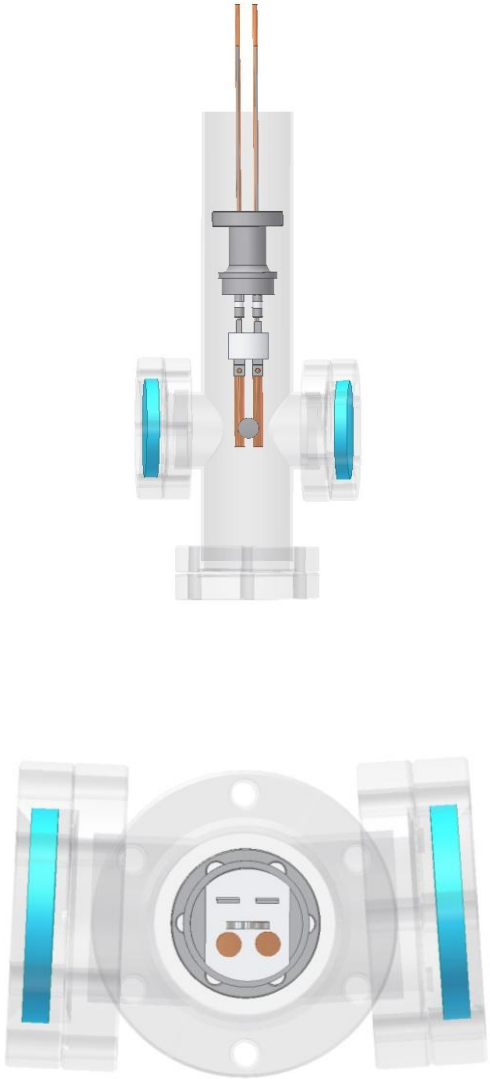

Figure 2.8 Schematic plot of our six-way high pressure cell with feedthroughs
Top: side view; bottom: top view.

vibrational properties on surfaces. It is an incisive, non-destructive tool for examining interfaces and surfaces [23]. A study of infrared absorption spectra of adsorbed molecules can give, in some cases, very detailed information about the geometry of the adsorbed species, the nature of their attachment on the surface, and the strength of the adsorption forces [24].

The fundamental of all infrared techniques is the interaction of the electromagnetic field of infrared radiation with the oscillation dipole associated with a particular normal vibrational mode of the molecules. This excitation manifests itself by the absorption of a proportion of the transmitted or reflected radiation in the infrared experiment. Dipole selection rules and other factors influence absorption intensities and frequencies in the gas, liquid, and solid states, and form the basis for the interpretation of RAIRS spectra[25].

Due to the high resolution of RAIRS (~4 cm^{-1}), inspection of the spectra for simple molecules yields important information. In general, RAIRS is seen as a useful method for elucidating molecular reaction mechanism at surfaces. If ambiguities arise in the assignment of surface IR bands, particularly those associated with hydrogen, isotopic substitution can often be used to clarify the nature of the intermediate. Another advantage

about RAIRS is that it does not require UHV conditions, as is the case with other vibrational spectroscopy techniques like high-resolution electron energy loss spectroscopy (HREELS). This has allowed the application of RAIRS in systems with pressures close to one atmosphere. Under high-pressure conditions, the RAIRS technique is also able to discriminate between adsorbed- and gas-phase species.

In our setup, the IR beam is taken from a BRUKER TENSOR 27 IR spectrometer and passed through a polarizer and focused through a NaCl window onto the sample surface at grazing incidence (~85^{o}). The surface acts as a mirror. The reflected beam is then passed through a second NaCl window and focused onto a mercury-cadmium-telluride (MCT) detector. Figure 2.9 shows a schematic plot and a picture taken for the RAIRS system arrangement used in our case. The entire beam path will be enclosed in a sealed box purged with dry air, purified using a scrubber for CO_2 and water removal to minimize interference from gas phase absorption bands associated with atmospheric H_2O and CO_2. In this high pressure cell, the crystal surface can be exposed to gases at pressures near atmosphere without the risk of losing the ultrahigh vacuum in the main chamber. The crystal can be transferred from ultrahigh vacuum to a ‘high pressure’ environment similar to that in atomic layer deposition conditions and back without exposure to outside air, and probed in-situ. Later, the surface can be characterized by XPS, LEIS and TPD.

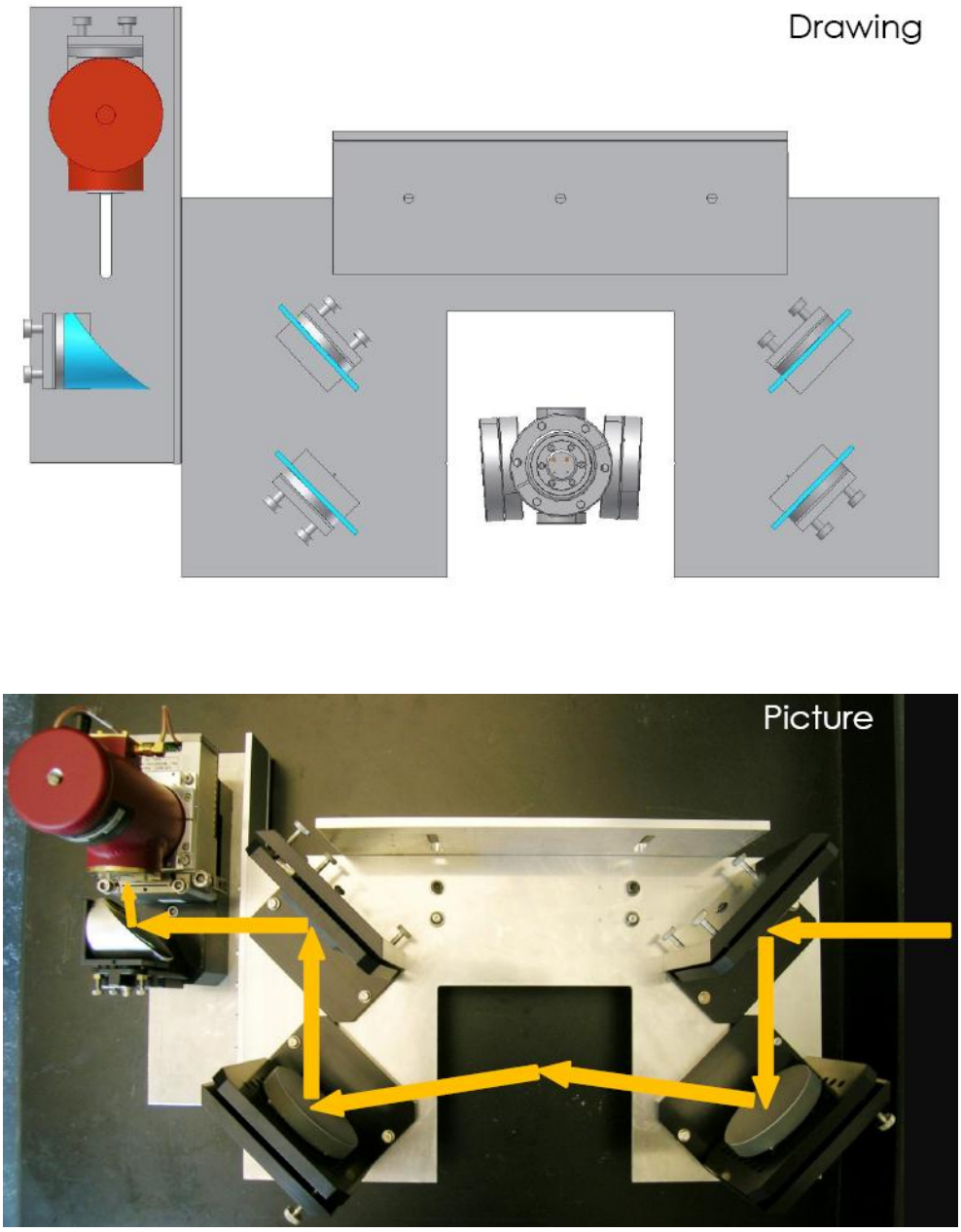

Figure 2.9 Schematic plot and picture of the RAIRS system arrangement.

2.9. References

[1] M. W. Roberts, *Catalysis Letters*, **2000**, *67*, 1.

[2] G. A. Somorjai, *Introduction to Surface Chemistry and Catalysis*, New York, Wiley, **1994**.31

[3] Z. Ma, F. Zaera, *Surface Science Reports* **2006**, *61*, 229.

[4] W. M. Lau, X.-W. Wu, *Surf. Sci*. **1991**, *245*, 345

[5] D. P. Smith, *J. Appl. Phys.* **1967**, *18*, 340

[6] H. Niehus, W. Heiland, E. Taglauer, *Surface Science Reports* **1993**, *17*, 213

[7] D. P. Woodruff, T. A. Delchar, *Modern Techniques of Surface Science*, 2nd ed.; Cambridge University Press: Cambridge, **1994**.

[8] D. Menzel, *Interaction of Metal Surfaces*, Springer-Verlag, Berlin and New York, **1975**.

[9] D. A. King, *Surf. Sci.* **1975**, *47*, 384-402.

[10] P. A. Redhead, *Vacuum* **1962**, *12*, 203

[11] H. Ofner, F. Zaera, *J. Phys. Chem. B* **1997**, *101*, 9069.

[12] D. Chrysostomou, J. Flowers, F. Zaera, *Surf. Sci.* **1999**, *439*, 34.

[13] Q. Ma, H. Guo, R. G. Gordon and F. Zaera. *Chemistry of Materials.* **2010**, *22*, 352

[14] C. D. Wagner, W. M. Riggs, L. E. Davis, J. F. Moulder, G. E. Muilenberg, G. E.,

Handbook of X-Ray Photoelectron Spectroscopy, Perkin-Elmer Corp.: Eden Prairie, MN, **1978.**

[15] D. Chrysostomou, C. French, F. Zaera, *Catal. Lett.* **2000**, *69*, 117.

[16] C. J. Jenks, B. E. Bent, N. Bernstein, F. Zaera, *J. Am. Chem. Soc.* **1993**, *115*, 308.

[17] C. J. Jenks, B. E. Bent, N. Bernstein, F. Zaera, *surface science letter,* **1992**, *277*, L89

[18] B. S. Lim, A. Rahtu, J. –S. Park, R. G. Gordon, *Inorganic Chemistry.* **2003**, *42,* 7951.

[19] Z. Li, S. T. Barry, R. G. Gordon, *Inorganic Chemistry*. **2005**, *44,* 1728

[20] J. H. Forsberg, V. T. Spaziano, T. M. Balasubramanian, G. K. Liu, S. A. Kinsley, C. A. Duckworth, J. J. Poteruca, P. S. Brown, J. L. Miller, *Journal of Organic Chemistry*, **1987**, *52*, 1017.

[21] J. A. T. Norman, M. Perez, S. E. Schulz, T. Waechtler, *Microelectronic Engineering*, 2008, 85, 2159.

[22] H. J. Tobias, P. M. Kooiman, K. S. Docherty, P. J. Ziemann, *Aerosol Science and Technology*. **2000**, *33*,170.

[23] C. J. Hirschmugl, *Surf. Sci.* **2002**, *500*, *577*.

[24] R. G. Greenler, *J.Chem. Phys*. **1966**, *44*, 310.

[25] B. E. Hayden, *Vibrational spectroscopy of molecules on surfaces*, Plenum Press, New York, **1987**.

CHAPTER THREE

Uptake of the Copper Acetamidinate ALD Precursor on Nickel Surfaces

3.1. Introduction

Copper acetamidinates are one of the most promising precursors for copper ALD [1-3]. The advantages of these copper acetamidinates include their relative stability against to reactions with air and their reasonable vapor pressure (about 0.1 Torr at 85℃ for copper(I)-*N,N'*-di-*sec*-butylacetamidinate). Past work has indicated that, although Cu acetamidinates appear not to chemisorb onto clean metals at the temperatures needed for ALD, somewhere around 450-500 K they may be activated on hydrogen-presaturated surfaces. Under those conditions the deposition appears to be self-limited, and to leave a copper layer of about 0.5 Å in thickness on the surface [2]. Unfortunately, the deposit copper film always contains approximately 1%carbon. The surface chemistry responsible for this process is virtually unknown, and many questions remain, including the source of the impurities, the effect of coadsorption of hydrogen and, in general, the mechanism for this surface chemistry. The goal of our work is to develop a molecular-level understanding of the surface reactivity of these precursors to design more efficient and cleaner copper ALD processes.

In this chapter we report on results from XPS and LEIS studies on the adsorption and thermal decomposition of copper(I)-*N,N'*-di-*sec*-butylacetamidinate on (110) oriented nickel surfaces. Experiments in the presence of preadsorbed hydrogen were also carried out in order to study the effect of hydrogen on the surface. It is shown here that, with copper(I)-*N,N'*-di-*sec*-butylacetamidinate, activated adsorption on nickel surfaces is possible only above 300 K. Also, at least on nickel substrates and under vacuum conditions, the optimum deposition temperature was identified to be around 350 K, because by 400 K deposition past one monolayer is possible, and by 450 K decomposition and Cu multilayer deposition is rapid; the adsorption is no longer self-limiting as required for clean ALD processes. It is also reported that approximately three ALD cycles are required to deposit one full copper monolayer. No detectable changes in deposition rates or surface chemistry were observed upon presaturation of the substrate with hydrogen. A discussion is provided to justify this latter observation. Some figures shown in this chapter were published in an article in *Chemistry of Materials*, 2010, 22, 352 (copyright by American Chemical Society); most text of that article was reprinted in this chapter. The molecular structure and mass spectrum of copper(I)-*N,N'*-di-*sec*-butylacetamidinate were shown in Figure 3.1, the mass spectrum was acquired using the ACIF facilities of chemistry department of the University of California, Riverside.

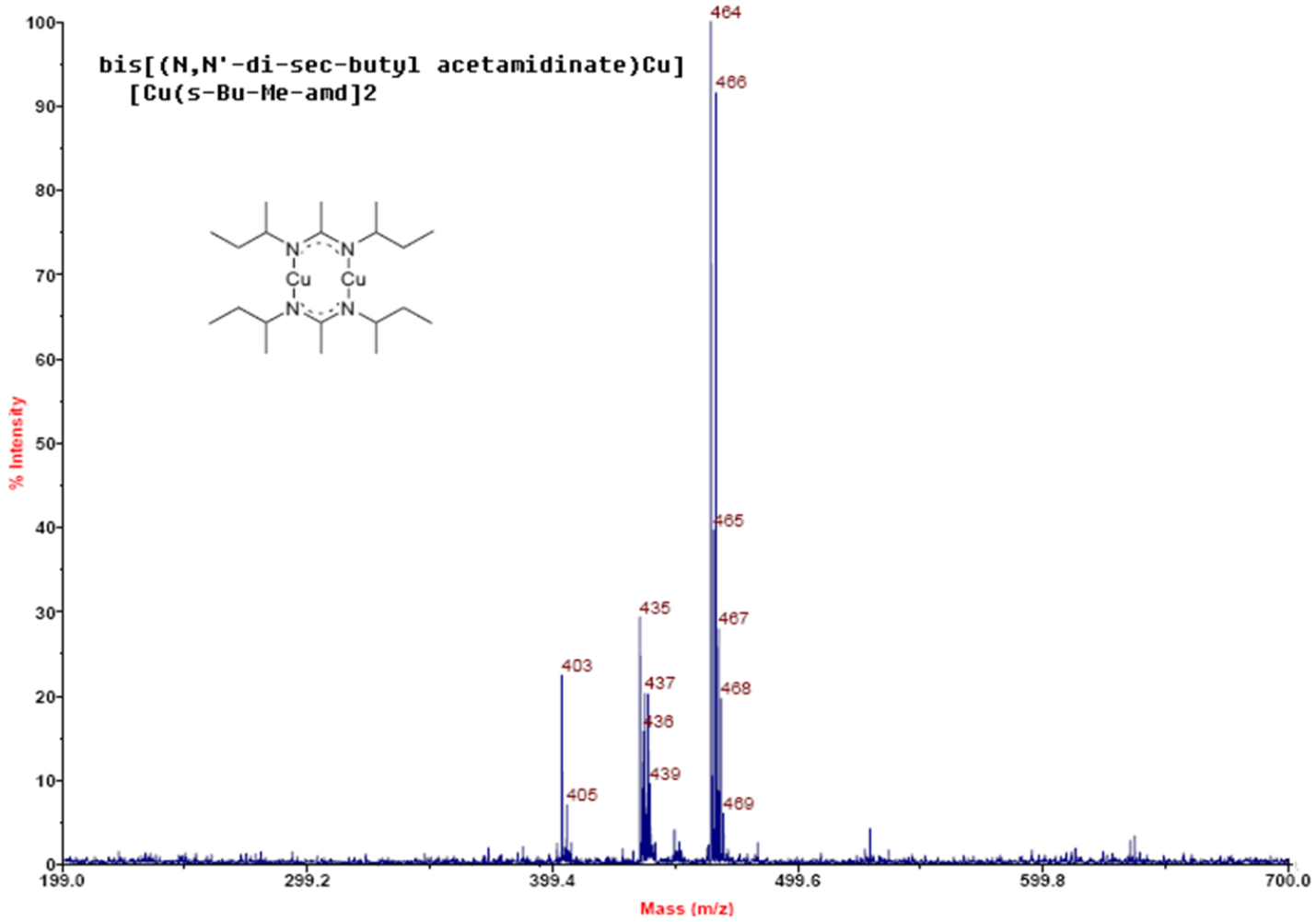

Figure 3.1 Molecular structure and mass spectrum of copper(I)-*N,N'*-di-*sec*-butylacetamidinate.

3.2. Results

3.2.1. XPS

The adsorption and activation of the copper acetamidinate on the Ni (110) surface was first investigated by XPS. Figures 3.2 to 3.5 display the Cu $2p_{3/2}$, C 1s, N 1s, and Ni $2p_{3/2}$ XPS data obtained after adsorption of 10.0 L of the acetamidinate at different temperatures. For each element, two sets of data are shown, one for the surface immediately after the adsorption at the indicated temperatures (left), and another obtained after annealing each of the surfaces of the first set to 500 K. The 10 L exposure was chosen to reach surface coverage close to one monolayer (see below). From Figure 3.2, the Cu $2p_{3/2}$data shows that adsorption at temperatures below 200 K results in the appearance of one XPS peak centered at 934.0 eV. This value is typical of Cu(I) species [4] and close to that reported for a copper acetylacetonate complex deposited onto a K10-montmorillonite clay [5], and is therefore indicative of molecular adsorption. The +1 oxidation state of the metal centers was confirmed by the kinetic energy of the L_3VV Auger electrons, which was determined to be 913.7 eV (the Auger parameter amounting to 361.1 eV; data shown in chapter 4, Figure 4.1) [6]. Adsorption at surface temperatures of 300 K or more, on the other hand, results in the Cu $2p_{3/2}$ peak shifting to at 932.5 eV, a typical metallic copper binding energy (details below). Figure 3.3 for C 1s and Figure 3.4 for N 1s show that adsorption at temperatures below 200 K results in the appearance of

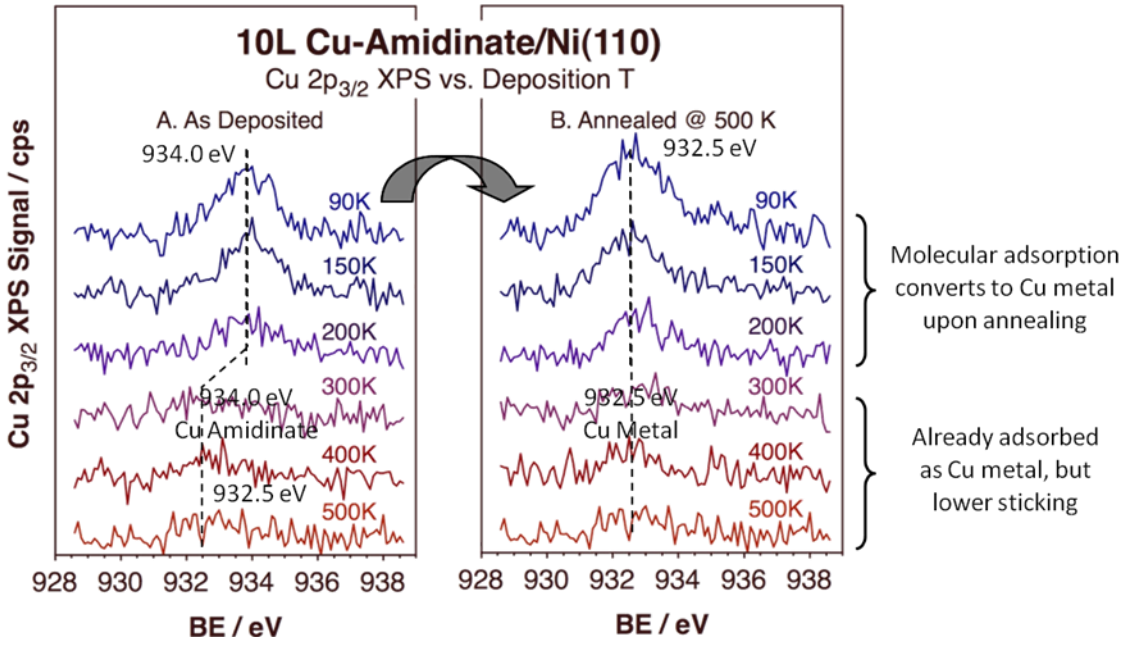

Figure 3.2 Cu $2p_{3/2}$ XPS for a Ni (110) single crystal surface dosed with 10.0 L of copper(I)-*N,N'*-di-*sec*-butylacetamidinate.

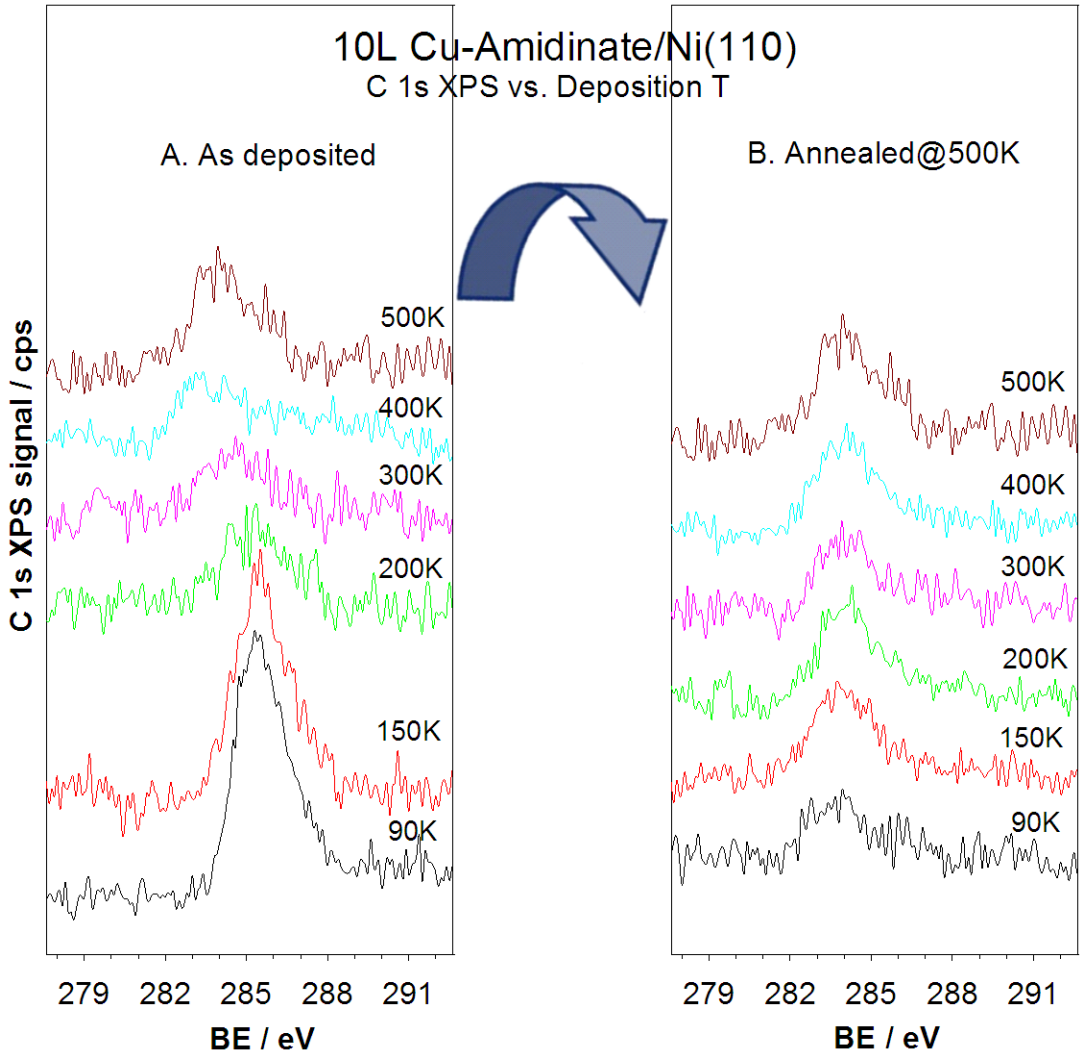

Figure 3.3 C 1s XPS for a Ni (110) single crystal surface dosed with 10.0 L of copper(I)-*N,N'*-di-*sec*-butylacetamidinate.

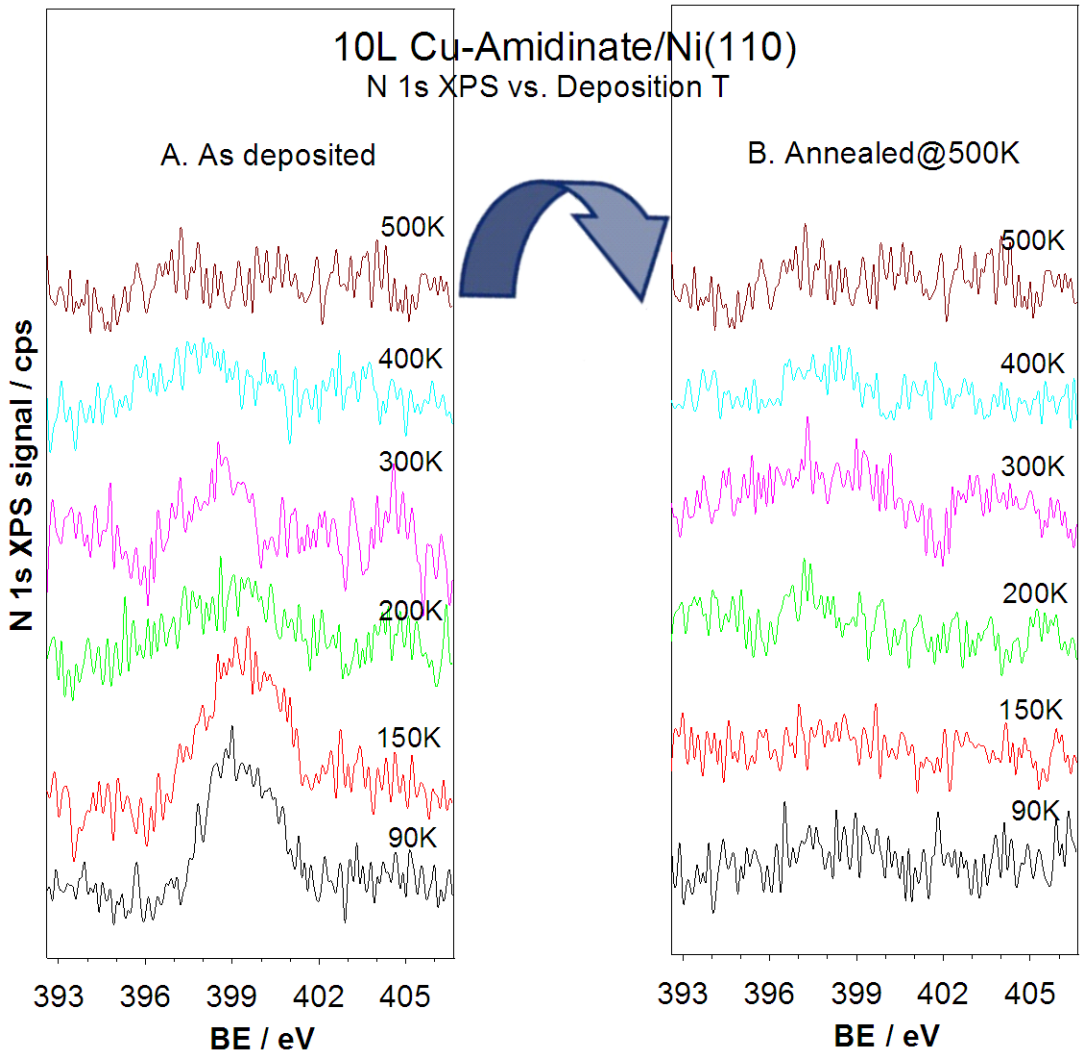

Figure 3.4 N 1s XPS for a Ni (110) single crystal surface dosed with 10.0 L of copper(I)-*N,N'*-di-*sec*-butylacetamidinate.

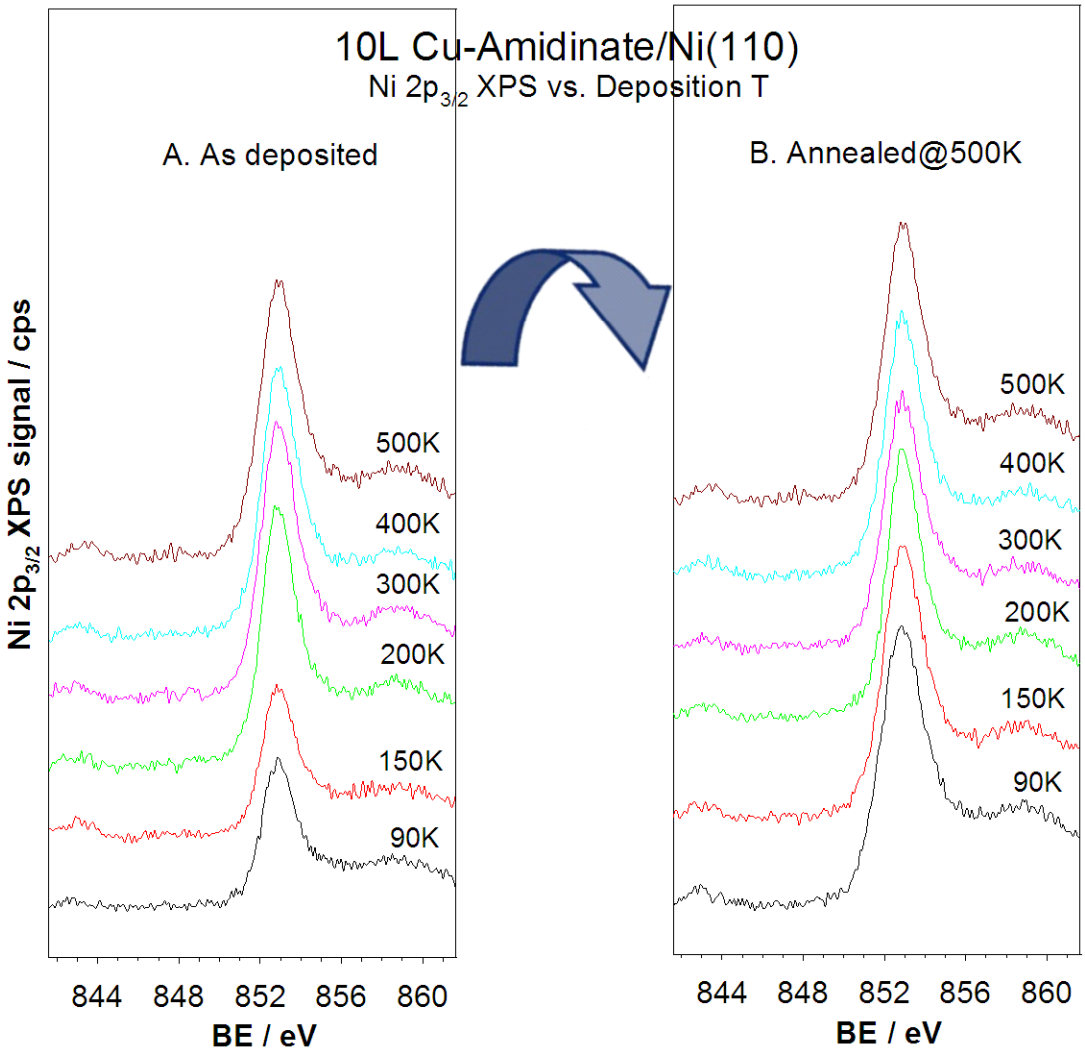

Figure 3.5 Ni $2p_{3/2}$ XPS for a Ni (110) single crystal surface dosed with 10.0 L of copper(I)-*N,N'*-di-*sec*-butylacetamidinate.

XPS peaks centered at 285.5 eV for C 1s and 399.5 eV for N 1s, and that both binding energies shift to lower values after annealing at 300 K or higher temperatures, indicating that the bonding between the copper atoms and their ligands breaks at the higher temperatures. All the shifts in binding energies (Cu $2p_{3/2}$, C 1s and N 1s) happen in the same temperature range. The binding energies of Ni $2p_{3/2}$ (Figure 3.5), on the other hand, stay constant while temperature is increased, but the peak intensity increases between 150 K and 200 K. That means that less copper acetamidinate molecules are adsorbed at 200 K than at 150 K, because of some desorption. The decrease in the C1s and N 1s peak in the same temperature range is consistent with this interpretation.

Annealing at 500 K the copper acetamidinate initially adsorbed at temperatures below 200 K results in a clear shift in the binding energy of the Cu $2p_{3/2}$ XPS peak of the adsorbed copper species, to 932.5 eV. The Auger L_3VV line shifts even more, to a kinetic energy of 919.0 eV (Auger parameter = 364.9 eV), consistent with the reduction of the copper atoms to a metallic state [4,6]. In fact, dosing of the copper acetamidinate on surfaces kept at temperatures of 300 K or above directly leads to the formation of adsorbed copper metal. This means that there is a switch in adsorption mode between 200 and 300 K from molecular to dissociative. Under no circumstances were other oxidation states identified for the copper-containing surface species; no

disproportionation reactions or formation of Cu(II) species were detected. Similarly, the C 1s and N 1s binding energies also shift down while annealing the lower-temperatures surfaces (200 K and below) to 500 K.

Finally, the dissociative adsorption of copper acetamidinate takes place with a lower effective sticking coefficient than that seen for molecular adsorption at lower temperatures, a fact indicated by the lower copper uptake (smaller Cu XPS peak, bigger Ni XPS peak) seen above 300 K. Clearly, activation and adsorption of the copper acetamidinate on the surface competes with molecular desorption at these higher temperatures. Such kinetic competition may explain why high doses of the precursor are required in ALD processes. The reason why ALD processes doses are always in the unit of million Langmuir is because at the high temperatures used there, most of the incoming molecules simply desorbed molecularly before having the opportunity to react and bond to the surface.

Further copper acetamidinate uptake experiments were carried out at surface temperatures between 300 and 460 K, a temperature range more in tune with those of interest for ALD. The Cu $2p_{3/2}$ XPS data obtained as a function of exposure for 350 (left panel), 400 (center), and 460 (right) K are provided in Figure 3.6. First to notice in this

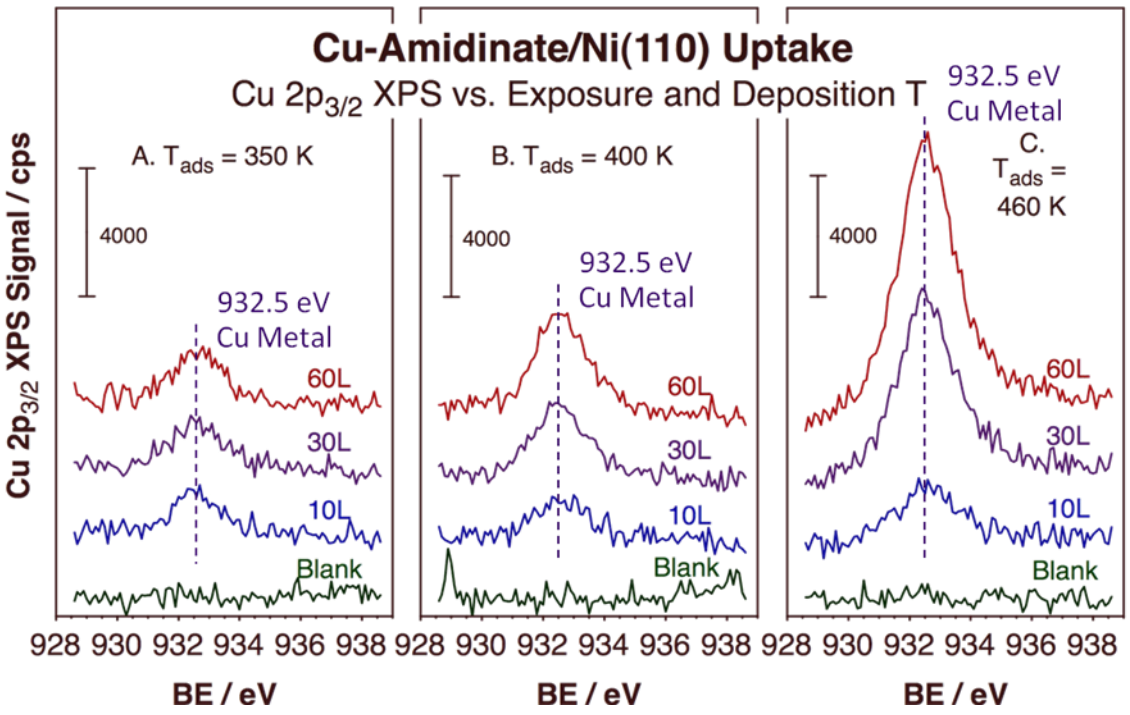

Figure 3.6 Cu $2p_{3/2}$ XPS uptake for copper(I)-*N,N'*-di-*sec*-butylacetamidinate on Ni (110) at 350 (left), 400 (center) and 460 (right) K.

figure is the fact that, again, all peaks are centered at 932.5 eV, the binding energy identified with metallic copper atoms. Moreover, a larger uptake is seen at higher temperatures, an observation indicative of the activated nature of the adsorption. In fact, at 350 K the copper surface coverage reaches saturation after exposures on the order of 10 L, after which no further uptake is possible. At 460 K, by contrast, the uptake appears to be unlimited, and certainly continues well past the first monolayer. Based on the attenuation of the Ni 2p XPS signal (Figure 3.7) and on comparisons with LEIS data (see below), a coverage of approximately three monolayers is estimated for the case of the 60 L exposure at 460 K (the term monolayer is used here relative to a value of one for monolayer saturation). A summary of the copper uptake derived by integrating the peaks area of curves in Figure 3.6 data is provided in Figure 3.12.

3.2.2. LEIS

Figure 3.8 displays results from LEIS experiments on the uptake of copper acetamidinate on a Ni (110) single-crystal surface at 90 K. It shows that most of the signal seen at 575 eV, which corresponds to Ne^+ scattering from the nickel surface atoms, is already suppressed after a 10 L exposure: only approximately 15% of the nickel surface remains uncovered at this stage of the uptake. Exposures of approximately 12 L are sufficient to saturate the surface at these low temperatures, and by 30 L no nickel atoms are any

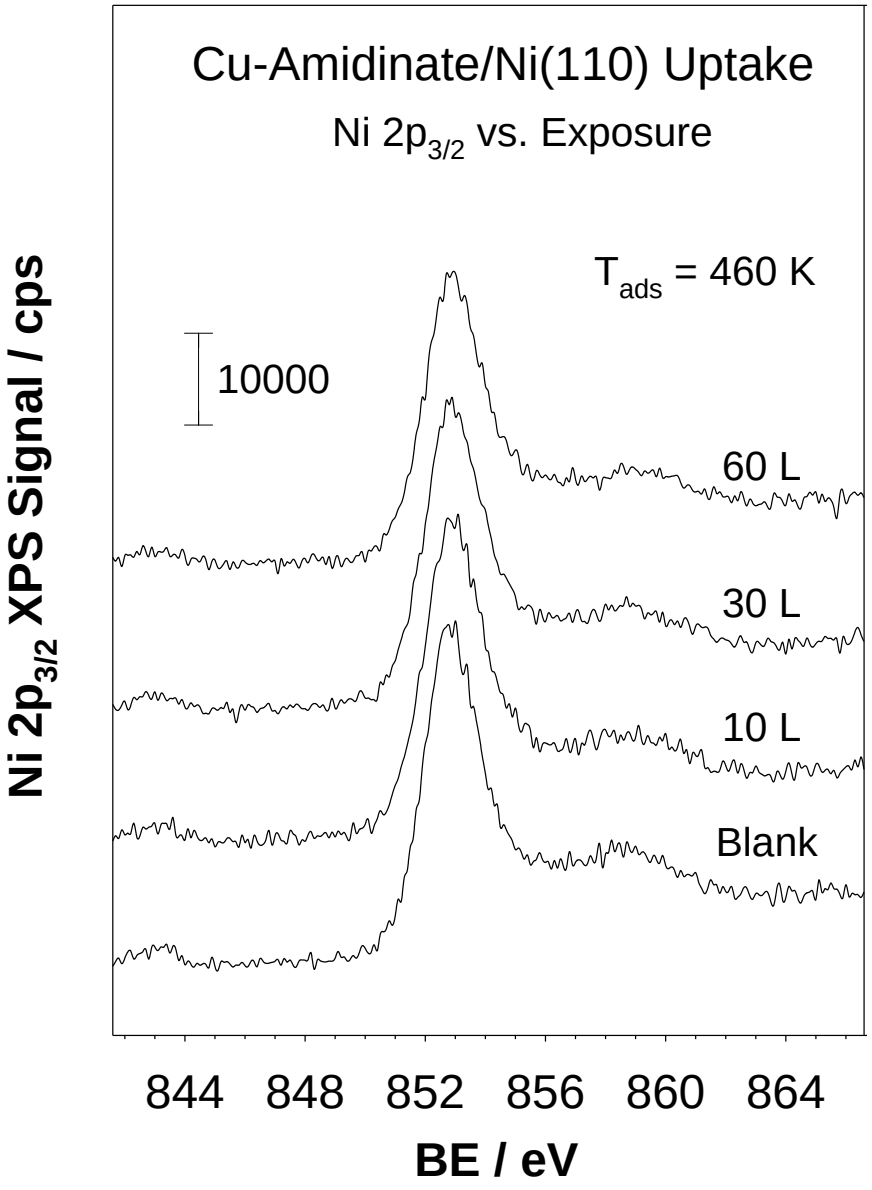

Figure 3.7 Ni $2p_{3/2}$ XPS uptake for copper(I)-*N,N'*-di-*sec*-butylacetamidinate on Ni (110) at 460 K.

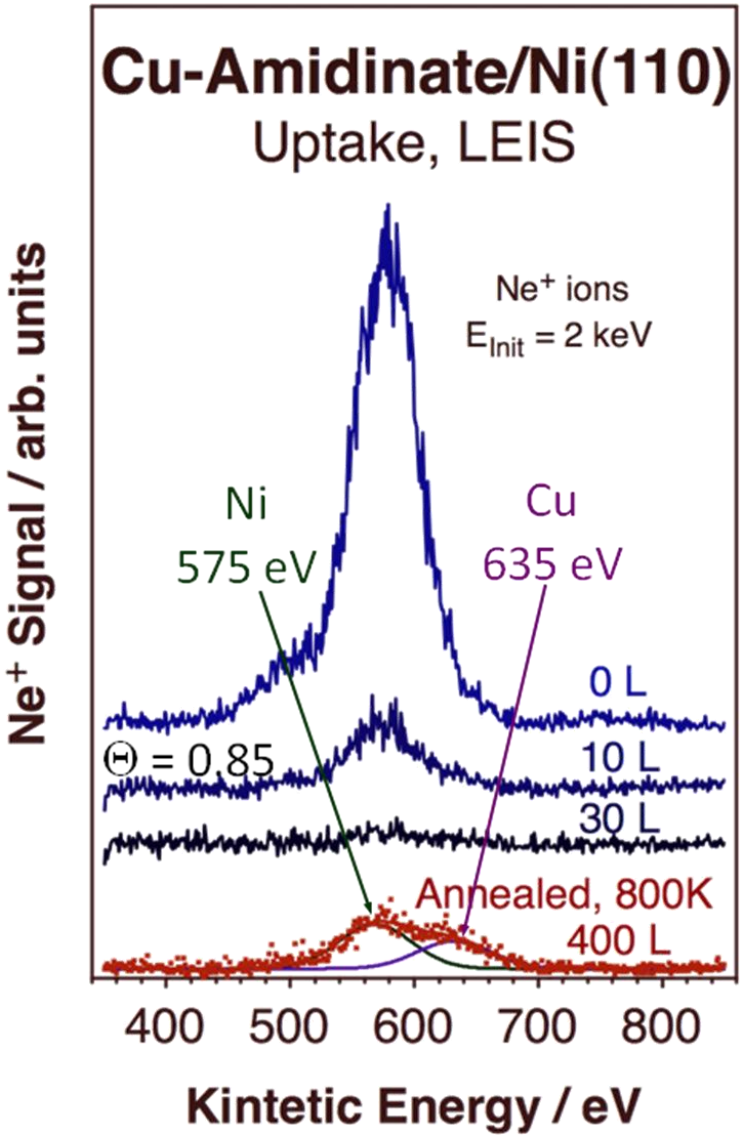

Figure 3.8 Ne^+ LEIS data from a Ni (110) single crystal surface dosed at 90 K with copper(I)-*N,N'*-di-*sec*-butylacetamidinate as a function of exposure.

longer exposed. It should be noted, though, that the adsorbed monolayer under these conditions is comprised of molecular copper acetamidinate, and that those molecules have a large footprint, much larger than that of the surface species obtained upon activated adsorption at higher temperatures. The bottom trace of Figure 3.8 corresponds to a surface dosed with 400 L of the copper acetamidinate at 90 K and then annealed to 800 K, which leads to some adsorbate decomposition and to the re-exposure of some nickel atoms. Two additional observations are worth highlighting from the data obtained after annealing: (1) a new peak develops in the LEIS data at 635 eV, associated with surface copper atoms, and (2) the combined signal from nickel and copper at this stage is much smaller than that of the clean surface. The latter observation is at least in part justified by the codeposition of carbon- and/or nitrogen-containing species on the surface upon thermal activation of the adsorbed copper acetamidinate, a fact that was corroborated by additional LEIS experiments using He^+ ions (Figure 3.9, the peak around 390 eV is from Ni surface, the broad peak below 200 eV comes from the combination of carbon or nitrogen). It should be pointed out, however, that differences in scattering cross section may also contribute to the overall decrease in LEIS signal intensity once the nickel is covered with copper.

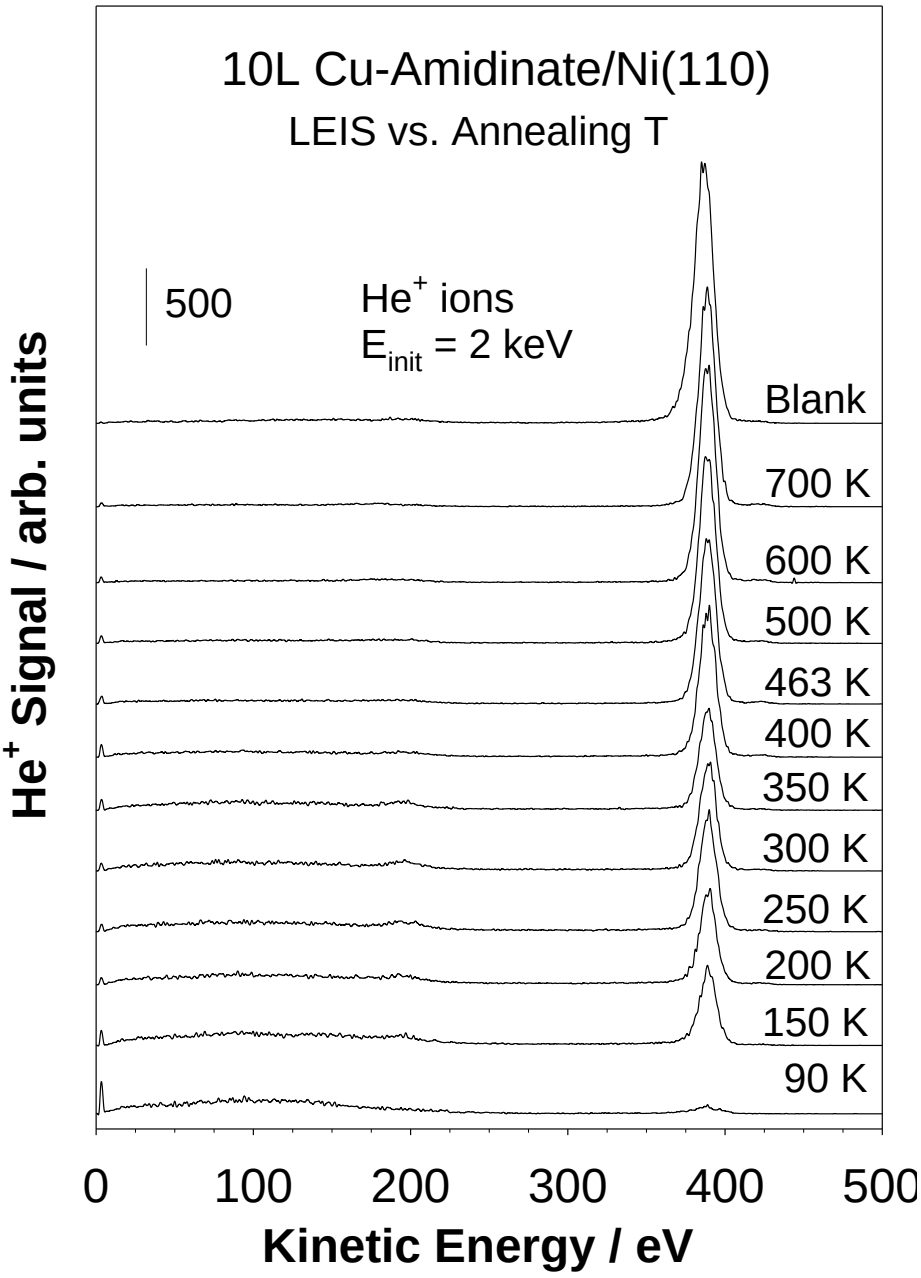

Figure 3.9 He^+ LEIS data from a Ni (110) single crystal surface dosed at 90 K with 10 L copper(I)-*N,N'*-di-*sec*-butylacetamidinate as a function of annealing temperature.

An estimate of the number of cycles needed for the buildup of one monolayer of copper atoms on the surface was obtained by performing several exposure-and-annealing cycles in sequence. Figure 3.10 reports the LEIS traces recorded after four of such cycles, in which the surface was first saturated with copper acetamidinate at 90 K and then annealed to 465 K to decompose the adsorbates and desorb the excess molecules of the precursor. A lower temperature than that used in the experiments in Figure 3.8 was used here for the annealing to minimize the dehydrogenation of the organic ligands in the hope to better reproduce the conditions seen in ALD. As expected, the LEIS peak associated with the nickel surface atoms decreases in size, by about a factor of two after each of those cycles, and disappears almost completely after the third. Quantification of the uptake, shown as a function of the number of cycles in the inset, indicates an exponential decrease in the amount of nickel atoms exposed as a function of the number of cycles performed, the result expected if new deposition occurs with constant probability on the uncovered nickel substrate. Also evident from the data in the main frame of Figure 3.10 is the appearance of the peak due to surface copper, which, again, is small because of a combination of codeposition of carbon- and/or nitrogen-containing species and changes in LEIS cross section. A deposition rate of ~ 0.33 monolayer/cycle, or 0.75 Å/cycle, was calculated from these LEIS data.

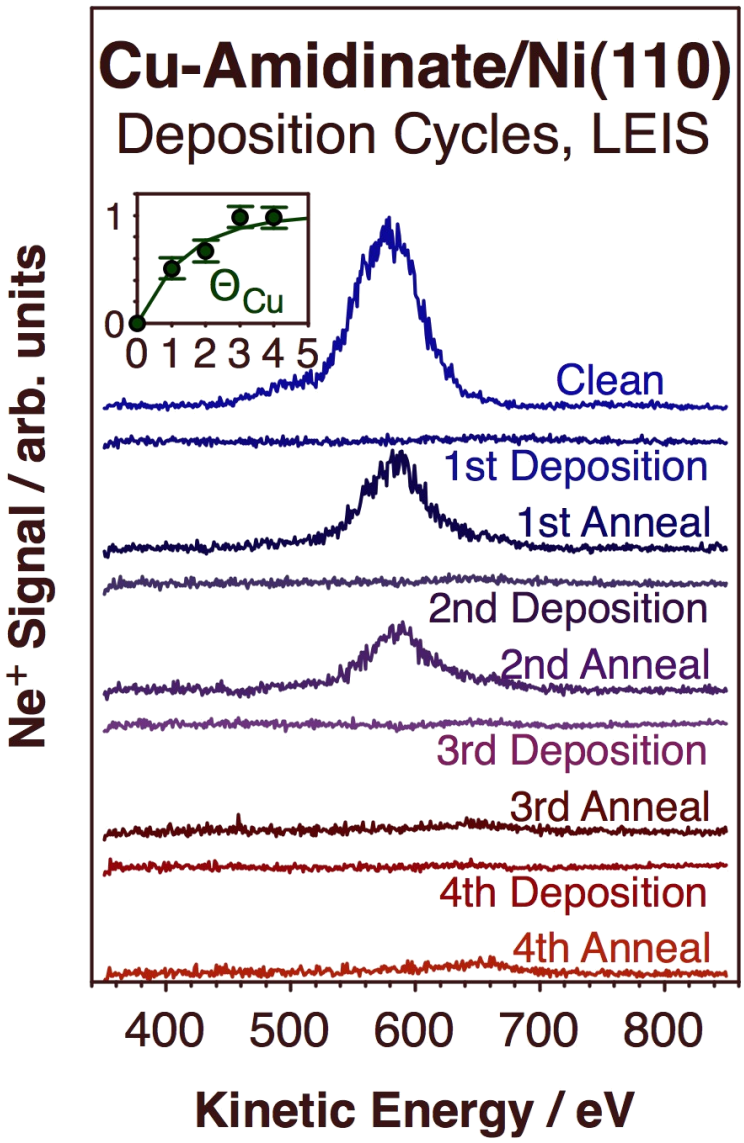

Figure 3.10 Ne^+ LEIS data obtained during the deposition of copper on Ni (110) using copper(I)-*N,N'*-di-*sec*-butylacetamidinate.

3.2.3. Experiments with Coadsorbed Hydrogen

In order to investigate the effect that coadsorbed hydrogen exerts on the adsorption and decomposition of copper acetamidinate on Ni (110), experiments similar to those reported in Figure 3.6 were carried out on surfaces previously saturated with hydrogen (by dosing 150 L H_2 at 90 K). Figure 3.11 displays Cu $2p_{3/2}$ XPS data for copper(I)-*N*,*N'*-di-*sec*-butylacetamidinate on the H-Saturated Ni (110) surface after10, 30 and 60 L exposures, all peaks are centered at 932.5 eV as those on clean surface, a value typical for metallic copper. Also, the uptake is faster at higher temperatures, as more clearly illustrated in Figure 3.12.

All the XPS peaks in Figures 3.6 for clean surface and 3.11 for H-Saturated surface were integrated and plotted in Figure 3.12. No significant changes are apparent upon hydrogen preadsorption from these data: a slightly different deposition rate may have been seen on the H-presaturated surface at 460 K, but the difference is most likely within the experimental error of the experiments. No appreciable differences were seen in the XPS peak shapes, and no differences were detected in the XPS signals for carbon and nitrogen either (Figures 3.13 and 3.14). It appears that, at least under vacuum, preadsorption of hydrogen does not lead to any appreciable changes in the surface chemistry of copper acetamidinates in the temperature range relevant to ALD processes.

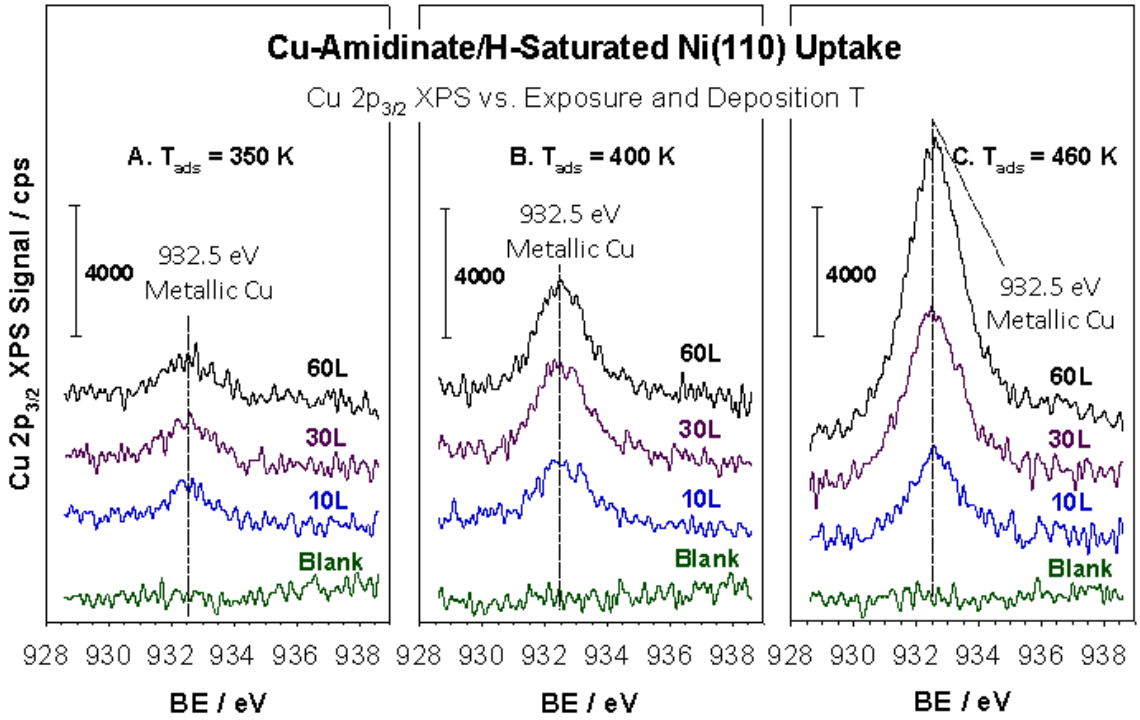

Figure 3.11 Cu $2p_{3/2}$ XPS uptake for copper(I)-*N,N'*-di-*sec*-butylacetamidinate on H-Saturated Ni (110) at 350 (left), 400 (center) and 460 (right) K.

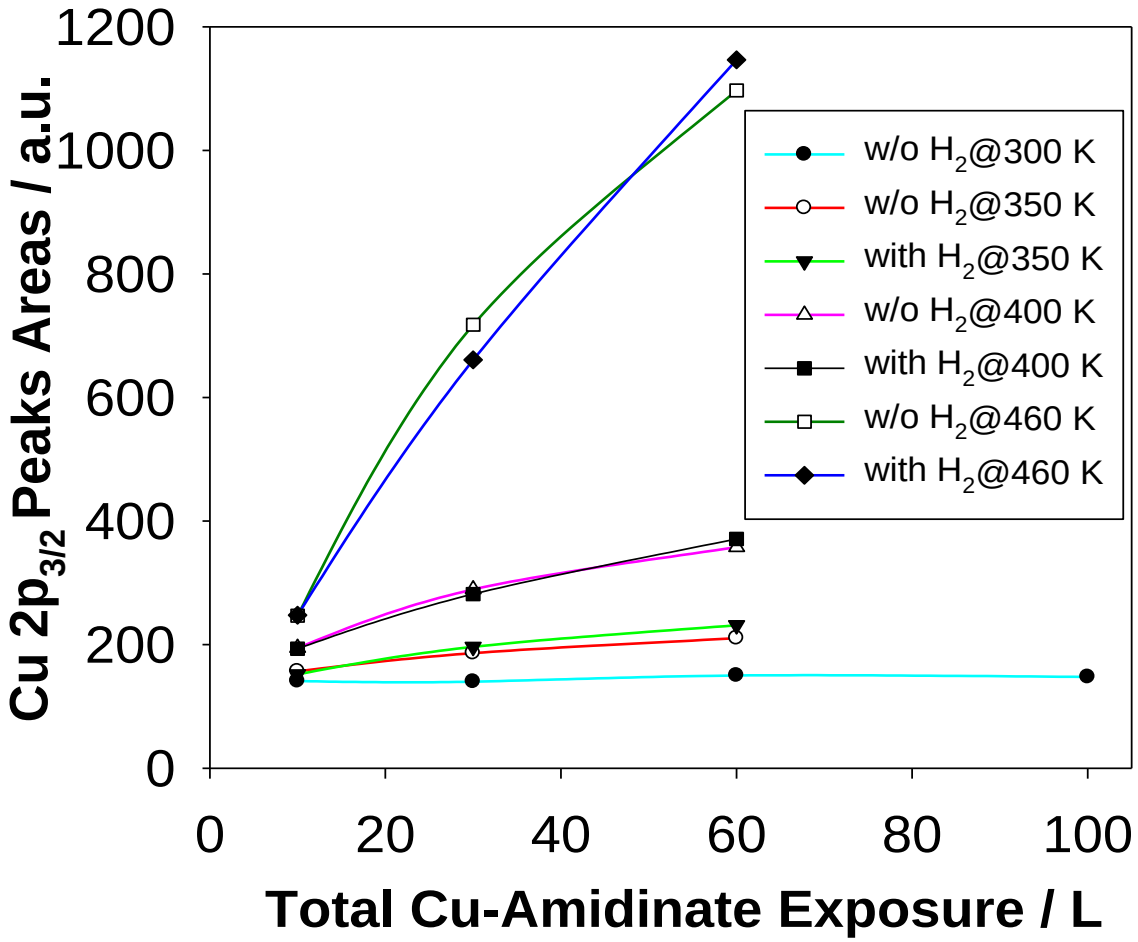

Figure 3.12 Copper uptake estimated from Cu $2p_{3/2}$ XPS experiments such as those shown in Figures 3.6 and 3.11 for copper(I)-*N,N'*-di-*sec*-butylacetamidinate on clean (as marked) and H-Saturated (as marked) Ni (110) as a function of surface temperature.

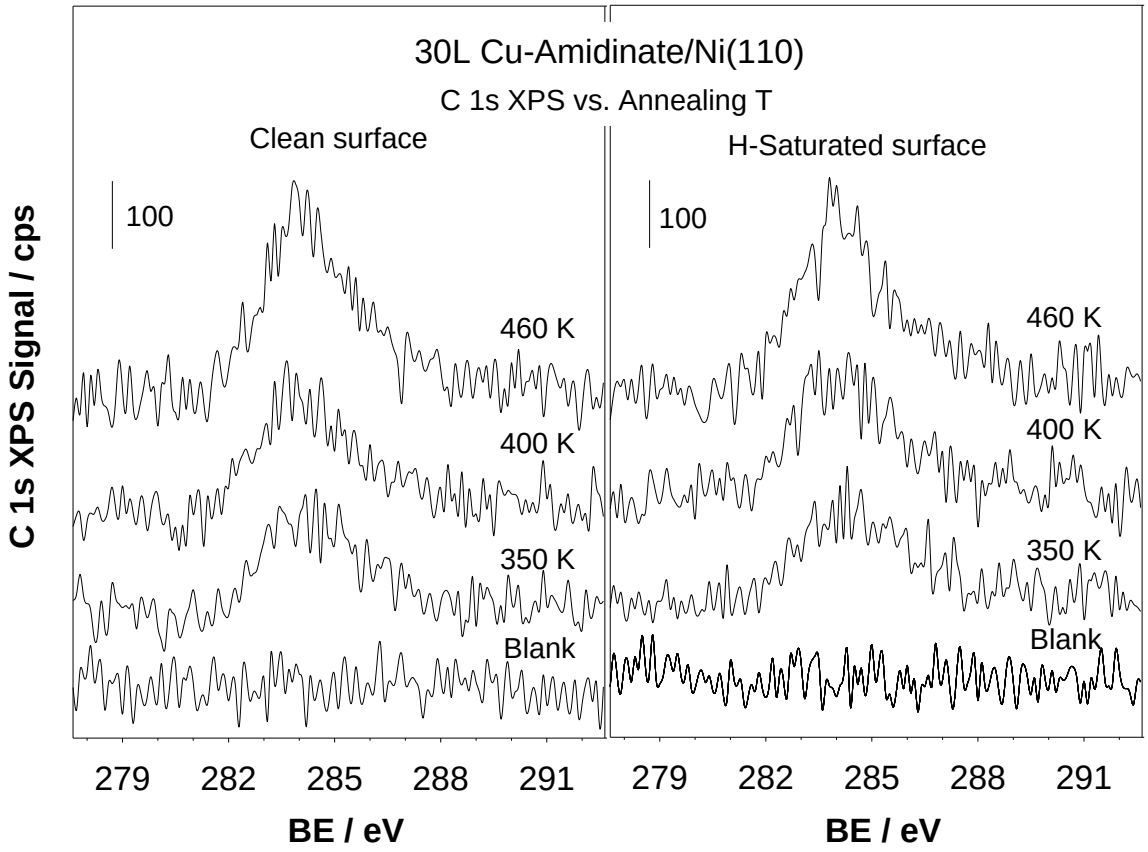

Figure 3.13 C 1s XPS for a Ni (110) single crystal surface dosed with 30.0 L of copper(I)-*N,N'*-di-*sec*-butylacetamidinate as a function of annealing temperature (left panel, clean surface; right panel, H-Saturated surface).

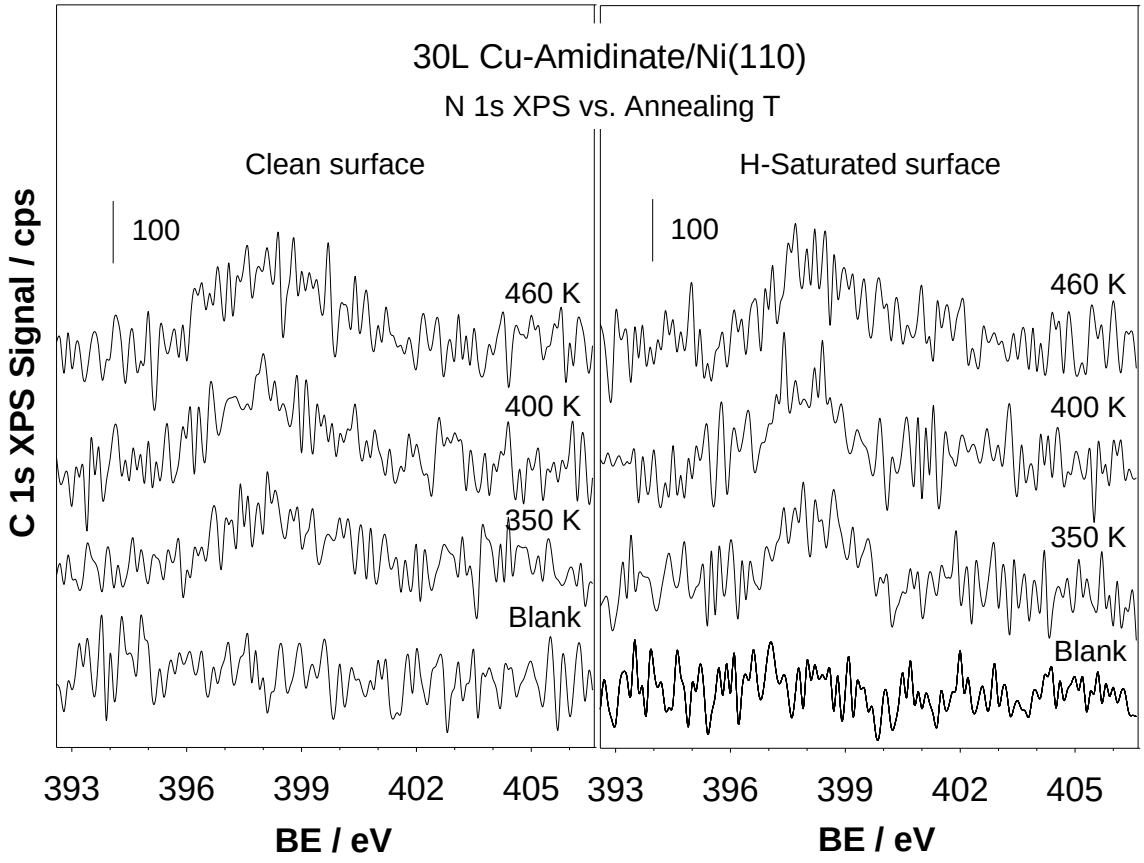

Figure 3.14 N 1s XPS for a Ni (110) single crystal surface dosed with 30.0 L of copper(I)-*N,N'*-di-*sec*-butylacetamidinate as a function of annealing temperature (left panel, clean surface; right panel, H-Saturated surface).

The latter conclusion is quite important, and at first sight surprising given that H_2 has been successfully used as the second reactant in ALD processes with copper acetamidinates [3]. However, our observation can be easily explained by the fact that hydrogen recombination and desorption from metal surfaces typically occurs at low temperatures, lower than those being considered here [7,8]. This is certainly true with Ni (110), where all adsorbed hydrogen desorbs by approximately 350 K as indicated by the H_2 TPD trace from H-saturated Ni (110) shown at the bottom of Figure 3.15. Also shown in that figure are the H_2 TPD data obtained from monolayers of *N,N'*-di-*sec*-butylacetamidine and copper(I)- *N,N'*-di-*sec*-butylacetamidinate for comparison. Note that in those cases the traces extend to higher temperatures, indicating that the surface chemistry of both compounds is complex and involves several dehydrogenation steps. Clean ALD processes aim to avoid the high-temperature reactions implied by the H_2 TPD signals seen here above 400 K, in particular if those lead to the formation of dehydrogenated surface species that cannot removed in the second half-cycle of the ALD process with H_2. More details of surface chemistry of the copper acetamidinate are presented in the next chapter.

3.3. Discussion

The surface-science studies reported in this chapter corroborate and expand on some of

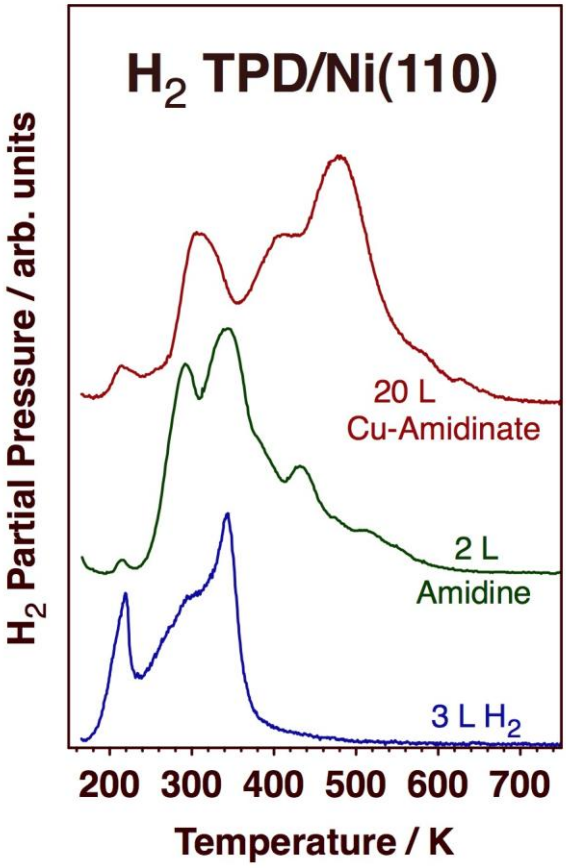

Figure 3.15 H_2 (2 amu) TPD traces from a Ni (110) single-crystal surface dosed with 3.0 L H_2 (bottom trace), 2.0 L di-*sec*-butylacetamidine (middle), and 20.0 L copper(I)-*N*,*N*′-di-*sec*-butylacetamidinate (top), all at 100 K.

the knowledge on the chemistry associated with the deposition of copper films using copper acetamidinates, copper(I)-*N*,*N*-di-*sec*-butylacetamidinate in particular, as precursors. In general, the work reported here attests to the power of using a surface-science approach to look into the details of the surface chemistry involved in ALD processes [9-12]. In this particular case, it was shown that the copper acetamidinate adsorbs dissociatively on nickel surfaces only above approximately 300 K. Moreover, the buildup of a copper-containing monolayer was deemed possible only at temperatures of 350 K or above. These temperatures are slightly lower than the onset of the thermal decomposition of the pure compound [1,2] , indicating that the metal substrate plays a role in promoting adsorption. On the other hand, our value agrees reasonably well with the ~ 390 K threshold reported in ALD experiments [3]. The adsorption is not only dissociative but also activated, since it is faster at higher temperatures. Moreover, the effective sticking probability reflected by the copper uptake is quite high even at 350 K. It appears that ALD processes using copper acetamidinates can, at least in principle, be designed to operate at fairly low temperatures (at least as far as the need to activate the copper precursor is concerned), and to require small copper acetamidinate exposures per cycles (for film deposition on metal substrates).

Perhaps more important is the establishment of an upper limit for the temperatures that

can be used in ALD. The main criterion for this is the need to promote the desired self-limiting dissociative adsorption while avoiding further decomposition and uptake beyond a monolayer coverage. In that regard, our data indicate that, under UHV conditions, some slow decomposition occurs on the surface at temperatures as low as 400 K, and that a fast and continuous copper deposition is achieved by 460 K, well beyond the saturation of the first layer. These temperatures are somewhat lower than those reported in ALD kinetic studies: most ALD-grown Cu films have typically been deposited at temperatures between approximately 425 and 465 K, and significant carbon codeposition (>10%) appears to occur only above 575 K [3].

A number of issues are worth discussing in connection with the apparent discrepancy between the surface-science and ALD experiments. First, the possibility of competing CVD processes taking place during ALD film growth has not been fully ruled out, and is quite likely given the high deposition rates seen on some substrates (see below). In fact, increasing the temperature used in ALD results in the deposition of rougher and less conductive films, an observation suggestive of side reactions associated with nucleation and further copper acetamidinate decomposition. On the other hand, our uptake data in Figure 3.12 indicate reasonably slow CVD-like processes even at 460 K, a competing pathway that could in fact be minimized by minimizing the total copper acetamidinate

dose used per cycle in the ALD process (ideally by reducing the cycle time in well-designed ALD reactors). Next, it is quite possible for the dissociative adsorption and surface decomposition of copper acetamidinate to be slowed down by the competitive adsorption of the carrier gas in ALD applications, a factor not relevant in the UHV environment used for our surface-science studies. Finally, after the deposition of the first layer of the metal, Cu deposition in ALD processes effectively occurs on the growing copper film, not on the original substrate; given the generally mild surface chemistry exhibited by copper [13-15], that is likely to result in slower hydrocarbon decomposition, and therefore a wider temperature window for ALD (The details of copper acetamidinate reacts on copper surface will be investigated in chapter 5). Based on all these points, it can be concluded that, from the point of view of the cleanliness of the surface chemistry of the copper acetamidinate precursor, although low temperatures are preferred in ALD processes, temperatures around 460 K are still acceptable.

From a practical point of view, the high reactivity of the copper acetamidinate precursor on nickel (and presumably other metal) surfaces has important implications in terms of the handling of the compound for its delivery in ALD reactors. As stated in the Experimental Details section, the copper acetamidinate proved quite stable in glass bubblers but decomposed rapidly in bubblers made out of stainless steel. It is easy to

conclude that metal surfaces may aid in the decomposition of the precursor within the gas handling and/or reactor hardware at relatively low temperatures. In fact, the temperatures typically used in ALD bubblers (395 K) are quite close to those reported here for the onset of decomposition on the nickel surface (400 K). The take-home lesson is that an effort must be made to expose the precursor only to non-catalytic surfaces such as glass. Fortunately, there are simple ways to coat stainless steel surfaces with silica, as done regularly on fittings and tubing in gas chromatography in order to avoid the catalytic destruction of the compounds being analyzed. Actually, the above results conflict with some reports [3] that claim that the copper acetamidinate shows faster deposition to form copper films on silica and other oxide surfaces than on metal surfaces. If this is true and the processes are still ALD, it is not easy to explain why the copper acetamidinate is much more stable in glass bubblers than in bubblers made out of stainless steel.

An issue related to that of activation temperatures is that of the deposition rate expected in copper ALD processes. The relevant information from our work on this issue comes from the LEIS data summarized in Figure 3.10. Those experiments do not exactly reproduce the situation encountered in ALD, where a second reactant is used to clean up the surface from the byproducts, but still provide a rough estimate for the expected growth rate. This is so because the film growth rate measured in our LEIS studies is

controlled by the large footprint of the original copper acetamidinate precursor, which limits the density of copper atoms deposited on the first monolayer. After thermal activation of the precursor-saturated monolayer, the conversion of the initial acetamidinate into the final surface species does free some surface sites and makes them available for further Cu deposition, but that occurs afterwards; the new sites can be filled with more copper only in the next deposition cycle.

As long as the rate of the ALD is also determined by the adsorption of the original precursor, the same argument should hold true there as well, and the deposition rate in both cases should be the same. Such analogy provides an estimate for the rate of film growth in pure ALD mode of approximately 0.75Å/cycle. Moreover, because in the experiments in Figure 3.10 the surface was heated to temperatures similar to those in ALD between adsorption cycles, the same organic side species are likely to form on the surface. It is worth remembering that in ALD the surface produced after the first half-cycle is also expected to be covered with a combination of copper and organic surface species. The extra organic species are allegedly removed by H_2 in the second half-cycle of the ALD, but that is not what controls the maximum amount of copper deposited in each cycle; the uptake of the acetamidinate is. According to our data, the fraction of the surface covered by copper in each cycle is constant and determined by the

amount of copper that can be fit in a monolayer by using the copper acetamidinate precursor; the same argument is likely to apply to ALD.

Another difference to consider between the LEIS experiments and ALD processes is that under ALD conditions the adsorption of the precursor is done at higher temperatures, and may therefore be accompanied by partial decomposition. In the case of the copper acetamidinate, one desirable possibility is for one of the two acetamidinate ligands to be hydrogenated as it dissociative bonds to the surface and to desorb as a free acetamidine molecule. In that case, additional sites would be freed during the copper acetamidinate dosing for further copper uptake, and a somewhat higher deposition rate per cycle could be possible. However, this chemistry is not likely to occur, at least on metals, because there are no obvious chemical pathways for the clean elimination of the organic ligands in the copper precursor without the deposition of irreversibly adsorbed moieties. In particular, given that no significant hydrogen from the second half-cycle remains on the surface once the H_2 is pumped away (see below), hydrogenation of the acetamidinate ligands would require surface hydrogen from decomposition of other organic moieties, and that would be likely to deposit other irreversibly adsorbed species, which would end up as impurities in the growing films. If no ligand elimination takes place during the first half-cycle, the metal uptake rate in ALD may be similar to that seen in the LEIS

experiments. The deposition rate value obtained here is certainly within the range reported in many ALD studies [3].

Hydrogen from specific surface groups in non-metallic substrates such as hydroxyl moieties in oxides may aid in promoting the type of hydrogenation reactions mentioned above during the initial stages of deposition. Higher deposition rates may therefore be seen in those types of substrates [3]. They are certainly expected to have a higher density of reactive sites (hydroxyl groups in oxides, for instance), and to facilitate the removal of at least one ligand from the precursor as it dissociatively adsorbs on the surface (the hydroxyl groups may provide the hydrogen needed to hydrogenate acetamidinate ligands to the free acetamidine). If this is the case, there would be fewer bulky ligands left on the adsorbed species, and more space for further copper acetamidinate uptake within a given cycle. However, although such reaction would lead to the existence of more nucleation sites on the initial surface and perhaps to the ability to grow smoother films as a result, it would still not be able to account for faster film growth rates once the surface is covered with the first layer of metallic copper. Consistent high deposition rates, even in this case, are likely to be indicative of a CVD component.

Lastly, we turn our attention to the role of hydrogen in the surface chemistry of Cu ALD

using copper acetamidinates. As indicated above, no significant effect was observed in our surface-science experiments upon dosing of hydrogen before or after the copper acetamidinates on the surface; similar copper deposition rates were measured on the clean versus H-Saturated surfaces in all temperatures ranges (Figure 3.12). The reason for this was traced back to the early desorption of the hydrogen from the surface, which occurs at temperatures below those used for the Cu film growth (Figure 3.15). The potential energy of H_2 adsorption on Ni surface is shown as a function of distance in Figure 3.16. Hydrogen adsorption is non-activated on nickel, whereas desorption is activated, therefore less hydrogen adsorbs at high temperatures. A more comprehensive argument in this respect can be made by using kinetic data available in the literature for hydrogen adsorption and desorption from metal surfaces [8]. Figure 3.17 displays the steady-state H coverage expected on Ni (110) surfaces as a function of both temperature and H_2 pressure estimated from such kinetic data. It can be clearly seen that increasing temperatures and/or decreasing pressures result in a decrease in steady-state hydrogen surface coverage, and that, in the temperature regime of interest (400 - 600 K), significant H surface coverage can only be maintained under H_2 pressures above approximately 10^{-6} bar. Our calculations rely on kinetic parameters measured under UHV conditions, but recent in-situ coverage measurements under atmospheric pressures have confirmed their validity [16]. It is also worth pointing out that the results reported here

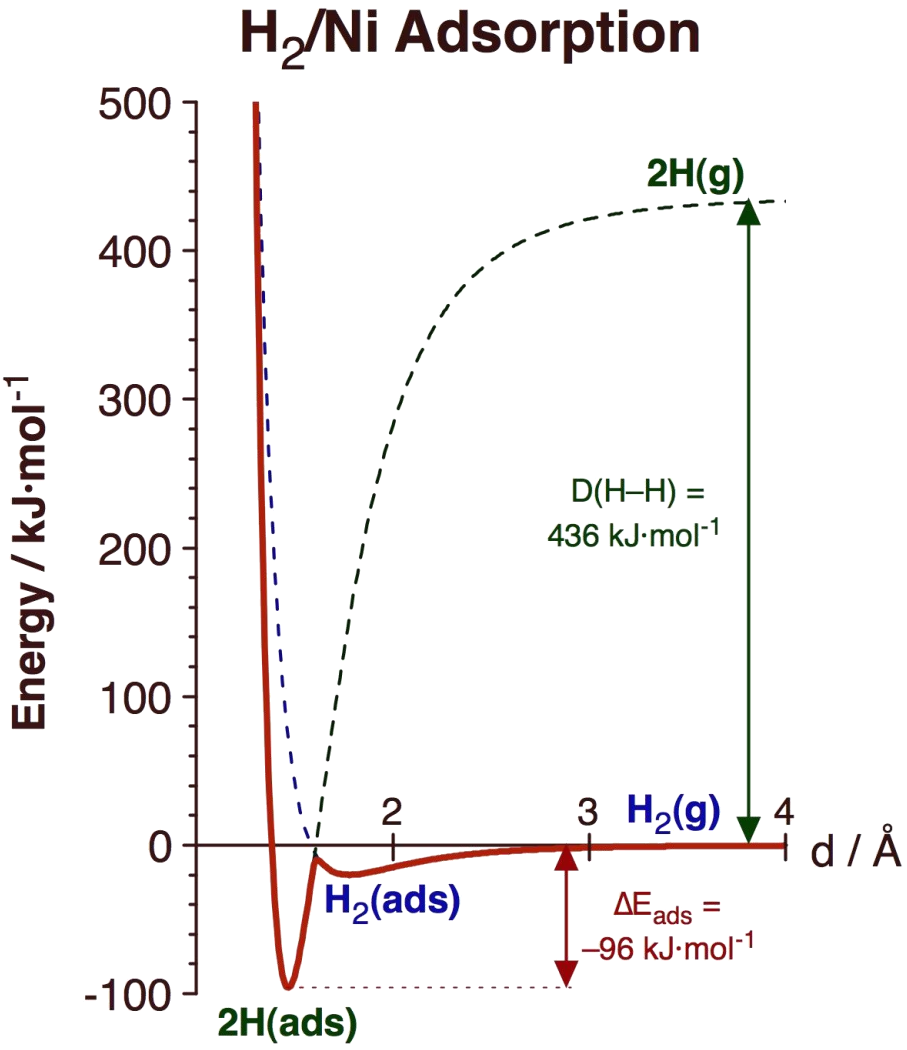

Figure 3.16 Potential energy plot for H_2 adsorption on Ni surfaces.

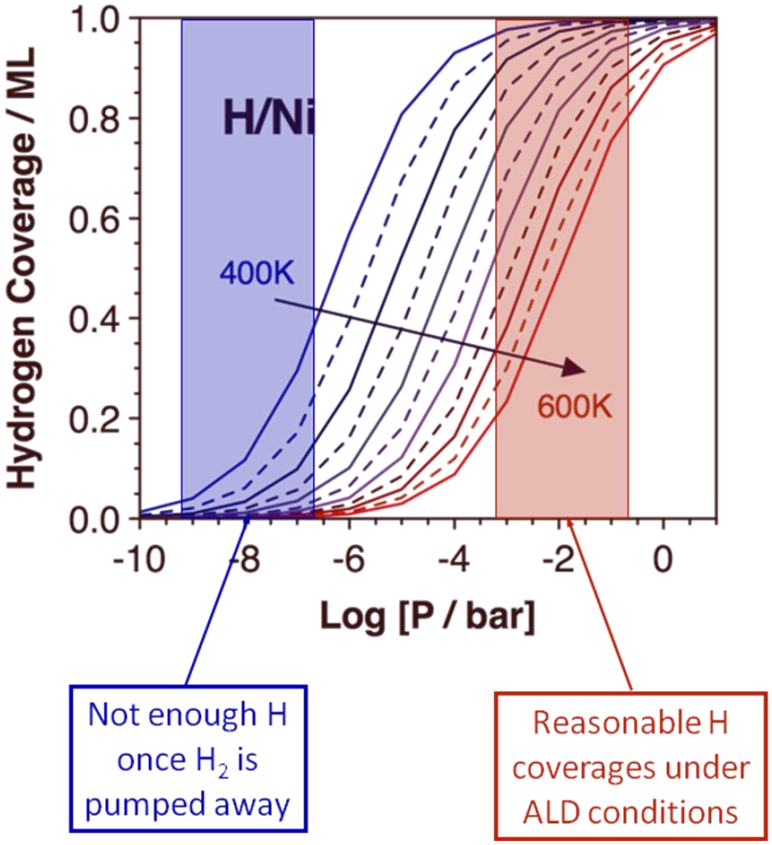

Figure 3.17 Estimated steady-state hydrogen surface coverage on Ni (110) as a function of hydrogen pressure and surface temperature, as calculated using adsorption and desorption parameters from the literature.

for nickel are quite representative of the chemistry that takes place on most transition metals, and that the kinetic parameters for hydrogen adsorption on cobalt, a substrate of interest in the microelectronic industry [17,18], are almost identical to those on nickel.

The implication from the fast and reversible nature of hydrogen adsorption on transition metal surfaces is that any adsorbed hydrogen generated by exposure of the substrate to H_2 in the second half-cycle of the copper acetamidinate + H_2 ALD cycles is rapidly lost upon pumping or flushing of that gas. Consequently, any organic intermediates formed on the surface upon activated adsorption of copper acetamidinate need to be sufficiently stable under the temperatures used for ALD to survive the purging typically done in between half-cycles so they can be hydrogenated once the hydrogen gas is introduced in the system. Otherwise, they are likely to dehydrogenate and form irreversible adsorbates, and ultimately incorporate carbon and/or nitrogen impurities in the growing films. Both the temperatures used for ALD and the nature of the copper acetamidinate (or any other organometallic precursor used in ALD processes based on reduction with H_2) need to be tuned to fulfill this requirement.

3.4. Conclusions

The adsorption and thermal activation of copper(I)-*N,N'*-di-*sec*-butylacetamidinate on Ni

(110) single crystal surfaces was studied under ultrahigh vacuum conditions by using a combination of X-ray photoelectron spectroscopy and low-energy ion scattering. Two adsorption modes were identified, molecular at low temperatures, and dissociative above 300 K. The latter is activated, and leads to the reduction of the copper atoms directly from Cu(I) to a metallic copper state. Monolayer saturation is seen when the deposition is carried out at 350 K, but some additional decomposition and copper deposition is seen over time at temperatures as low as 400 K, and almost a linear dependence of copper growth on exposure is observed by 460 K.

Because of the large footprint of the original adsorbed copper acetamidinate, the maximum uptake of copper atoms per cycle in ALD is limited by the initial dissociative adsorption of the precursor, even if its subsequent thermal treatment on the surface leads to the opening of some additional sites (presumably via the desorption of some organic byproducts). It was determined that approximately three cycles of low-temperature surface saturation and annealing are needed to reach a monolayer coverage of copper on the surface, the equivalent of a film growth rate of ~ 0.75 Å/cycle. It is likely for similar growth to define pure ALD processes, and that significantly larger values would be a reflection of additional CVD.

Finally, it was established that, under the conditions of these experiments, dosing of hydrogen either before or after the copper acetamidinates on the Ni does not result in any significant changes in the deposition of copper via copper acetamidinate dissociative adsorption. The absence of any effect here was ascribed to the low temperatures needed for hydrogen desorption (≤ 350 K), below those temperatures typically used in ALD processes. Based on calculations using published kinetic parameters, it was determined that significant steady-state hydrogen surface coverage above ~ 400 K is possible only under pressures of gas-phase hydrogen above approximately 10^{-6} bar. This suggests that the organic intermediates that may form on the surface upon thermal activation of adsorbed copper acetamidinate need to be stable at the temperatures used in ALD in order to be available for hydrogenation and removal from the surface in the second half-cycle rather than decomposing and incorporating as impurities in the growing films.

3.5. References

[1] B. S. Lim, A. Rahtu, J. –S. Park, R. G. Gordon, *Inorganic Chemistry.* **2003**, *42,* 7951.

[2] Z. Li, S. T. Barry, R. G. Gordon, *Inorganic Chemistry*. **2005**, *44*, 1728.

[3] Z. Li, A. Rahtu, R. G. Gordon, *Journal of the Electrochemical Society.* **2006**, *153,* C787.

[4] C. D. Wagner, W. M. Riggs, L. E. Davis, J. F. Moulder, G. E. Muilenberg, G. E., *Handbook of X-Ray Photoelectron Spectroscopy,* Perkin-Elmer Corp.: Eden Prairie, MN, **1978.**

[5] C. Pereira, S. Patricio, A. R. Silva, A. L. Magalhaes, A. P. Carvalho, J. Pires, C. J. Freire, *Colloid Interface Sci.* **2007**, *316,* 570.

[6] D. Briggs, *Handbook of X-ray and Ultraviolet Photoelectron Spectroscopy*, Heyden: London, **1978**.

[7] G. A. Somorjai, *Chemistry in Two Dimensions: Surfaces*, Cornell University Press: Ithaca, NY, **1981**.

[8] K. Christmann, O. Schober, G. Ertl, M. Neumann, *J. Chem. Phys.* **1974**, *60*, 4528.

[9] F. Zaera, *J. Mater. Chem*. **2008**, *18*, 3521.

[10] M. Xu, H. Tiznado, B. –C. Kang, M. Bouman, I. Lee, F. Zaera, *J. Korean Phys. Soc.* **2007**, *51*, 1063.

[11] H. Tiznado, M. Bouman, B. –C. Kang, I. Lee, F. Zaera, *J. Mol. Catal. A,* **2008**, *281,*

35.

[12] B. –C. Kang, J. –H. Boo, I. Lee, F. Zaera, *J. Phys. Chem. A*, **200**9, *113*, 3946.

[13] Z. Ma, F. Zaera, *Surface Science Reports*, **2006**, *61*, 229.

[14] F. Zaera, F. *Chem. Rev.* **1995**, *95*, 2651.

[15] B. E. Bent, *Chem. Rev.* **1996**, *96*, 1361.

[16] M. Johansson, O. Lytken, I. Chorkendorff, *J. Chem. Phys*. **2008**, *128*, 034706.

[17] P. Singer, *Semicond. Int.* **2004**, *27*, 40.

[18] Z. Li, R. G. Gordon, D. B. Farmer, Y. Lin, J. Vlassak, *Electrochemical and Solid-State Letters*. **2005**, *8*, G182.

CHAPTER FOUR

Surface Chemistry of the Copper Acetamidinate ALD Precursor on Nickel Surfaces

4.1. Introduction

In the previous chapter, the uptake and hydrogen coadsorption effect of copper(I)-*N,N'*-di-*sec*-butylacetamidinate on Ni (110) single crystal surface were investigated. The results from that work show that the uptake was self-limited at 350 K and became CVD style while the surfaces were hotter than 400 K. The copper acetamidinate directly convert from Cu(I) to metallic copper. It takes three cycles of low-temperature surface saturation and annealing to reach one monolayer coverage of copper on the surface, the equivalent of a film growth rate of ~ 0.75 Å/cycle. The effect of coadsorption of hydrogen on the surface is not appreciable because under UHV no enough hydrogen retained at 350 K and above.

Further research was carried out to unveil the chemical mechanism of the conversion of the copper acetamidinate and the source of impurities observed in the deposited films. In this chapter we report results from XPS and TPD studies on the surface chemistry of

copper(I)-*N,N'*-di-*sec*-butylacetamidinate on (110) oriented nickel surfaces. Experiments in the presence of preadsorbed hydrogen were carried out in order to study possible hydrogenation reactions on the surface at different temperatures. It is shown here that, with copper(I)-*N,N'*-di-*sec*-butylacetamidinate, molecular desorption happens around 215 K. Decomposition of some of the monolayer release the amidine ligand which adsorbs on the surfaces and reacts to produce several by-products. At 300 K, a small amidine (^{s}But-NH-C(CH_3)=NH) is formed and desorbs from the surfaces. 2-butene is also produced at 480 K via β-hydride elimination. Some carbon species are retained on the surface even after the surface is heated to 800 K, the likely source for the impurities that incorporate into the copper film. No detectable changes in surface chemistry were observed upon presaturation of the substrate with hydrogen.

4.2. Results

4.2.1. XPS

The thermal chemistry of copper(I)-*N,N'*-di-*sec*-butylacetamidinate on clean Ni (110) surface was first surveyed by XPS. The main frames of Figures 4.1 and 4.2 display the XPS spectra obtained after dosing50.0 L Cu-Amidinate on the Ni (110) surface at 90 K and after annealing temperatures at 150, 200, 250, 300, 400, 500, 600, 700, and 800 K.

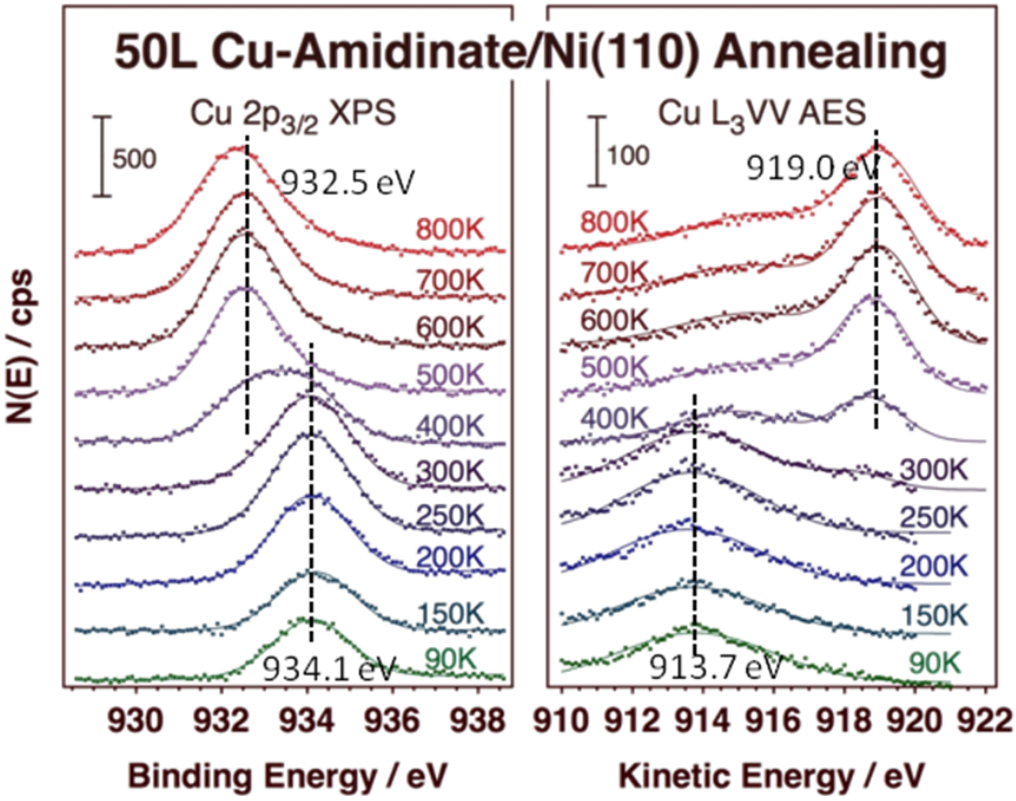

Figure 4.1 Cu $2p_{3/2}$ and AES data from 50.0 L copper acetamidinate on clean Ni (110), after dosing at 90 K and after annealing to 150, 200, 250, 300, 400, 500, 600, 700 and 800 K.

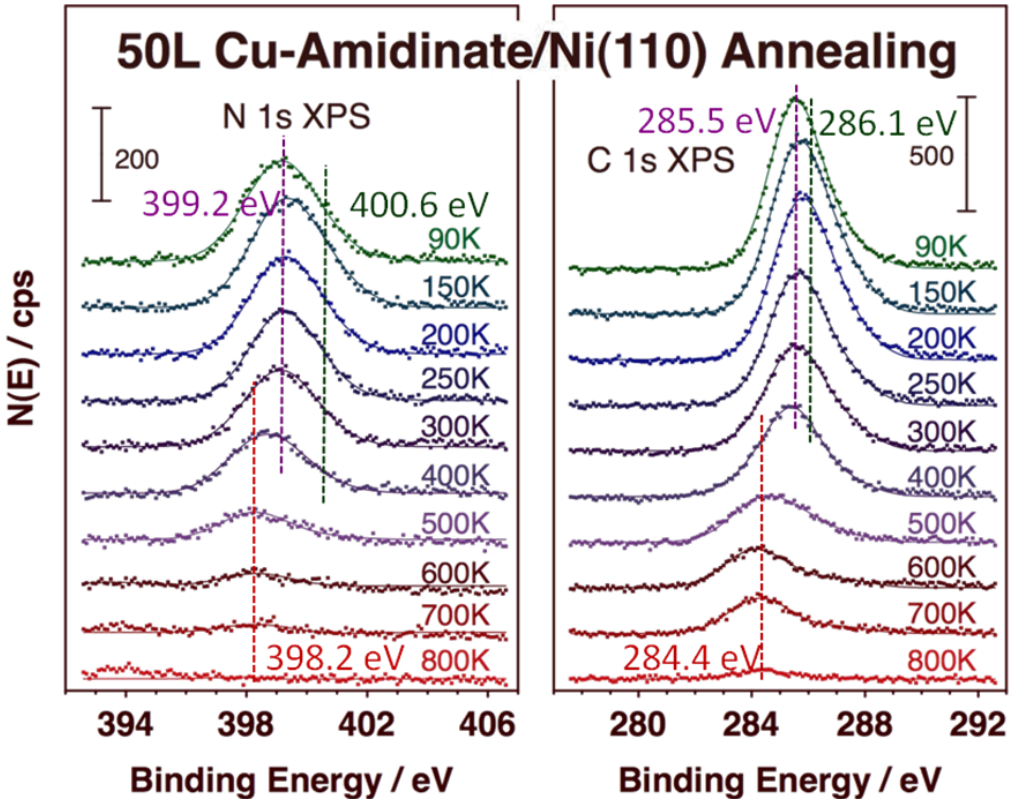

Figure 4.2 N 1s and C 1s data from 50.0 L copper acetamidinate on clean Ni (110), after dosing at 90 K and after annealing to 150, 200, 250, 300, 400, 500, 600, 700 and 800 K.

The left panel of Figure 4.1 corresponds to the Cu $2p_{3/2}$ data. The XPS data look quite similar from 90 K to 300 K, which a peak position at 934.1 eV; that can be assigned to a Cu(I) species [1]. The main change is seen between 300 K and 500 K: two chemical states are seen at 400 K, at 834.1 and 932.5 eV, which are indicated with copper bonded to the ligand and metallic copper atom respectively. Above 500 K, the peaks intensities and positions remain the same, with one peak centered at 932.5 eV, typical of metallic copper [1].

The right panel of Figure 4.1 reports the Cu L_3VV AES data. Those data display the same trend as the Cu $2p_{3/2}$ data: They remain the same from 90 K to 300 K, with a peaks position at 913.7 eV, assigned to the Cu(I) species [2]. Again, two chemical states are seen at 400 K, the second peak appearing at 919.0 eV, a value typical of metallic copper [2]. No further changes are seen. Combining the AES and XPS data, a firm conclusion can be drawn that the copper acetamidinate decomposes on the Ni (110) single crystal surface directly from a Cu(I) molecular species to Cu(0) metal even when no hydrogen provided; no other chemical state of Cu is observed in the temperature range from 90 to 800 K. This result is different from that in previous reports, that it has been claimed Cu(II) species form during the copper acetamidinate decomposition [3,4].

With regard to the N 1s XPS data (Figure 4.2, left panel), no changes are seen from 90 to 200 K, with peaks at 400.6 and 399.2 eV. Between 200 and 250 K, the total peak intensity decreases a little because of some molecular desorption. Between 250 and 300 K, the peak intensity decreases further, but the peak positions are almost the same. Between 300 and 500 K, the peak intensity decreases but now the peaks position also shift down to 398.2 eV, indicating some decomposition. Further annealing leads to further decreases in peaks intensity, and no nitrogen-containing species are left on the surface after 800 K.

The C 1s data (Figure 4.2, right panel), shows almost, but not quite, the same behavior. Two peaks are seen at 286.1 and 285.5 eV between 90 and 200 K, the peak intensities decrease a little between 200 and 250 K. This matches the TPD data, where some molecular desorption is seen around 215 K (shown later). Between 250 and 300 K, the peak intensity continues to decrease, and between 300 and 600 K, the peak intensities decreases and the position shifts down to 284.4 eV. This indicates some desorption of by-products. Between 600 K and 700 K, both the intensity and position of the remaining C 1s peak remain the same; no further reaction occurs in that temperature range. Above 700 K, additional carbon loss is seen.

From Figure 4.2, at least three temperature regimes can be identified where the signals for carbon and nitrogen change. Those are slightly dephased, however. The data from Figures 4.1 and 4.2 in the form of the areas of each peak, are summarized in Figure 4.3. Three or four regions are observed. Molecular desorption is seen at around 250 K, then the nitrogen and carbon signals decrease following the decomposition of the Cu(I) species. New surface nitrogen and carbon species are formed as the copper metal film is deposited on the Ni (110) surface at temperatures above 400 K.

4.2.2. TPD

The XPS data shows that the copper acetamidinate decomposes on the Ni (110) single crystal surface as the surface temperature is increased, producing several by-products in addition to copper metal. To unveil the mechanism of this process, TPD data was also acquired. Copper acetamidinate was dosed on the Ni (110) surface at 90 K at different exposures: 0.5, 1.0, 2.0, 6.0, 10.0, 15.0, and 20.0 L. signal intensities were collected for 2, 39, 41, 42, 43, 54, 56, 57, 58, 70, 71, 72, 112, 114, 154, 155, and 170 amu. The signal for 56 amu, which corresponds to 2-butene formation, is drawn in Figure 4.4 and that for 114 amu, originating from a new small amidine, ^{s}But–NH–C(CH_3)=NH_2, is drawn in Figure 4.5.

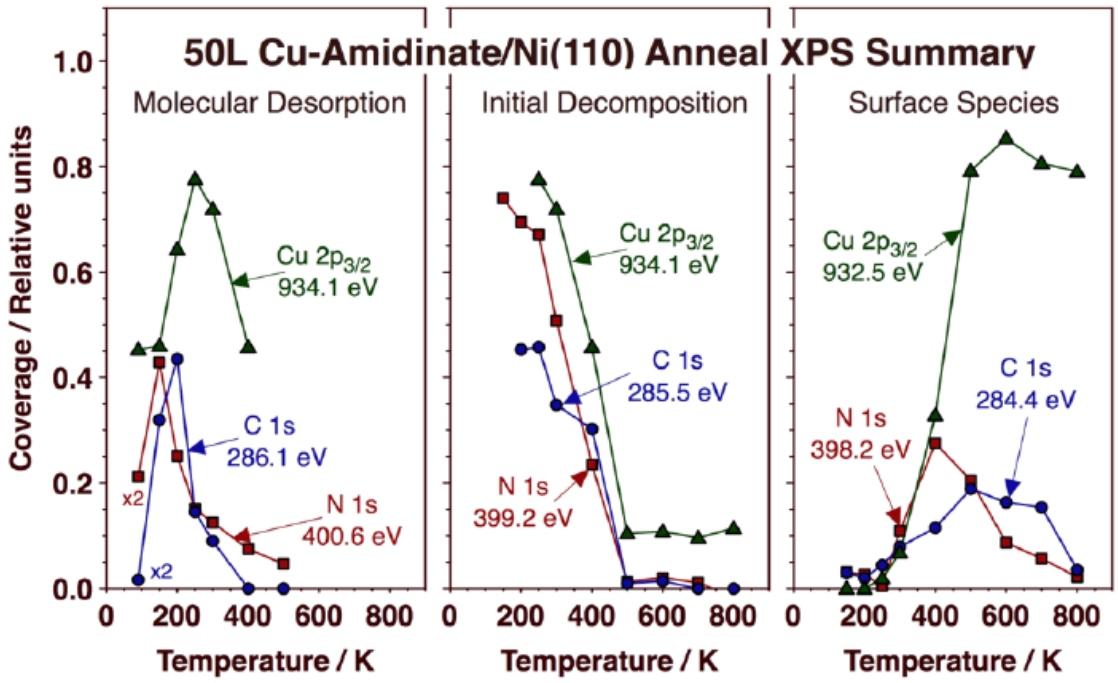

Figure 4.3 Summary of integrated XPS peaks areas from the data in Figure 4.1 and 4.2 versus surface temperature.

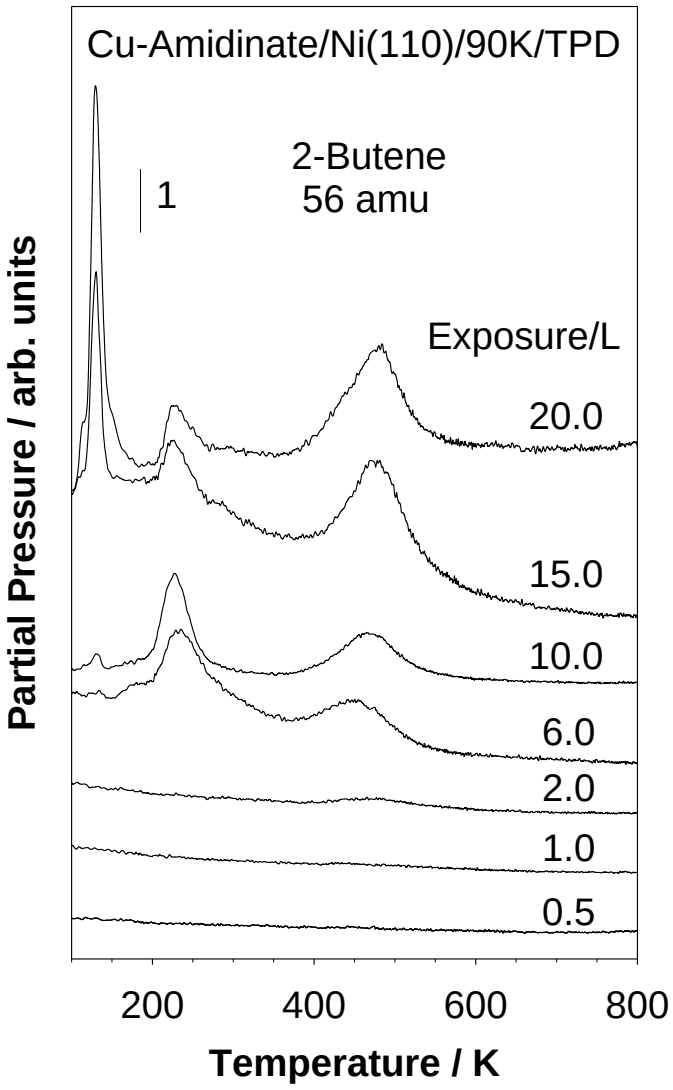

Figure 4.4 2-butnen TPD from copper acetamidinate decomposition on clean Ni (110) surface as a function of exposure.

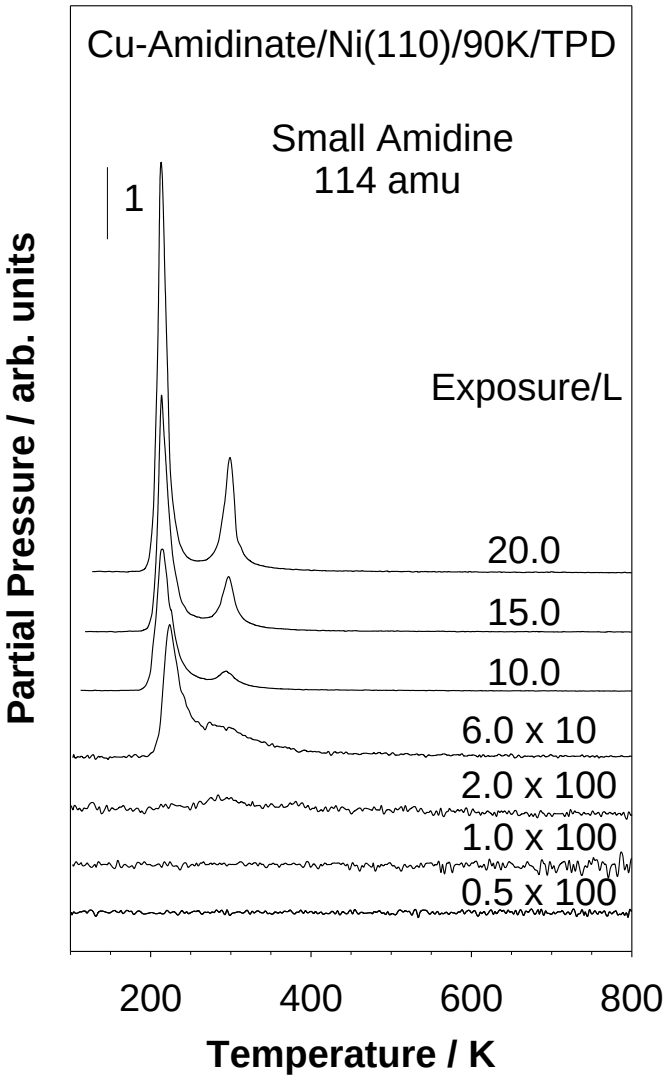

Figure 4.5 Small amidine TPD from copper acetamidinate decomposition on clean Ni (110) surface as a function of exposure.

In Figure 4.4, for exposure less than 2.0 L, there is almost no signal, but when the exposure is increased to 6.0 L, two dominant peaks appear at around 215 and 480 K. Both of those peaks increase in size while increasing the dose up to 15 L, but then they saturate and a third desorption peak appears at around 140 K, which comes from cracking of the multilayer molecular desorption. The 215 amu peak is assigned to cracking from monolayer molecular desorption, as corroborated by TPD data for mass numbers above 200 amu (such as 218 amu). Desorption of the amidine ligand was ruled out by checking on the signal for 170 amu. The 480 K is identified with one of the decomposition products of copper acetamidinate, 2-butene.

Some intensity was detected for the TPD of 114 amu, but the intensity there was too weak to be used for the identification of products. Several experiments were carried out and added together to overcome the problem. In additional to the peak at 215K, one new peak is observed at around 300 K (Figure 4.5). Similar as in the TPD of 2-butene, the 114 amu TPD displays no signal for exposure less than 2.0 L, and two peaks at around 215 and 300 K starting at 6.0 L. Both of the peaks increase in intensity with increased dosing size. The 215 peak is assigned to the cracking of the monolayer molecular desorption, as in Figure 4.4. The 300 K is a new feature, presumably from a new decomposition product of copper acetamidinate.

114 amu matches the molar mass of ^{s}But-NH-C(CH_3)=NH, a small amidine that may form after the original ligand losses one butene molecule. To make sure that the 300 K peak in the 114 amu TPD is from this new product, further TPDs were carried out for additional masses. Figure 4.6, shows a comparison of peak intensities at 215 and 300 K for 112, 114, 154, 155, and 170 amu after a 20.0 L exposure of copper acetamidinate on the Ni (110) surface. It can be seen there that the 112 and 114 amu traces do not follow the expected ratios with 154, 155 and 170 amu for molecular desorption, the later almost having no intensity at 300 K. Therefore, it is concluded that the 300 K peak does not come from the cracking of the original copper acetamidinate. Combined with the information obtained from experiments with 6 L exposure of acetamidine on the Ni (110) surface shown in Figure 4.7 (where it is shown that the 113, 114 and 170 amu TPD peaks also have no intensity at 300 K), the formation of the smaller amidine is corroborated.

Based on our experimental data, the following reaction mechanism is proposed: the copper acetamidinate adsorbs on the Ni surface at lower temperatures, but decomposes while heating the surface. The acetamidine ligand decomposes to form butyl and the –N(^{s}But)-C(CH_3)=N– fragments. The butyl moiety then dehydrogenates to form 2-butene while the –N(^{s}But)-C(CH_3)=N– fragment hydrogenates to form ^{s}But-NH-C(CH_3)=NH. The summary of the TPD information is provided in Figure 4.8 for 20 L exposure of

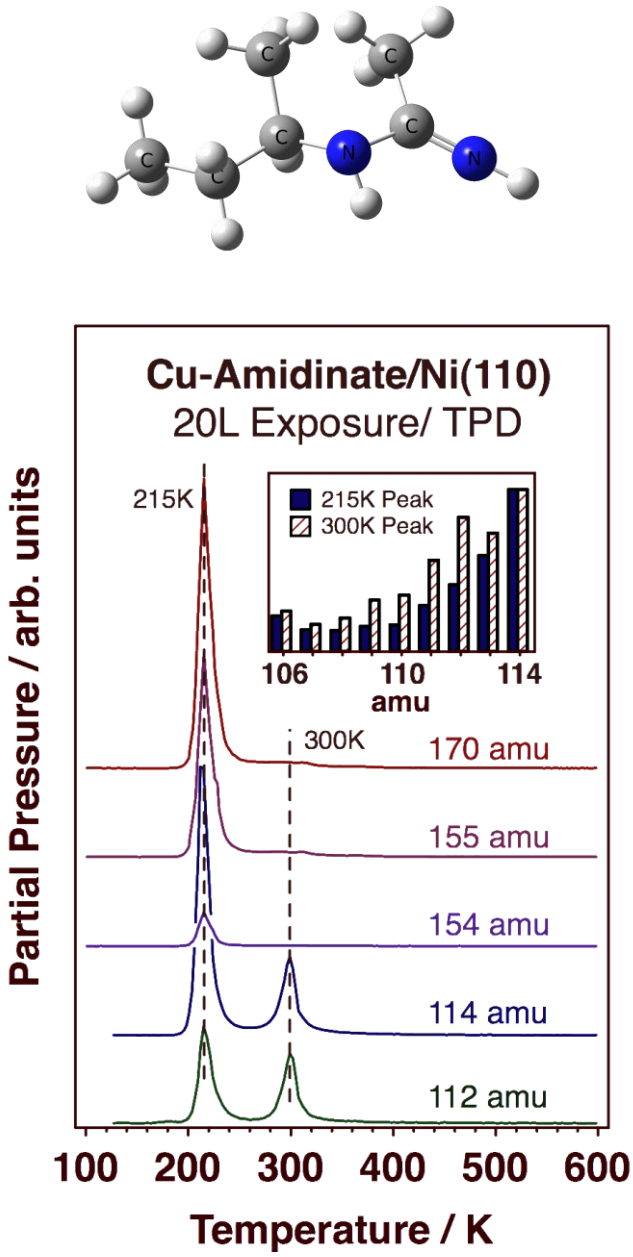

Figure 4.6 Small amidine (^{s}But–NH–C(CH_3)=NH_2) structure (top), and relative intensities for the signals for 112, 114, 154, 155 and 170 amu in the peaks at 215 and 300 K after 20 L exposure of copper acetamidinate on Ni (110).

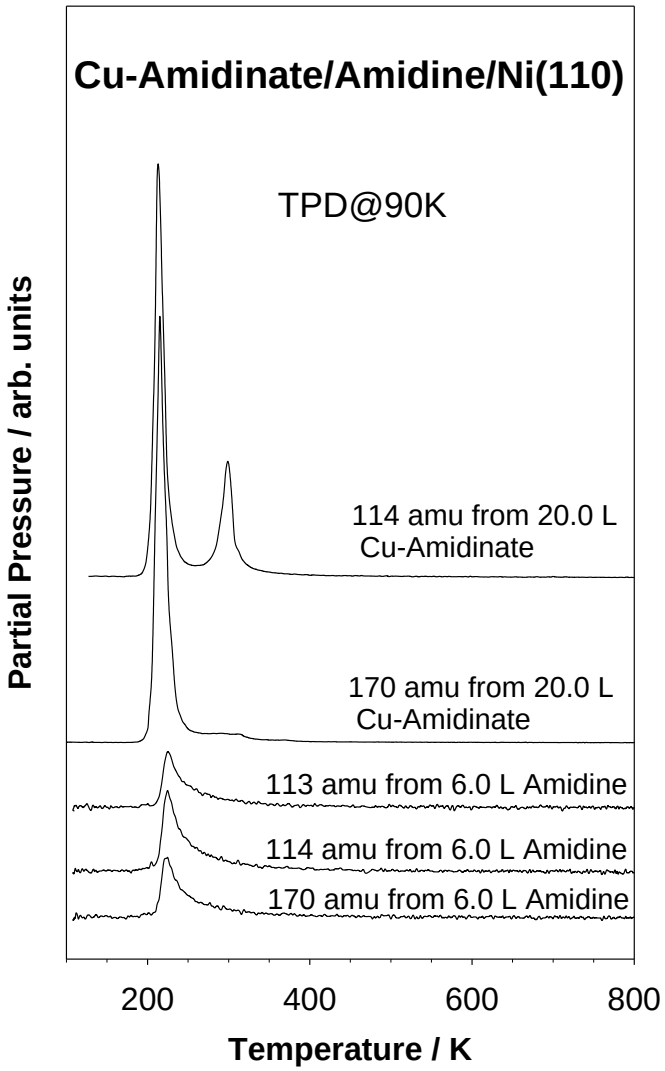

Figure 4.7 114 and 170 amu TPD from 20 L of copper acetamidinate on Ni (110), and 113, 114, 170 amu TPD from 6.0 L amidine on Ni (110).

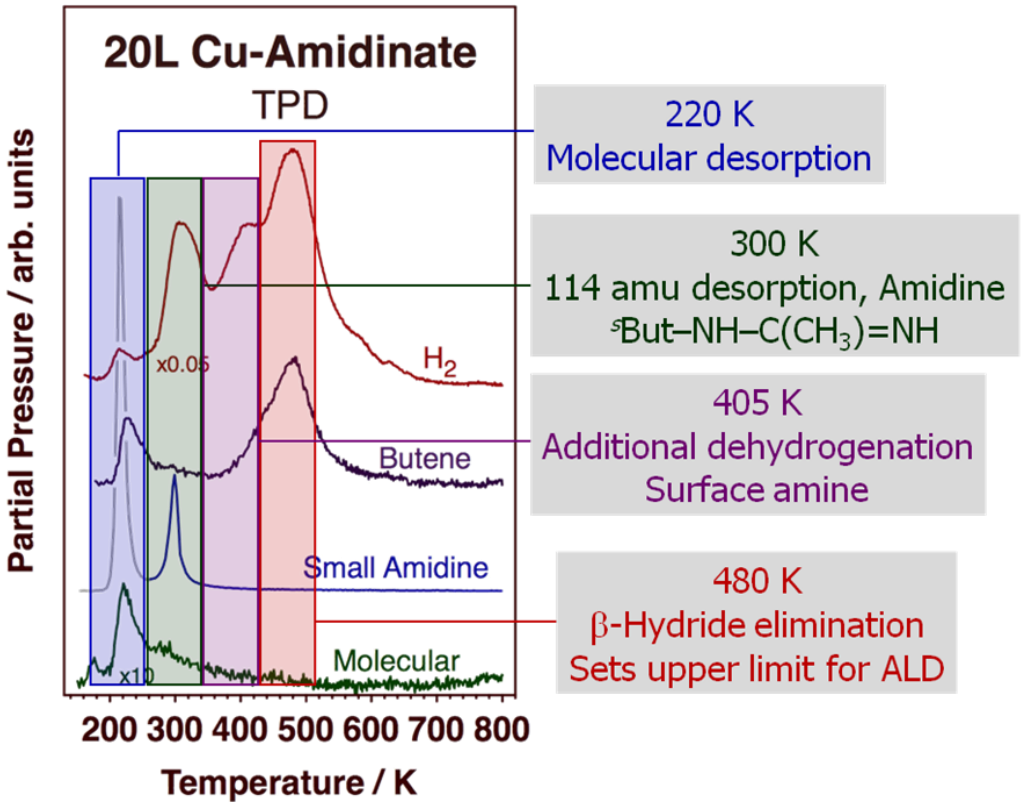

Figure 4.8 TPD from 20 L of copper acetamidinate on Ni (110).

copper acetamidinate on the Ni (110) single crystal surface. Except for hydrogen, two products were identified, the small amidine, that desorbs at 300 K, and 2-butene, which desorbs at 480 K. Molecular desorption happens at 215 K. The hydrogen TPD trace indicates that there is an additional peak at 405 K, due to further dehydrogenation, from products not identified by our experiment.

4.2.3. Experiments with Coadsorbed Hydrogen

In the previous chapter, presaturation the Ni (110) surface with hydrogen was investigated by XPS and LEIS at relatively lower temperature to investigate the effect that hydrogen causes on the decomposition of copper acetamidinate. In this chapter, the hydrogen was preadsorbed on the Ni (110) surface at 90 K. Then XPS and TPD were used to identify any differences in chemistry compared with the clean surface. Experiments similar to those reported in section 4.2.1 were carried out. The main frame of Figure 4.9 displays the XPS spectra obtained after 50.0 L copper acetamidinate was dosed on the Ni (110) surface previously saturated with hydrogen at 90 K. That surface was then annealed at 90, 150, 200, 250, 300, 400, 500, 600, 700, and 800 K.

From left to right, XPS data are shown for C 1s, N 1s , Ni $2p_{3/2}$, and Cu $2p_{3/2}$ features. The Cu $2p_{3/2}$ data was also deconvoluted, to better identify their different peaks. For

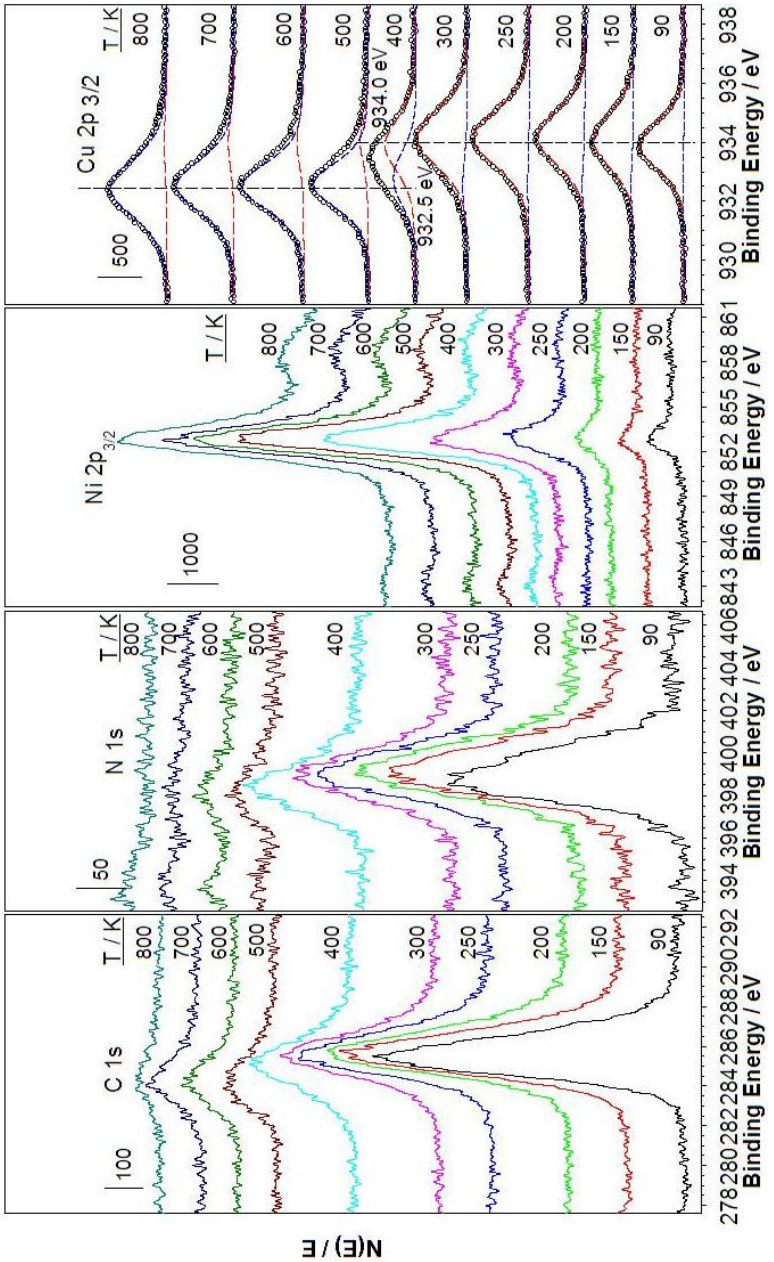

Figure 4.9 C 1s, N 1s, Ni $2p_{3/2}$ and Cu $2p_{3/2}$ XPS from 50.0 L copper acetamidinate dosed on a Ni (110) surface previously saturated with hydrogen at 90 K as a function of temperature.

comparison, a similar set of XPS data acquired on the clean Ni (110) is displayed in Figure 4.10. In the case of the XPS for Cu $2p_{3/2}$, both two sets of data display peaks with binding energies at 934.1 eV for the Cu(I) species [1] at lower temperature. One clear transition happens at 400 K, where two chemical states are seen in the deconvolution, for the copper (I) species and metallic copper (at 934.1 and 932.5 eV, respectively). The copper acetamidinate is totally converted to metallic copper after heating above 400 K, at which point the binding energy shifts down to 932.5 eV [1]. No other cooper chemical state is observed regardless of the presence or absence of presaturated hydrogen on the Ni (110) surface.

Comparing the XPS data for C 1s, N 1s and Ni $2p_{3/2}$ panels with versus without predosed hydrogen, not only the peaks shapes, but also their intensities and their positions match each other. No significant changes are apparent from these data. It appears that, at least under vacuum, preadsorption of hydrogen does not lead to any appreciable changes in the surface chemistry of copper acetamidinates.

The conclusion from this work is quite important to ALD processes with copper acetamidinates, and is different from that in other report [5]. As explained in the previous chapter, hydrogen recombination and desorption from the metal surfaces typically occurs

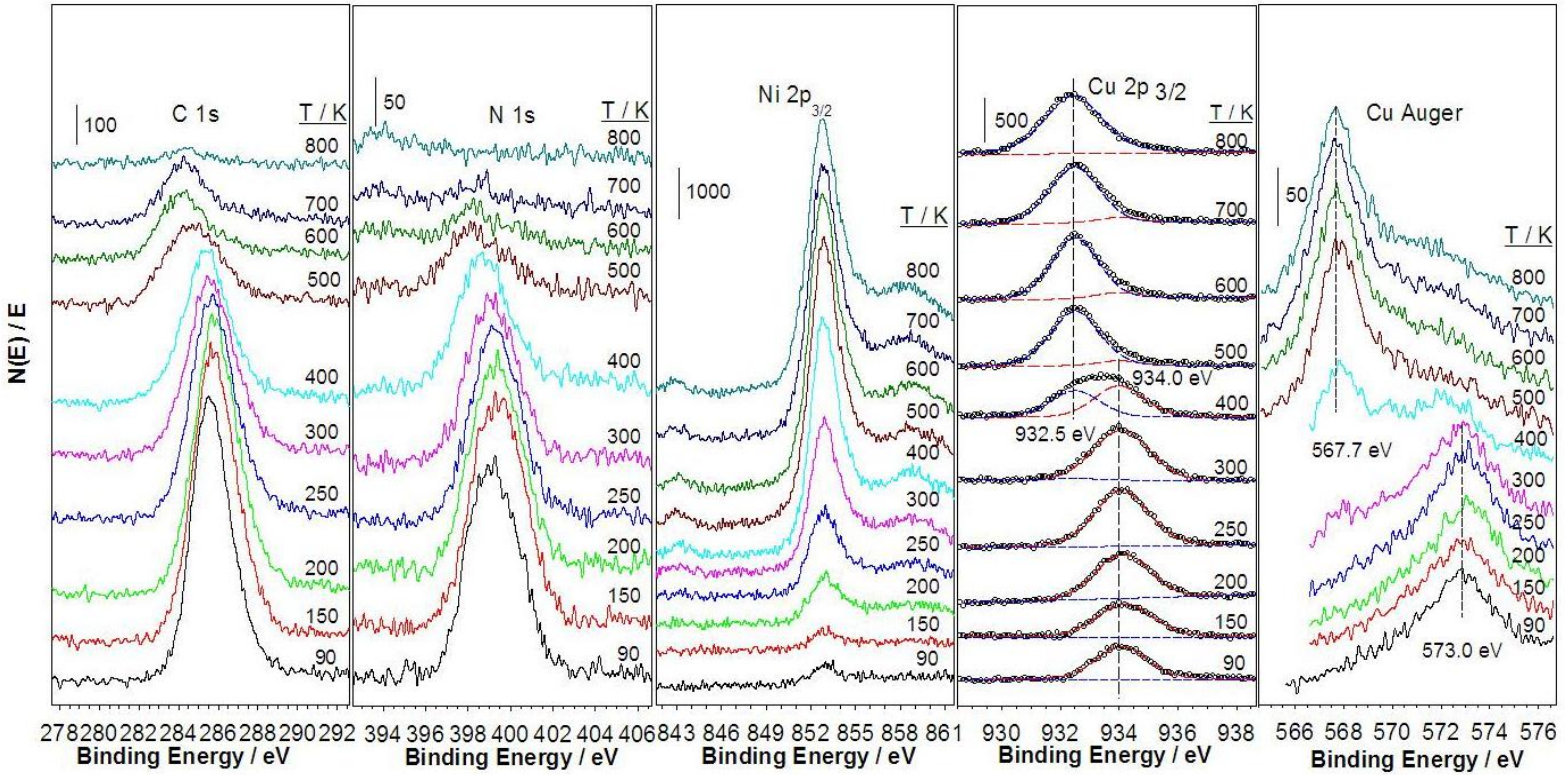

Figure 4.10 C 1s, N 1s, Ni $2p_{3/2}$ and Cu $2p_{3/2}$ XPS and Cu AES from 50.0 L copper acetamidinate dosed on a Ni (110), at 90 K and after annealing to the indicated temperatures.

at low temperatures, lower than those at which copper acetamidinates begin to react on the surface [6,7].

4.3. Discussion

By combining TPD and XPS results from studies on copper acetamidinate adsorbed on Ni (110), the following reaction mechanism was proposed: copper acetamidinate adsorbs on the Ni (110) surface at lower temperatures, and the Cu-N bonds are broken only upon heating the surface above 300K. The N atom may then bind directly to the nickel metal surface. Further chemistry follows, where one of the hydrogen atom is transferred from *sec*-butyl group to a N atom in a β–H elimination step. A N-C bond breaks, and di-σ 2,3-butene fragments (CH_3-CH(Ni)-CH(Ni)-CH_3) and –N(^{s}But)-C(CH_3)=N– fragments from on the nickel surface. The di-σ butene then desorbs at around 480 K.

In order to check on the role of butyl intermediates in the production of the 2-butene, additional TPD experiments were done with 2-iodobutane on the Ni (110) surface. No butene is produced at lower butane, 3 L; only some butane is desorption observed (58 amu). However, after a 4 L dose, the desorption of butene (56 amu) is indeed observed (Figure 4.11). The desorption temperature of butane is lower than that of butene, but both of them desorbed by 300 K. Given that the desorption temperature of the butene seen

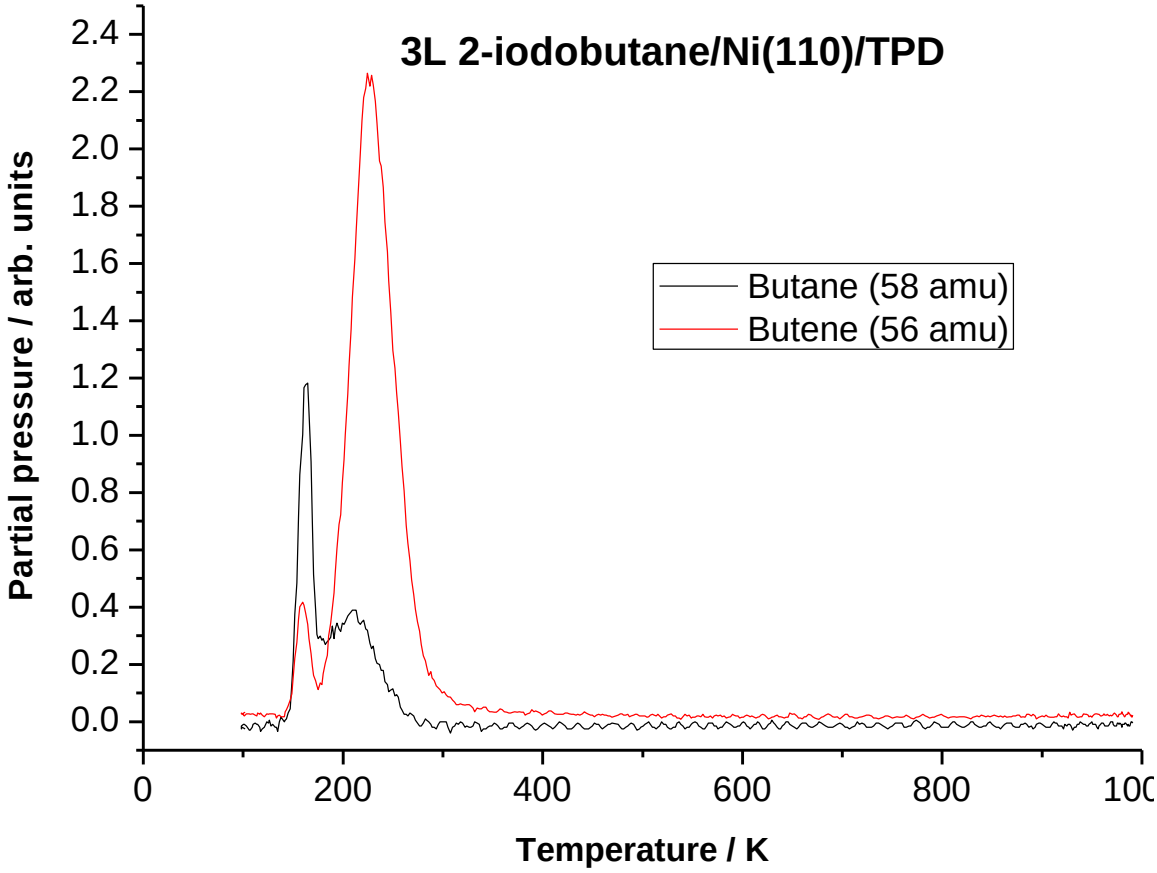

Figure 4.11 56 and 58 amu TPD from 2-iodobutane dosed on Ni (110).

from copper acetamidinate decomposition is much higher (480K), is concluded that, the butene desorption in that case is reaction limit; the butene desorbs immediately after being produced. Since no butane was observed during the TPD of copper acetamidinate, It is concluded that at high temperature the butyl fragment prefers to undergo dehydrogenation on the Ni (110) surface, and that the extra hydrogen is consumed to produce the smaller amidine by-product.

Given that butene desorbs at around 480 K, a temperature higher than that reported for copper acetamidinate ALD conversion in past references (150 ~190 ℃) [5,8-11]. It is inferred that some organic fragments form and adsorb on the Ni (110) surface in between. Most ALD-grown Cu films are deposited at temperatures between approximately 425 and 465 K, and in this temperature range, the carbon codeposition is about 1%.[5]. The reason for those deposits of carbon impurities could therefore be the deposited copper atoms may bury some hydrocarbon fragment into the film. On the other hand, the –N(^{s}But)-C(CH_3)=N– moiety hydrogenates to form ^{s}But-NH-C(CH_3)=NH (the small amidine, identified by the 114 amu signal) and desorbs at around 300 K, below the ALD reaction temperatures. This is the reason why no nitrogen has been detected in the films[5].

As discussed above, the small amidine (^{s}But-NH-C(CH_3)=NH) is another product of the copper acetamidinates decomposition on the Ni (110) surface. The supporting evidence for this was provided by the results in Figures 4.6 and 4.7. Jason P. Coyle *et al* have proposed a similar mechanism for a copper (I) guanidinate precursor, which, according to them, decomposes to form a smaller guanidine [12,13]. An interesting observation is that both copper precursors can deposit copper by themselves, they do not require a second, reducing agent (H_2) to produce copper metal.

Another point driving from our data is that in our results, under ultrahigh vacuum, preadsorption of hydrogen does not lead to any appreciable changes in the surface chemistry of copper acetamidinates. This can be explained on Ni (110) surface by the fact that all the adsorbed hydrogen desorbs by approximately 350 K, as indicated by the H_2 TPD trace from H-saturated Ni (110) shown at the bottom of Figure 3.12. This temperature is lower than that used for ALD processes with copper acetamidinates. When that temperature is reached, no enough hydrogen is available on the Ni (110) surface for reaction. For a 20 L copper acetamidinates exposure on the Ni (110) surface, in the hydrogen desorption trace shown in Figure 4.8, the 215, 300, and 480 K peaks are from the cracking of the molecular desorption, the small amidine, and the butene.

4.4. Conclusions

The surface chemistry of copper(I)-*N,N'*-di-*sec*-butylacetamidinate on Ni (110) single crystal surfaces was studied under ultrahigh vacuum conditions by using a combination of XPS and TPD. Two by-products were identified, butane, which forms via β-hydride elimination and desorbs at 480 K, and a small amidine (^{s}But–NH–C(CH_3)=NH_2), which desorbs at 300 K. Molecular desorption happens at 215 K.

Combined with the result from the previous chapter, it is concluded that, under the ultrahigh vacuum conditions, dosing of hydrogen either before or after the copper acetamidinate on the Ni (110) surface does not result in any significant changes in surface chemistry. The absence of any effect was ascribed to the low temperatures needed for hydrogen desorption (≤ 350 K), below those typically used in ALD processes [5].

The copper acetamidinate precursor can be used to deposit copper atoms on the Ni (110) surface by itself, without a second reducing precursor, and produce copper metal. This result is similar to that seen in some previous reports [12,13]. The copper acetamidinate decomposes directly on the Ni (110) single crystal surface from the Cu(I) molecular species to Cu(0) metal film; no other chemical state of Cu is observed. This conclusion differs from those from other reports [3,4], which claim that Cu(II) species may form

during ALD processes with the copper acetamidinate on silica surfaces.

4.5. References

[1] C. D. Wagner, W. M. Riggs, L. E. Davis, J. F. Moulder, G. E. Muilenberg, G. E., *Handbook of X-Ray Photoelectron Spectroscopy*, Perkin-Elmer Corp.: Eden Prairie, MN, **1978.**

[2] D. Briggs, *Handbook of X-ray and Ultraviolet Photoelectron Spectroscopy*, Heyden: London, **1978**.

[3] M. Dai, J. Kwon, M. D. Halls, R. G. Gordon, Y. J. Chabal, *Langmuir*, **2010**, *26*, 3911

[4] O. Seitz, M. Dai, F. S. Aguirre-Tostado, R. M. Wallace, Y. J. Chabal, *J. Am. Chem. Soc.* **2009**, *131*, 18159

[5] Z. Li, A. Rahtu, R. G. Gordon, *Journal of the Electrochemical Society*. **2006**, *153*, C787.

[6] G. A. Somorjai, *Chemistry in Two Dimensions: Surfaces*, Cornell University Press: Ithaca, NY, **1981**.

[7] K. Christmann, O. Schober, G. Ertl, M. Neumann, *J. Chem. Phys.* **1974**, *60*, 4528.

[8] Z. Li, S. T. Barry, R. G. Gordon, *Inorganic Chemistry*. **2005**, *44*, 1728.

[9] Z. Li, R. G. Gordon, *Chemical Vapor Deposition*. **2006**, *12*, 435.

[10] Z. Li, R. G. Gordon, D. B. Farmer, Y. Lin, J. Vlassak, *Electrochemical and Solid-State Letters*. **2005**, *8*, G182.

[11] M. Dai, J. Kwon, E. Langereis, L. Wielunski, Y. J. Chabal, Z. Li, R. G. Gordon,

ECS Trans. **2007**, *11*, 91.

[12] J. P. Coyle, P. A. Johnson, G. A. DiLabio, S. T. Barry, J. Müller, *Inorg. Chem*. **2010**, *49*, 2844.

[13] J. P. Coyle, W. H. Monillas, G. P. A. Yap, S. T. Barry, *Inorg. Chem*. **2008**, *47*, 683.

CHAPTER FIVE

Surface Chemistry of the Copper Acetamidinate ALD Precursor on Copper Surfaces

5.1. Introduction

After the deposition of the first layer of the metal, Cu deposition in ALD processes effectively occurs on the growing copper film, not on the original substrate. Given the generally mild surface chemistry exhibited by copper [1-3], that is likely to result in slower hydrocarbon decomposition, and therefore a wider temperature window for ALD. A Cu (110) single crystal surface was used here to simulate the ALD processes after the deposition of first copper layer.

In this chapter we report results from XPS and TPD studies on the surface reactivity of copper(I)-*N,N'*-di-*sec*-butylacetamidinate on (110) oriented copper surfaces. It is shown that copper(I)-*N,N'*-di-*sec*-butylacetamidinate, molecular desorption happens around 220 K. In the remaining adsorbed molecules, the amidine ligand is displaced onto the surface, and reacts and produces several by-products. At 480 K, the same small amidine (^{s}But-NH-C(CH_3)=NH) seen on Ni (110) is formed and desorbs from the surface.

2-butene forms via β-hydride elimination and desorbs at 560 K. Some carbon species are retained on the surface even after the surface is heated to 800 K, again the potential source of impurities in the copper film.

5.2. Results

5.2.1. XPS

The XPS of copper acetamidinate on a clean Cu (110) single crystal surface were acquired first. Since the Cu XPS peaks from copper acetamidinate overlap with the signal from the Cu substrate, some clues on the chemistry seen here may be drawn from the changes in the carbon/nitrogen binging energies.

50.0 L copper acetamidinate was dosed on Cu (110) surface at 90 K, and the surface was then annealed to 150, 200, 250, 300, 400, 500, 600, 700, and 800 K. The XPS data for the Cu $2p_{3/2}$, Cu L_3VV AES, C 1s and N 1s photoelectrons acquired at all those temperatures are reported in Figures 5.1 and 5.2. The Cu $2p_{3/2}$ data (Figure 5.1, left panel) shows constant binding energies from 90 to 200 K at 934.1 eV, but the peak broadens. This peak can be assigned to Cu(I) species [4]. The main change happens between 250 and 400 K, where the signal of XPS peaks intensity increases dramatically and shifts down to 933.3 eV. Above 400 K, and up to annealing temperatures of 800 K, the peak intensity remains

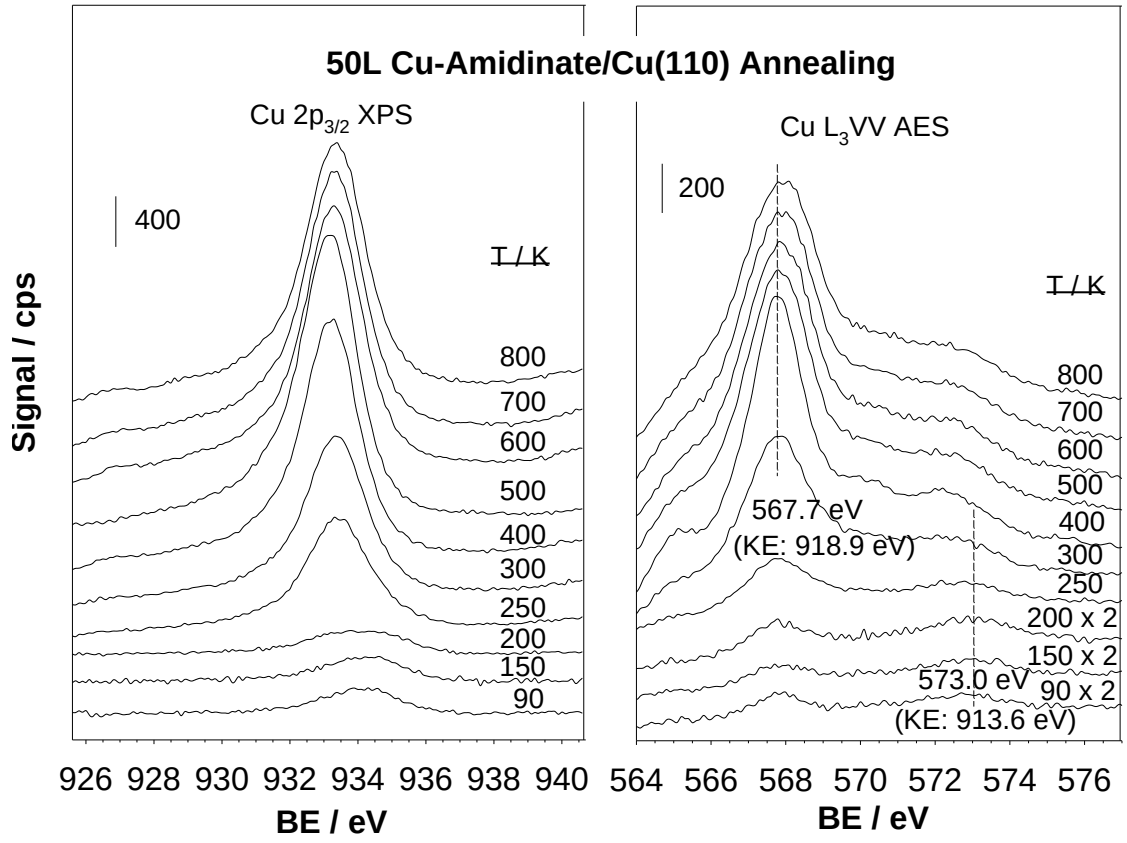

Figure 5.1 Cu $2p_{3/2}$ XPS and Cu AES from 50.0 L copper acetamidinate on clean Cu (110), dosed at 90 K and after annealing to the indicated temperatures.

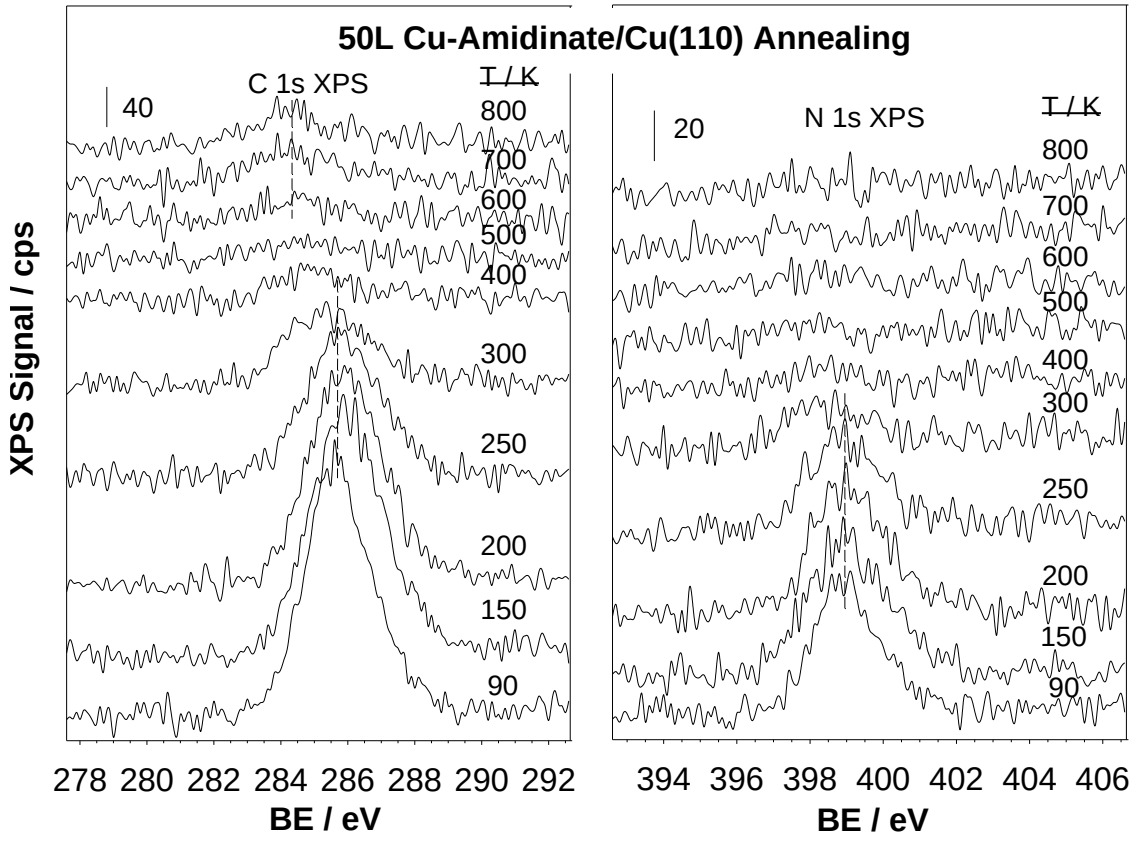

Figure 5.2 C 1s and N 1s XPS from 50.0 L copper acetamidinate on clean Cu (110), dosed at 90 K and after annealing to the indicated temperatures.

constant and the peak position stays within 0.1 eV of 933.2 eV. This new signal is most likely due to the copper substrate, which becomes visible after multilayer desorption of the copper amidinate. The Cu $2p_{3/2}$ binding energy shift seen here is smaller than on the Ni (110) surface.

The right panel of Figure 5.1 shows the Cu L_3VV AES data, which displays the same trends as the Cu $2p_{3/2}$ XPS data. The peak look almost the same from 90 to 200 K, it is centered at 913.6 eV (kinetic energy) the value for Cu(I) species [5]. Similar as with the Cu $2p_{3/2}$ XPS peak, the main change in the AES peaks occurs between 250 and 400 K, where the peak intensity increases dramatically, and the position shift to 918.9 eV (kinetic energy), typical of metallic copper [5]. No more changes are seen above 400 K.

Combining the AES data and XPS data, a firm conclusion can be drawn, that the copper acetamidinate decomposes directly on the Cu (110) single crystal surface from Cu(I) molecular to Cu(0) metal, as in Ni (110).

Regarding the C 1s XPS data (Figure 5.2, left panel), no changes are seen from 90 to 200 K, with a peak at 285.7 eV. Between 200 and 250 K, the peak intensity decreases a little, but the position remains the same. This matches the C 1s XPS data from the Ni (110)

surface, where some molecular desorption happens at around 220 K (a little more desorption occurs on Cu (110) than on Ni (110) see later). Between 250 and 300 K, the peak intensity decreases continuously, and the peak binding energy also decreases. Between 400 and 600 K, the peak intensity decreases more and the peak position shifts down to 284.4 eV. This indicates desorption of some by-products. Above 600 K, both the intensity and position of the C 1s XPS peak keep constant; some carbon species are retained on the Cu (110) surface even after annealing to 800 K.

The N 1s XPS data (Figure 5.2, right panel) follows the behavior of the C 1s XPS: almost no changes are seen from 90 to 200 K, with a peak position at 399.0 eV. Between 200 K and 250 K, the peak intensity decreases a little, and the position is the same; some molecular desorption takes place. Between 250 and 300 K, the peak intensity decreases continuously, and peak position also decreases. Between 300 and 500 K, the peak intensity decreases and the peak position shift down to 398.2 eV because of some decomposition and desorption of surface intermediates. Further increases in annealing temperature lead to further the peak intensity decreases. No nitrogen containing species are left on the surface after annealing at 800 K.

5.2.2. TPD

TPD was used to identify the chemical reactions of copper acetamidinate on the Cu (110) surface. Exposures from 0.5 to 20 L were used; the initial temperature of Cu (110) surface was 90 K. signals were followed for 55 and 56 (for butene), 57and 58 (for butane), 113 and 114 (for small amidine), and 170 and 171 amu (for copper acetamidinate). Figure 5.3 displays the spectra for 114 and 171 amu, and Figure 5.4 for 56 and 58 amu.

The 171 amu TPD displays desorption peaks at 220 and 300 K, matching the C 1s and N 1s XPS signals decreases seen before in the same temperature range. The spectra for 114 amu display a small additional desorption peak at 480 K, which we assigned to a small amidine (^{s}But-NH-C(CH_3)=NH). The temperature here is higher than on Ni (110) surface. The TPD spectra for 58 amu follows the spectra for 114 and 171 amu, and no additional peaks are observed, indicating that no butane is produced from copper acetamidinate TPD on Cu (110). The spectra for 56 amu, on the other hand, display an additional peak at 560 K, a temperature higher than that from copper acetamidinate on Ni (110). Also, the intensities of both 480 and 560 K TPD peaks here were small compared with that for molecular desorption, the reason why the changes in the C 1s and N 1s XPS results were not significant. The spectra for 55, 56, 57, 58 and 114, 170, 171 amu from 15 L copper acetamidinate TPD on Cu (110) shown in Figure 5.5 for comparison. The difference

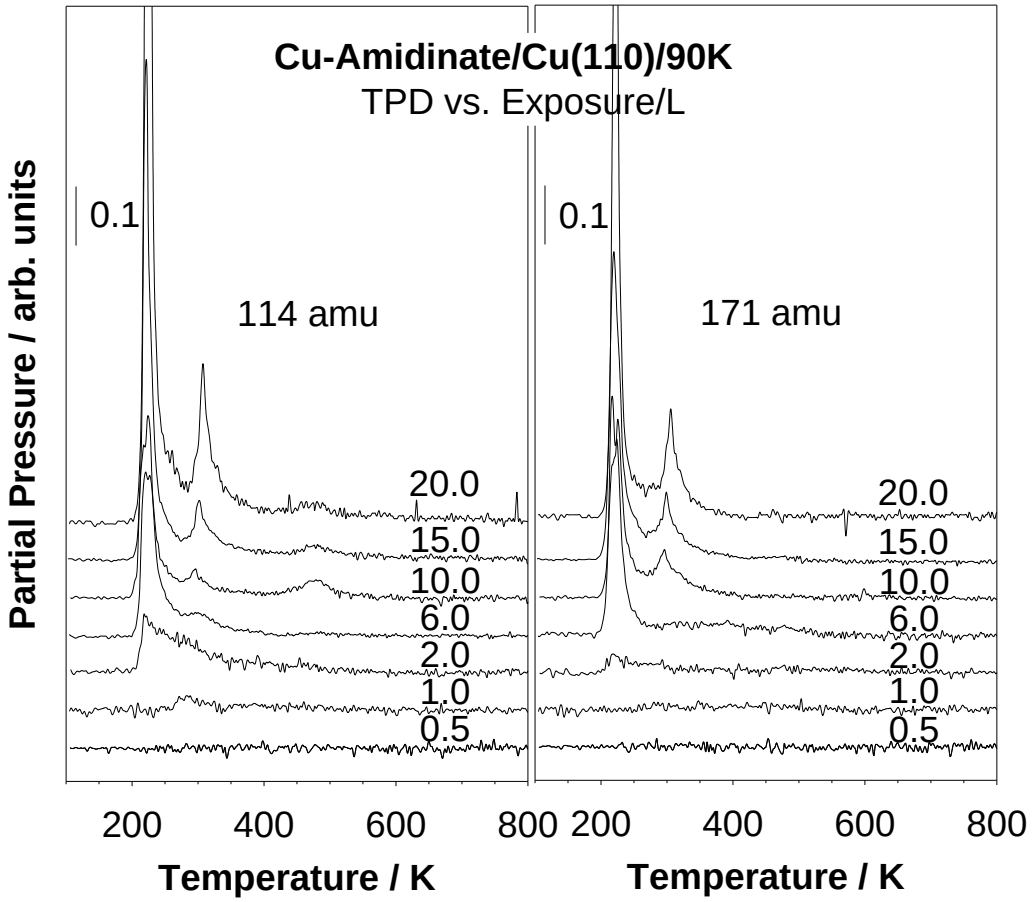

Figure 5.3 114 and 171 amu TPD from copper acetamidinate on clean Cu (110) surface versus exposure.

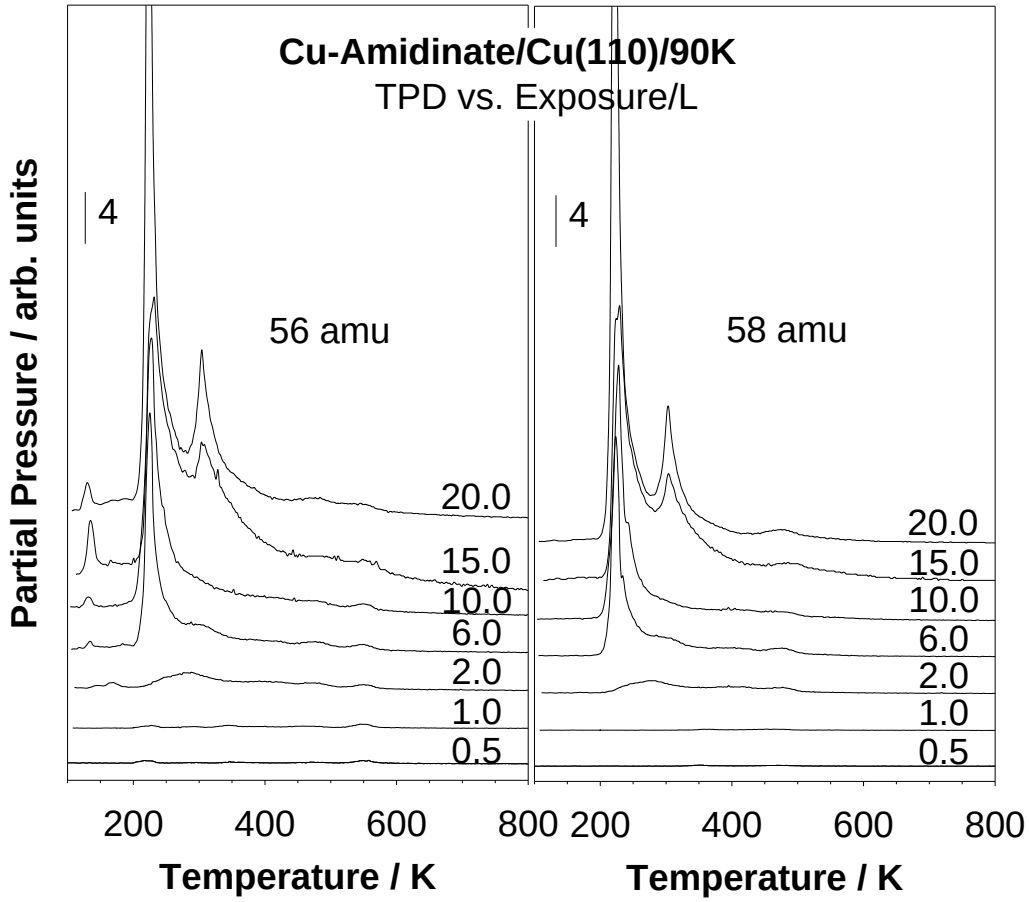

Figure 5.4 56 and 58 amu TPD from copper acetamidinate on clean Cu (110) surface versus exposure.

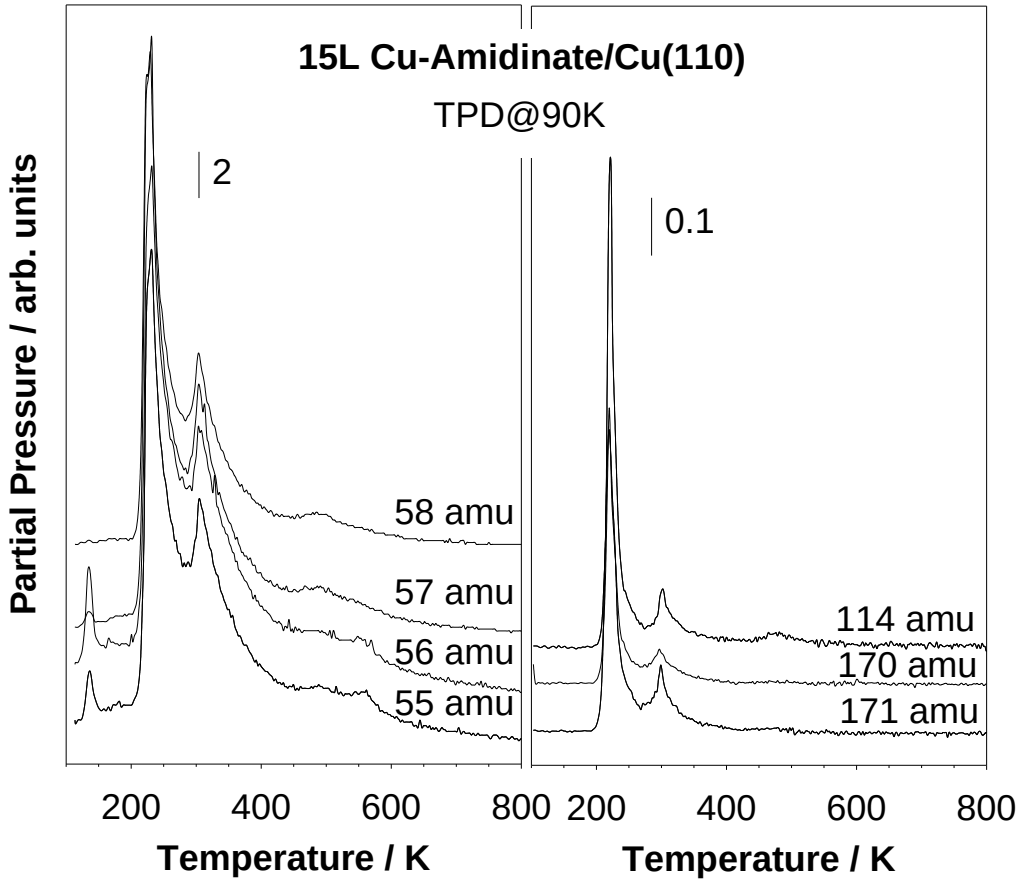

Figure 5.5 55, 56, 57 and 58 (left) and 114, 170 and 171 amu (right) TPD from 15.0 L copper acetamidinate on clean Cu (110).

between the spectra for 56 and 58 amu is obvious at 560 K. Some of the 220 K desorption peak are out of scale in these figures since there are much more intense than the signal for the 480 and 560 K peaks. Sounds the copper acetamidinate reaction on Cu (110) surface was relative weak given the generally mild surface chemistry exhibited by copper [1-3].

5.3. Discussion

Combining the TPD and XPS results from our studies on the surface chemistry of copper acetamidinate on Cu (110), it can be concluded that the reaction mechanism is similar to that on the Ni (110). The copper acetamidinate adsorbs on the Cu (110) surface, and the Cu-N bonds are broken upon annealing of the surface. 2-butene is produced via β-hydride elimination, and desorbs at 560 K. No butane is observed during the TPD of copper acetamidinate on the Cu (110) single crystal surface, indicating that butyl fragments from decomposition of the copper amidinate prefer to dehydrogenate rather than hydrogenate on the Cu (110) surface.

The butene produced here desorbs at around 560 K, a temperature higher than that for used the copper acetamidinate ALD reaction as described in the literatures [6-10].That means that before 560 K, there are some organic fragments adsorbed on the Cu (110)

surface, and, as most ALD-grown Cu films are typically deposited at temperatures between approximately 425 and 465 K, in this temperature range, some carbon incorporation in the copper films may be expected. Interestingly, though the reported carbon codeposition in these ALD is only about 1% [6].

The small amidine identified before (^{s}But-NH-C(CH_3)=NH) is another product obtained from copper acetamidinate decomposition on the Cu (110) surface. A mechanism for its formation was discussed in Chapter four. On the Cu (110), both the 2-butene and the small amidine desorb with smaller yields and at higher temperatures than on Ni (110). It appears that the surface chemistry of amidinate on copper is milder than on nickel [1-3].

5.4. Conclusions

The surface chemistry of copper(I)-*N,N'*-di-*sec*-butylacetamidinate on a Cu (110) single crystal surface was studied under ultrahigh vacuum conditions by using a combination of XPS and TPD. Two decomposition products were identified, butene, which forms via β-hydride elimination and desorbs at 560 K, and a small amidine (^{s}But–NH–C(CH_3)=NH_2), which desorbs at 480 K. Molecular desorption happens at 220 K. The copper acetamidinate reaction on Cu (110) surface is relative mild compared to what is seen on Ni (110).

5.5. References

[1] Z. Ma, F. Zaera, *Surface Science Reports*, **2006**, *61*, 229.

[2] F. Zaera, F. *Chem. Rev.* **1995**, *95*, 2651.

[3] B. E. Bent, *Chem. Rev.* **1996**, *96*, 1361.

[4] C. D. Wagner, W. M. Riggs, L. E. Davis, J. F. Moulder, G. E. Muilenberg, G. E., *Handbook of X-Ray Photoelectron Spectroscopy,* Perkin-Elmer Corp.: Eden Prairie, MN, **1978.**

[5] D. Briggs, *Handbook of X-ray and Ultraviolet Photoelectron Spectroscopy*, Heyden: London, **1978**.

[6] Z. Li, A. Rahtu, R. G. Gordon, *Journal of the Electrochemical Society*. **2006**, *153*, C787.

[7] Z. Li, S. T. Barry, R. G. Gordon, *Inorganic Chemistry*. **2005**, *44*, 1728.

[8] Z. Li, R. G. Gordon, *Chemical Vapor Deposition*. **2006**, *12*, 435.

[9] Z. Li, R. G. Gordon, D. B. Farmer, Y. Lin, J. Vlassak, *Electrochemical and Solid-State Letters*. **2005**, *8*, G182.

[10] M. Dai, J. Kwon, E. Langereis, L. Wielunski, Y. J. Chabal, Z. Li, R. G. Gordon, *ECS Trans*. **2007**, *11*, 91.

CHAPTER SIX

Thermal Reactivity of Acetamidine on Nickel and Copper Surfaces

6.1. Introduction

In this chapter we report results from XPS, LEIS and TPD studies on the adsorption and thermal activity of *N,N'*-di-*sec*-butylacetamidine on (110) oriented nickel and copper surfaces. Those results are intend to help understand the ALD mechanism of the decomposition of copper(I)-*N,N'*-di-*sec*-butylacetamidinate. It is shown here that a little more than 10 L exposure of *N,N'*-di-*sec*-butylacetamidine can cover the Ni (110) surface with one monolayer, and that the acetamidine reacts on both surfaces to produce at least one by-product, butene. Some carbon species remain on both surfaces even annealing at 800 K, but no nitrogen containing species are observed by XPS.

The *N,N'*-di-*sec*-butylacetamidine was prepared by reaction of acetonitrile with *sec*-butylamine. Details of the synthesis and full characterization of the final product are provided elsewhere [1-3]. The molecular structure and mass spectrum of the *N,N'*-di-*sec*-butylacetamidine were shown in Figure 6.1, the mass spectrum was acquired using the ACIF facilities of chemistry department of the University of California, Riverside.

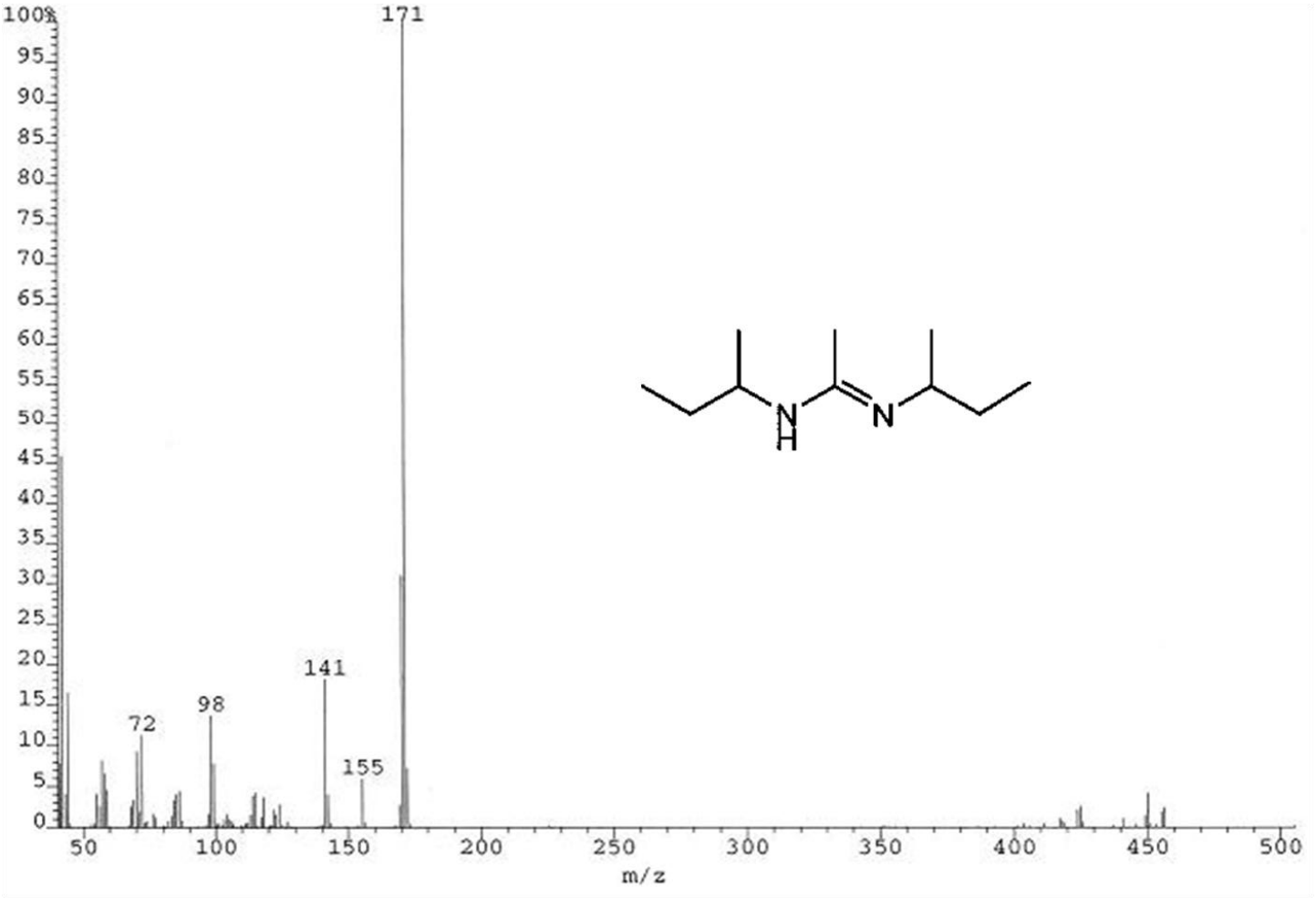

Figure 6.1 Molecular structure and mass spectrum of *N*,*N*'-di-*sec*-butylacetamidine.

6.2. Results

6.2.1. Nickel surface

Figure 6.2 displays results from LEIS experiments on the uptake of copper acetamidinate on a Ni (110) single crystal surface at 90 K. It shows that most of the signal seen at 1570 eV, which corresponds to He^+ scattering from the nickel surface atoms, is already suppressed after a 10 L exposure: only approximately 5% of the nickel surface remains uncovered at this stage of the uptake. Exposures of approximately 11 L are therefore sufficient to saturate the surface at these low temperatures, and by 20 L exposure no nickel atoms are exposed. The bottom trace of Figure 6.2 corresponds to a surface dosed with 20 L of the acetamidine at 90 K and then annealed to 800 K, a process that leads to some adsorbate decomposition and to the re-exposure of some nickel atoms. One additional observation is worth highlighting from the data obtained after annealing: a new peak develops in the LEIS data at 600 eV, associated with surface carbon atoms. This result is consistent with the results of XPS shown below.

C 1s, N 1s and Ni $2p_{3/2}$ XPS were also acquired after a 50 L acetamidine dose on the Ni (110) surface at 90 K. The data was first acquired at 90 K, then the sample was annealed at 150, 200, 250, 300, 400, 500, 600, 700, and 800 K. The data are shown in Figure 6.3. The C 1s XPS peak at 90 and 150 K are similar, centered at 285.6 eV, the same as the

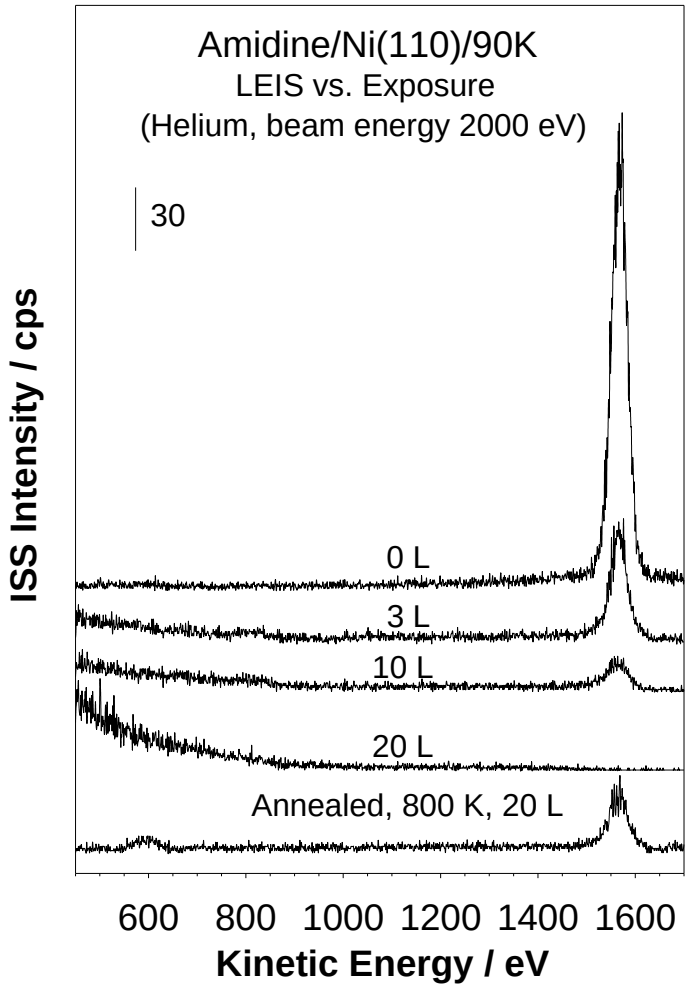

Figure 6.2 He^+ LEIS from a Ni (110) single crystal surface dosed at 90 K with *N*,*N'*-di-*sec*-butylacetamidine as a function of exposure.

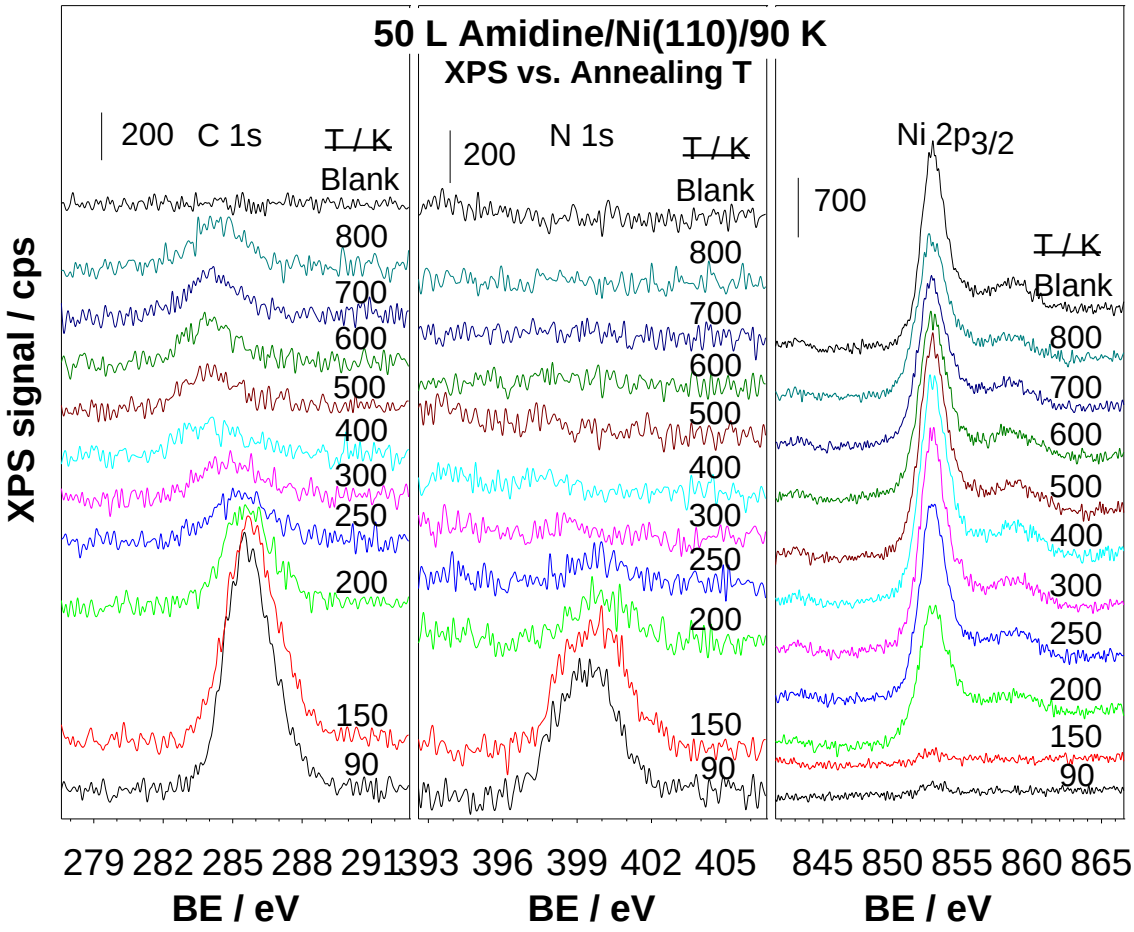

Figure 6.3 C 1s, N 1s and Ni $2p_{3/2}$ XPS form 50.0 L *N,N'*-di-*sec*-butylacetamidine on clean Ni (110) dosed at 90 K and after annealing to the indicated temperatures.

peaks position in copper acetamidinate. After annealing at 200 K, the peak position is still the same, but the intensity decreases, implying some desorption. This matches the TPD data show later, where, some molecular desorption was observed in this temperature range. Between 200 and 400 K, the intensity decreases continuously, and the peak position shifts down to 284.0 eV. From500 to 800 K, both the position and intensity of the C 1s XPS peak is almost constant.

In the N 1s XPS (Figure 6.3, center panel), a peak is first observed at 399.8 eV at 90 and 150 K. Annealing to 200 K, the peak position is still the same, but the intensity decreases as with the C 1s XPS. Between 200 and 300 K, the intensity continues to decrease, and almost vanishes; From 400 to 800 K, no obviously N 1s XPS peak was identified.

The Ni $2p_{3/2,}$ XPS peak position remains constant during annealing up to 800 K, always at 852.7 eV. The intensity increases from 90 to 400 K, then stays almost constant up to 800 K (Figure 6.3, right panel). From all these XPS data, it is conclude that some carbon retains on the surface even up to 800 K, but some desorption happens between 90 and 400 K. The details were probed by TPD.

From the TPD of acetamidine on the Ni (110) surface, it was found that the free

acetamidine is not as active as copper acetamidinate; most of the acetamidine desorbs molecularly at low temperatures, 223 K (Figure 4.7). this is seen in the traces for 113, 114, and 170 amu from 6.0 L acetamidine on Ni (110). The traces for 56 amu (butane), and 114 amu (small amidine) versus exposure are shown in Figure 6.4. For doses below 6 L, there is one additional peak in the TPD for 56 amu at around 525 K, from butene. Note that the peak position is higher than for the butene produced by decomposition of copper acetamidinate on Ni (110). There are no additional peaks in the 114 amu traces other than that for molecular desorption. No products are observed for doses below 2 L.

6.2.2. Copper surface

Similar as on Ni (110) surface, the XPS for C 1s, N 1s, and Ni $2p_{3/2}$ were acquired for 50 L acetamidine as a function of annealing temperature (Figure 6.5 left panel). The intensity of the C 1s peak, at 285.8 eV at 90 K, 0.2 eV higher than on Ni (110) surface, starts to decrease upon annealing at 200 K, and that continues up to 400 K as the peak position shifts down to 284.2 eV (still 0.2 eV higher than on Ni (110) surface). From500 K to 800 K, both the peak position and its intensity remains almost constant.

The N 1s XPS show a peak first observed at 399.6 eV at 90 K. That peak shifts after annealing to 150 K, to 399.8 eV. Annealing to 200 K leads to another ~0.2 eV peak shift

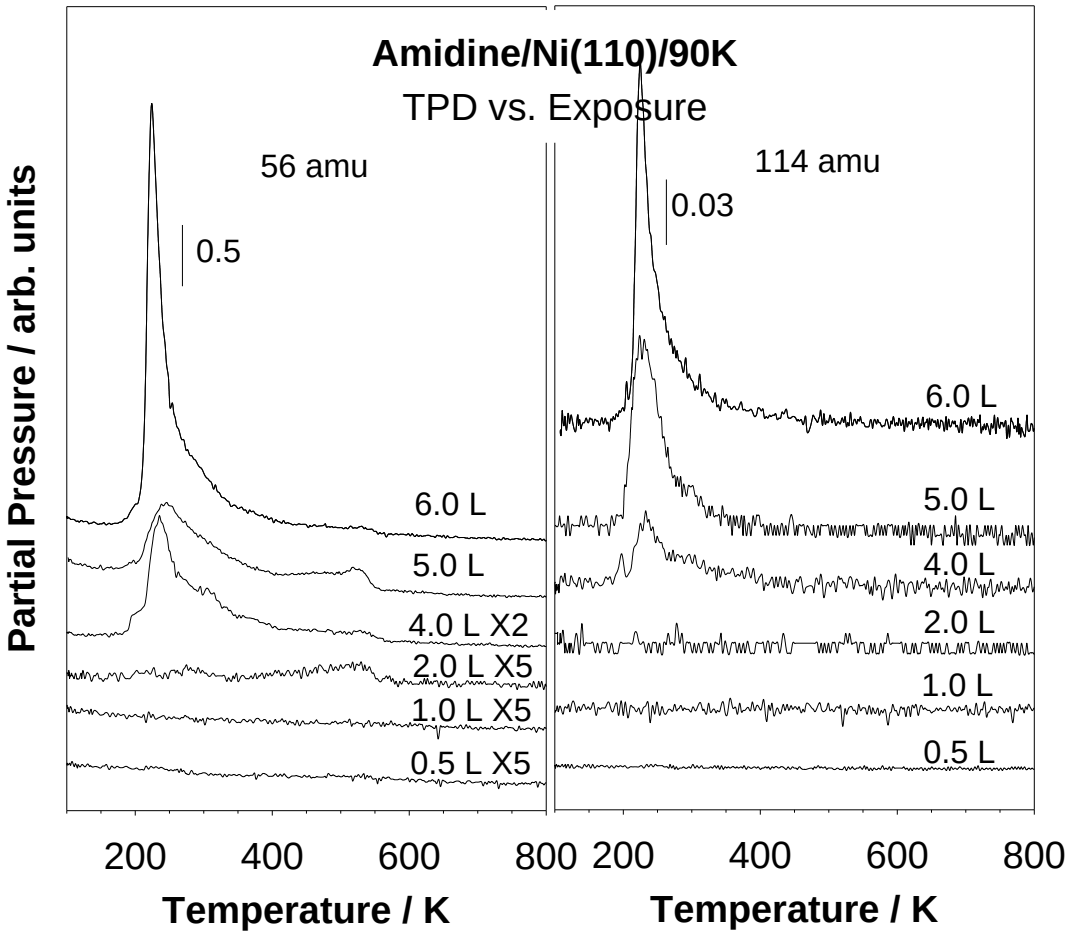

Figure 6.4 56 (2-butnen) and 114 amu TPD from acetamidine on clean Ni (110) versus exposure.

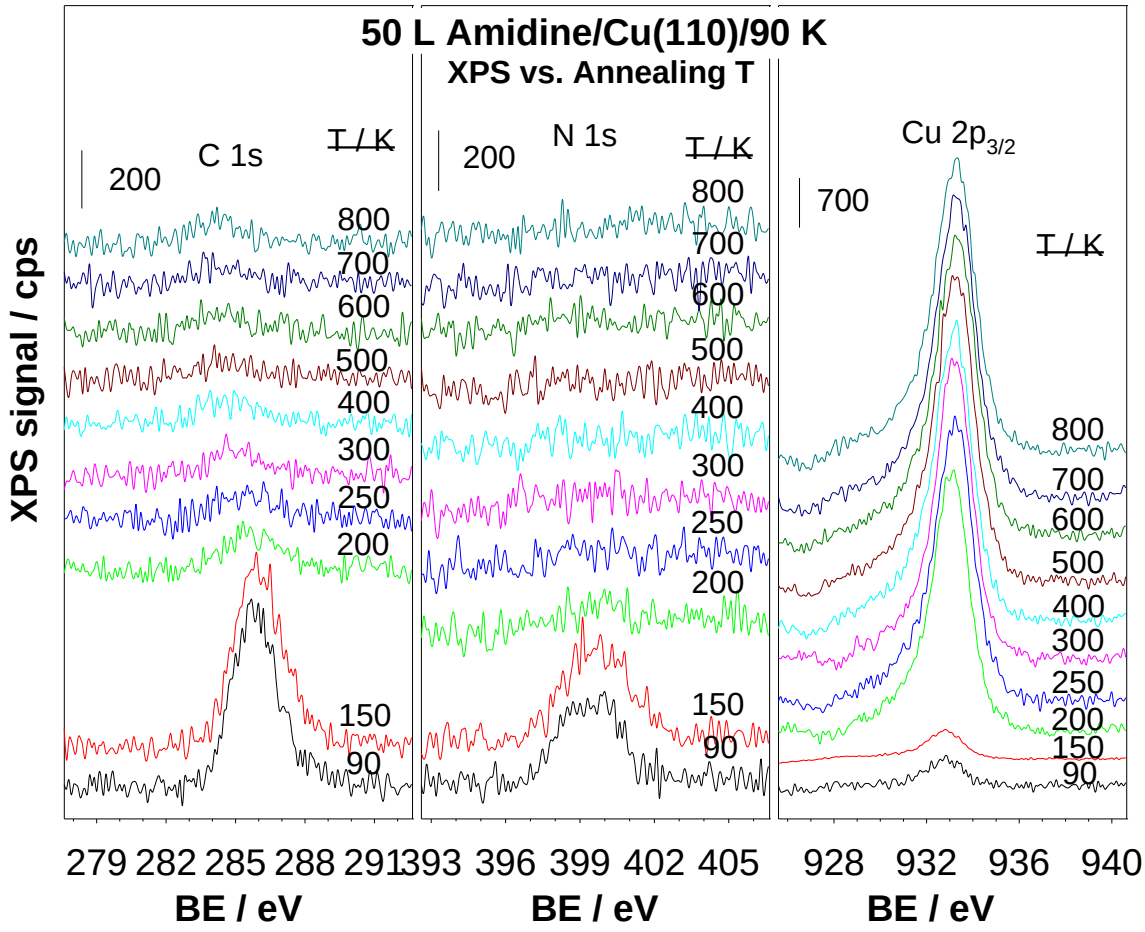

Figure 6.5 C 1s, N 1s and Cu $2p_{3/2}$ XPS form 50.0 L *N*,*N'*-di-*sec*-butylacetamidine on clean Cu (110) dosed at 90 K and after annealing to the indicated temperatures.

and, a large decrease of intensity. Between 200 and 300 K, the intensity continues to decrease, until almost vanishing. From 400 to 800 K, on obviously N 1s XPS peak was identified (Figure 6.5, center panel).

The XPS data of Cu $2p_{3/2,}$ shows a peak at 933.2 eV for all temperature. The intensity increases continuously from 90 to 300 K, then remains almost constant up to 800 K (Figure 6.5, right panel). These XPS data indicate that some carbon is retained on the surface up to 800 K, and some that desorption happens between 90 and 400 K.

The TPD of acetamidine on Cu (110) surface were carried out for a 20 L exposure, recording the signals for 113, 114, 155, 169, and 170 amu (Figure 6.6). A molecular desorption peak is seen around 223K, with a long tail. The 114 amu signal, which correspond to the small amidine, displays no additional peak other than that for molecular desorption peak.

The TPD spectra for 55, 56 (butene), and 57 and 170 (molecular) amu from a 10 L acetamidine exposure on clean Cu (110) (Figure 6.7, left panel), show a large peak at around 223 K, from molecular desorption, but also additional peaks at 495 K. This peak is also likely due to molecular desorption, perhaps from some parts around the Cu (110)

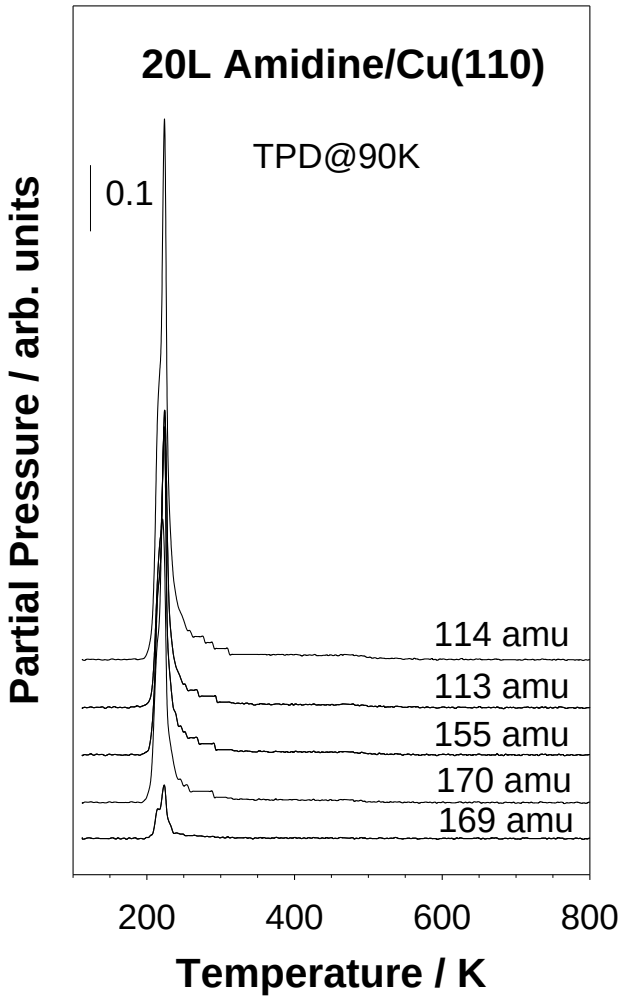

Figure 6.6 113, 114, 155, 169 and 170 amu TPD from 20.0 L *N,N'*-di-*sec*-butylacetamidine on clean Cu (110).

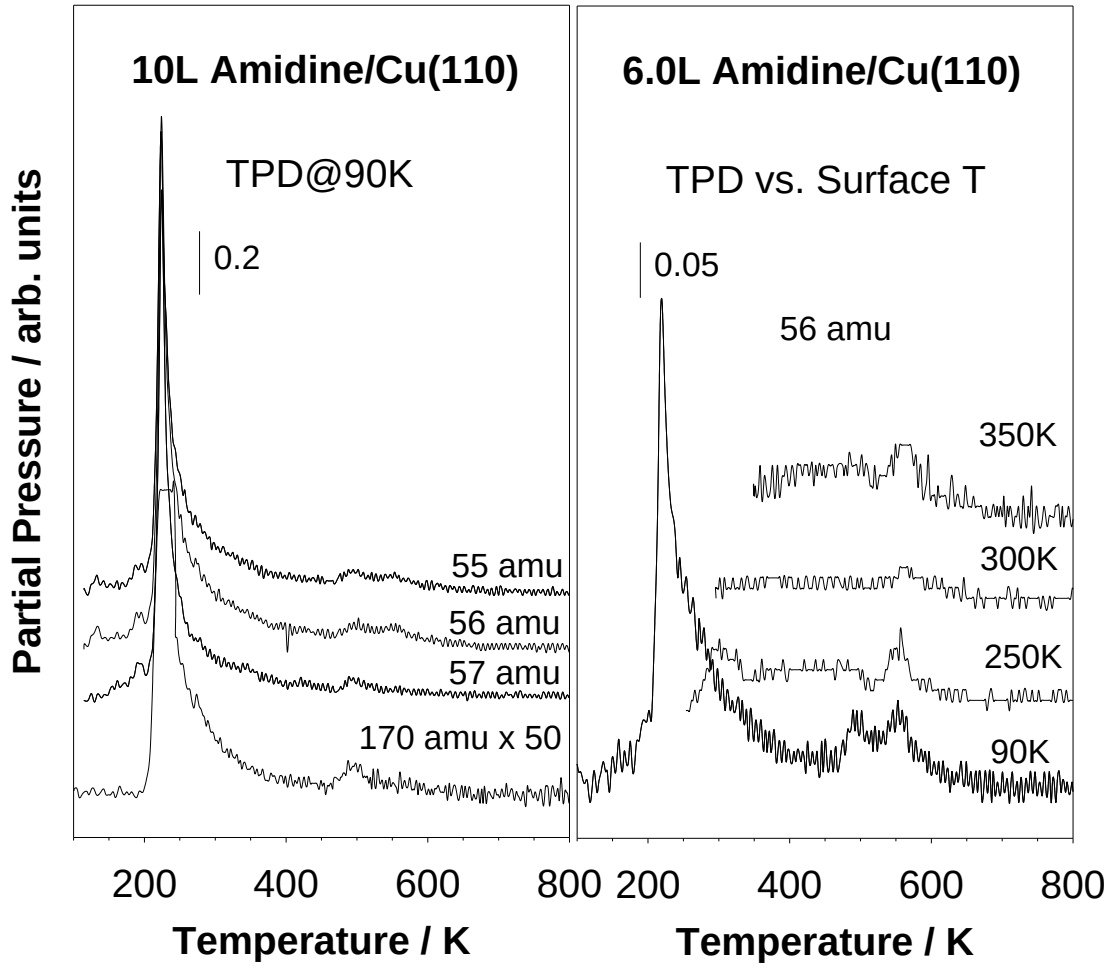

Figure 6.7 Left: 55, 56 (butene), 57 and 170 (molecule) amu TPD from10.0 L *N*,*N'*-di-*sec*-butylacetamidine on clean Cu (110). Right: 56 (butene) amu TPD from 6.0 L *N*,*N'*-di-*sec*-butylacetamidine on clean Cu (110) dosed at the indicated temperatures.

surface. In addition, the 55 and 56 amu TPD display a small peak at 560 K, which is assigned to butene. To eliminate the possibility that the 495 K desorption peak originates from Cu (110), a TPD for 6.0 L acetamidine was acquired, monitoring the 56 amu (butene) signal for experiment where the initial adsorption surface temperature was held at 90, 250, 300, and 350 K respectively (Figure 6.7, right panel). For adsorption temperatures above 250 K, the 495 K desorption peak disappears, and only 560 K desorption peak is left behind.

6.3. Discussion

For a clean ALD process, without impurities introduced into the deposit copper film [4], it would be desirable for the acetamidinate ligands in our precursor to be hydrogenated as it bonds to the surface, and to desorbs as a free acetamidine molecule without any further surface conversion. Is for that reason that is helpful to understand the surface reactivity of acetamidine on the nickel and copper surfaces.

According to our TPD results, acetamidine produces small amounts of butene, but to a less extent than copper acetamidinate on the same surface. Also, no small amidine is made here, although that could be obscured by the long molecular desorption tail seen in the TPD. Overall, not much chemistry happens with free amidine. This could be become,

once the amidinate ligand is hydrogenated to the amidine, it becomes much less reactive.

While comparing the XPS data of acetamidine versus copper acetamidinate on the same surface, the N 1s binding energies are different even at low temperatures. For 50 L exposure, for instance, the initial binding energies for N 1s are 399.8 eV for acetamidine and 399.2 eV for copper acetamidinate on Ni (110) surfaces, and 399.6 eV for acetamidine and 399.0 eV for copper acetamidinate on Cu (110) surfaces. Both those sets show a 0.6 eV difference between the Cu precursor and the free hydrogenated ligand. This difference may be caused by the N atoms being bonded to the Cu (I) atoms or not. Those results also prove that the copper acetamidinate adsorbs intact on the surface, and decomposes only at higher temperature.

Finally, butene from acetamidine desorbs at 525 K from Ni (110) surface. This temperature is higher than that for desorption of the butene produced from copper acetamidinate on the same surface. That may also indicate that the acetamidine is less active than copper acetamidinate.

6.4. Conclusions

The adsorption and thermal activation of *N,N'*-di-*sec*-butylacetamidine on Ni (110) and

Cu (110) single crystal surfaces was studied under ultrahigh vacuum conditions by using a combination of XPS, LEIS AND TPD. Only one product from the acetamidine decomposition was identified: butene, which desorbs at 525 K from Ni (110) and 560 K from Cu (110). The conversion of acetamidine on both surfaces is relatively small compared with copper acetamidinate, and less products are released. Molecular desorption happens at around 223 K.

Exposures of approximately 11 L acetamidine are sufficient to saturate the Ni (110) surface at 90 K. Some acetamidine decomposes on both Ni (110) and Cu (110) surfaces to left carbon species on the surfaces.

6.5. References

[1] B. S. Lim, A. Rahtu, J. –S. Park, R. G. Gordon, *Inorganic Chemistry.* **2003**, *42,* 7951.

[2] Z. Li, S. T. Barry, R. G. Gordon, *Inorganic Chemistry*. **2005**, *44*, 1728.

[3] J. H. Forsberg, V. T. Spaziano, T. M. Balasubramanian, G. K. Liu, S. A. Kinsley, C. A. Duckworth, J. J. Poteruca, P. S. Brown, J. L. Miller, *Journal of Organic Chemistry*, **1987**, *52*, 1017.

[4] Q. Ma, H. Guo, R. G. Gordon, F. Zaera, *Chemistry of Materials.* **2010**, *22*, 352.

CHAPTER SEVEN

Thermal Reactivity of Cu-KI5 on Copper Surfaces

7.1. Introduction

As discussed in the last several chapters, the copper(I)-*N,N'*-di-*sec*-butylacetamidinate is one promising precursors for copper ALD [1-3]. Other copper(I) precursors are also being considered, though, including Cu-KI5, copper(I) (N(1(dimethylvinylsiloxy)-1-methylethano)-2-imino-4-pentanoate) and CupraSelect^{TM} 2500, 1,1,1,5,5,5-hexafluoro-2,4-pentanedionato-copper(I)-trimethylvinylsilane. CupraSelect^{TM} 2500 is a known Cu(I) precursor for the deposition of copper films by CVD, a precursor from Air products and Chemicals Inc. [4,5]. The copper(I) (N(1(dimethylvinylsiloxy)-1-methylethano)-2-imino-4-pentanoate) precursor is a new version, an unfluorinated precursor with higher thermal stability and better vapor pressure [6,7]. The short name Cu-KI5 of this precursor will be used in the rest of this dissertation to save typing and space. The Cu-KI5 was provided by Air Products Inc. Details of this chemical are provided elsewhere [6], and the molecular structure is shown in Figure 7.1

In this chapter we report results from XPS and TPD studies on the adsorption and thermal

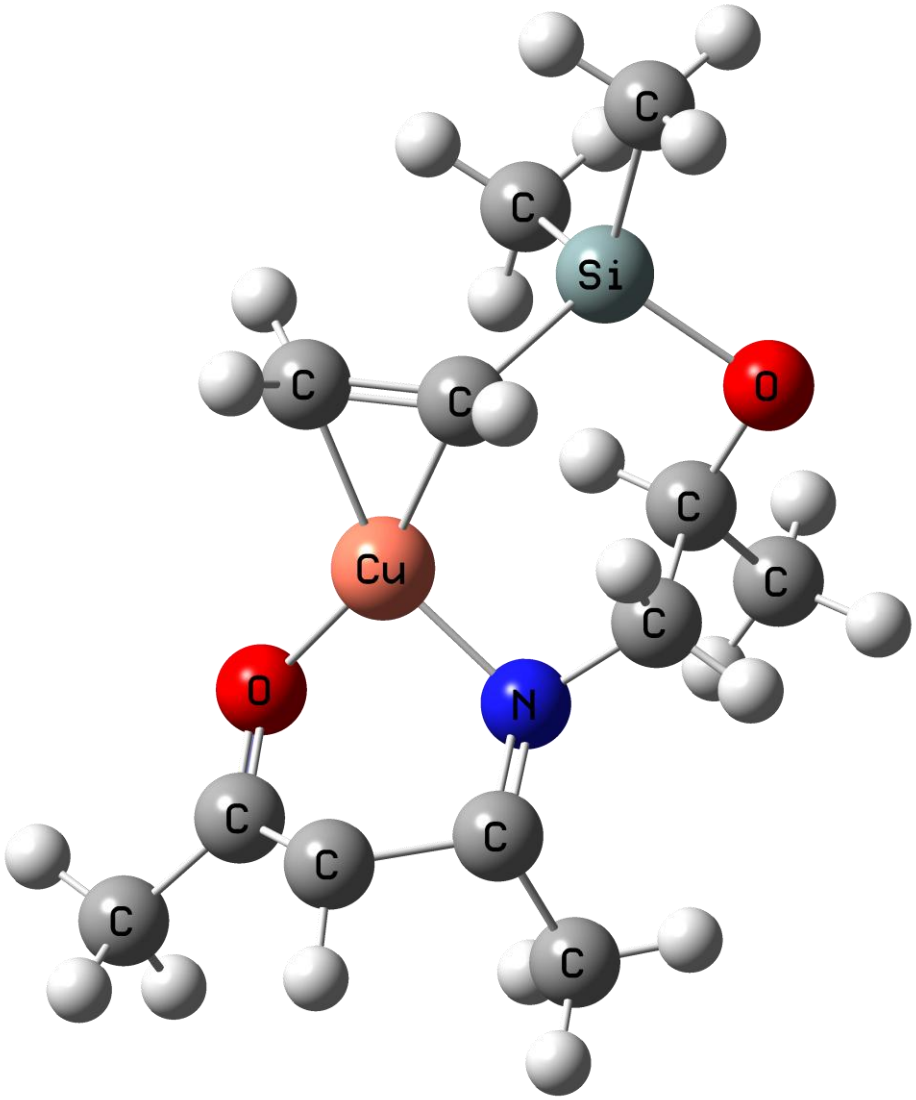

Figure 7.1 Molecular structure of Cu-KI5
copper(I)(N(1(dimthylvinylsiloxy)-1-methylethano)-2-imino-4-pentanoate).

activity of Cu-KI5 on (110) oriented copper surfaces. Those results, combined with the results about the copper(I)- *N,N'*-di-*sec*-butylacetamidinate, are directed to help understand the copper(I) species chemistry on late transition metal surfaces related to ALD processes. It is shown here that Cu-KI5 decomposes on Cu (110) upon annealing above 400 K. Carbon, oxygen, and even silicon-containing species are left on the surface, and copper oxide may form. Desorption peaks seen at 280 and 425 K may be attributed to decomposition products from the ligand during TPD.

7.2. Results

7.2.1. XPS

The thermal chemistry of Cu-KI5 on clean Cu (110) surface was first surveyed by XPS. The main frame of Figures 7.2 and 7.3 display the XPS spectra obtained after different exposures (50, 150, 300 L) of Cu-KI5 on the Cu (110) surface at 90 K.

With respect to the C 1s XPS data (Figure 7.2, left panel), the signal increases with dose, with a peak at 285.3 eV; no saturation is reached even after 300 L. The N 1s XPS signal for the Cu-KI5 molecule displays a peak at 399.6 eV (Figure 7.2, center panel), but only after a 300 L dose; no signal was seen for lesser exposures. The O 1s XPS signal also grows continuously, at 533.0 eV (Figure 7.2, right panel), from 50 to 300 L. based on the

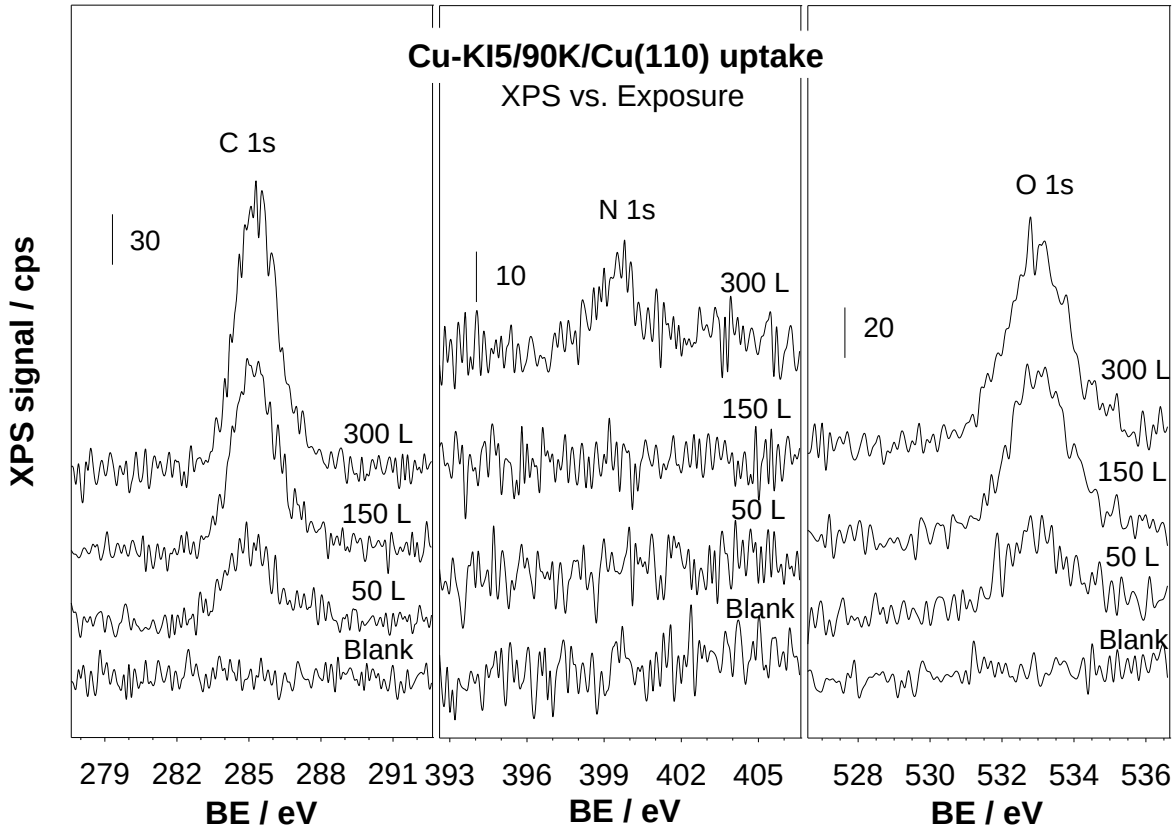

Figure 7.2 C 1s, N 1s and O 1s XPS from Cu-KI5 on clean Cu (110) dosed at 90 K versus exposure.

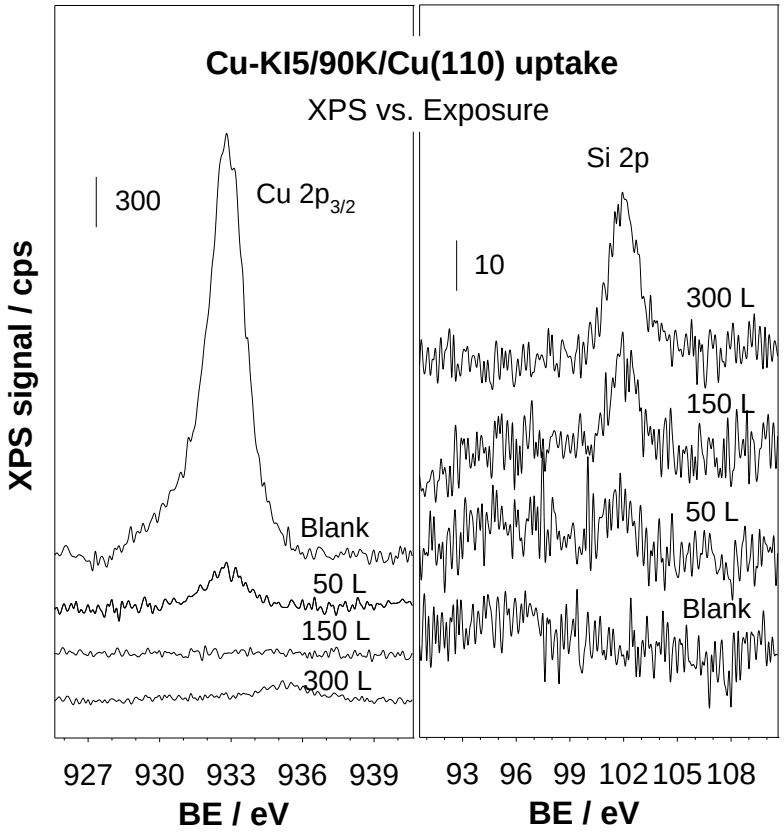

Figure 7.3 Cu $2p_{3/2}$ and Si 2p XPS from Cu-KI5 on clean Cu (110) dosed at 90 K versus exposure.

Cu $2p_{3/2}$ XPS data (Figure 7.3, left panel), the 932.8 eV peak due to the substrate is significantly attenuated after 50 L, and gone by 150. By 300 L, the Cu $2p_{3/2}$ XPS signal for Cu-KI5 molecule is seen at 935.2 eV. Finally, the Si 2p XPS signal continuously increases at 102.0 eV (Figure 7.3, right panel).

The main frames of Figures 7.4 and 7.5 display the XPS spectra obtained after dosing300 L Cu-KI5 on the Cu (110) surface at 90 K and annealing to the indicated temperatures. The C 1s XPS signal drops sharply between 150 and 200 K, and shifts from 285.3 to 285.0 eV (Figure 7.4, left panel), and continue to decrease up to 400 K as the binding energy also shifts downward. Beyond 400 K, the peak intensity stays almost constant, and the binding energy settles at 284.0 eV. The N 1s XPS signal displays a peak at 399.6 eV at 90 K (Figure 7.4, center panel) with an intensity that decreases continuously with temperature up to 300 K. No nitrogen was seen after annealing above 400 K. The O 1s XPS signal also drops sharply between 150 and 200 K and shifts from 533.0 to 532.7 eV, and decreases further up to 400 K (Figure 7.4, right panel). The final binding energy in this case is 531.6 eV. The Si 2p XPS signal drops sharply between 150 and 200 K and shifts from 102.0 to 101.8 eV (Figure 7.5, left panel), and continuously decreases and shifts to 101.5 eV upon annealing to 400 K. Annealing to 800 K, still leaves a small Si 2p signal at 101.5 eV. The trends of the O 1s and Si 2p XPS data follow those of C 1s.

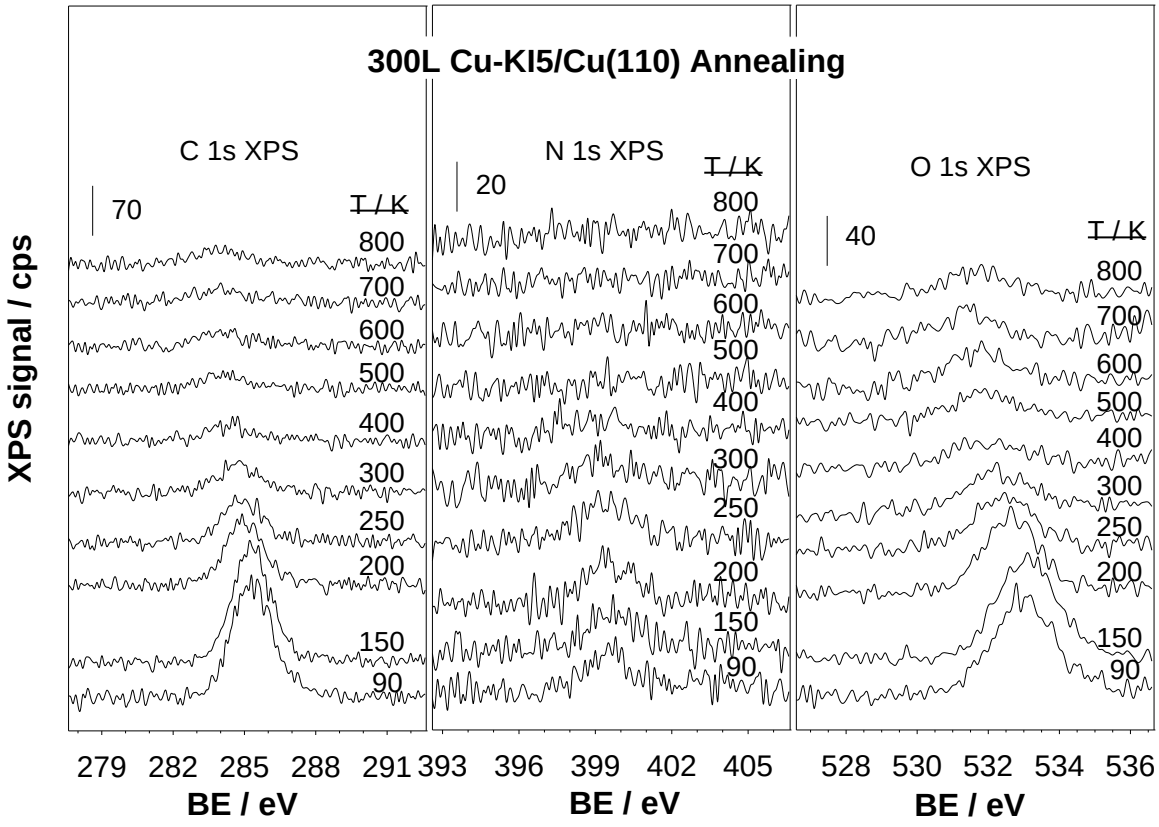

Figure 7.4 C 1s, N 1s and O 1s XPS from 300 L Cu-KI5 on clean Cu (110), dosed at 90 K and after annealing to the indicated temperatures.

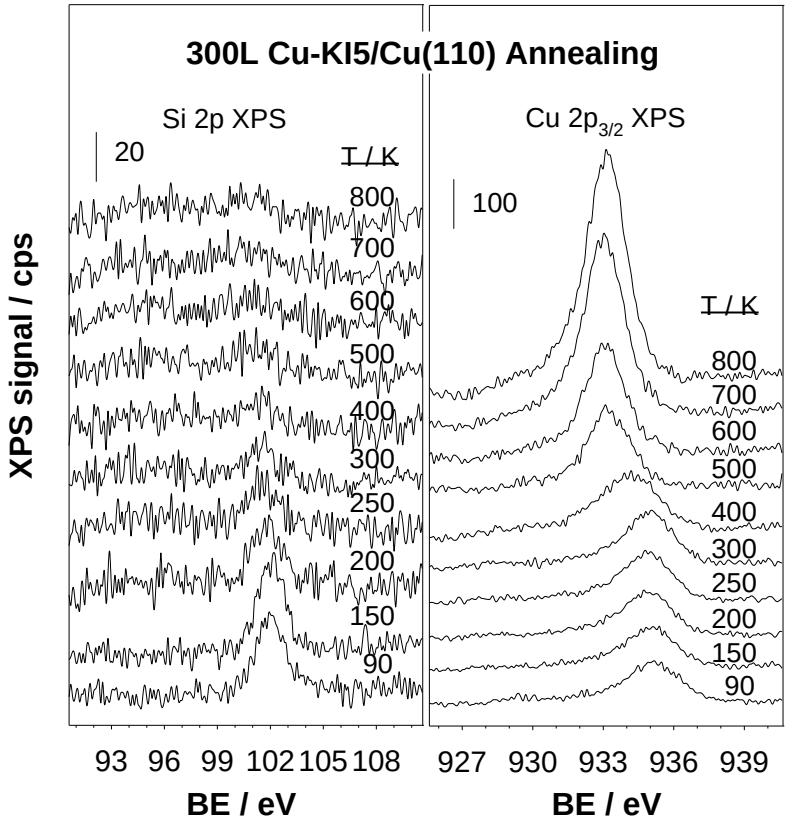

Figure 7.5 Si 2p and Cu $2p_{3/2}$ XPS from 300 L Cu-KI5 on clean Cu (110), dosed at 90 K and after annealing to the indicated temperatures.

For the Cu $2p_{3/2}$XPS signal, the peak is centered at 935.2eV with constant intensity from 90 to 300 K. At 400 K a broad feature observed, the combination of two peaks. A further shift is seen, to 933.1 eV at 500 K. When increasing the annealing temperature further, the intensity of the signal at 933.1eV continuously increases, all the way to 800 K. The Cu $2p_{3/2}$ signal is centered at 933.1 eV, which means that a copper compound other than metallic copper forms on the surface.

7.2.2. TPD

Some TPD experiment was carried out as well. Several small masses, including 59, 63 and 73 amu, were tested. Almost no peaks were observed from the TPD of a surface dosed with 10 L Cu-KI5. For doses of 20, 30 and 50 L, some peaks clear grow at around 165, 210, 280, and 425 K, as shown in Figure 7.6. For 59 amu, its 210 and 280 K peaks continuously increases with dose, the 165 K peak is always small, and the 425 K peak saturates around10 L. The 63 and 73 amu TPD also display all four peaks, except that the 425 K peak saturates at the beginning, and the 165, 210, and 280 K peaks continuously increase with dose. However, ratios of the intensities of the different peaks at different temperatures are different for each mass number (Figure 7.7, left panel). That means that these peaks do not come from the same chemical. To prove this, some higher masses, 96, 97, 98, 142, 143, 144, 239, 240 and 241 amu, were monitored as well (Figure 7.7, right

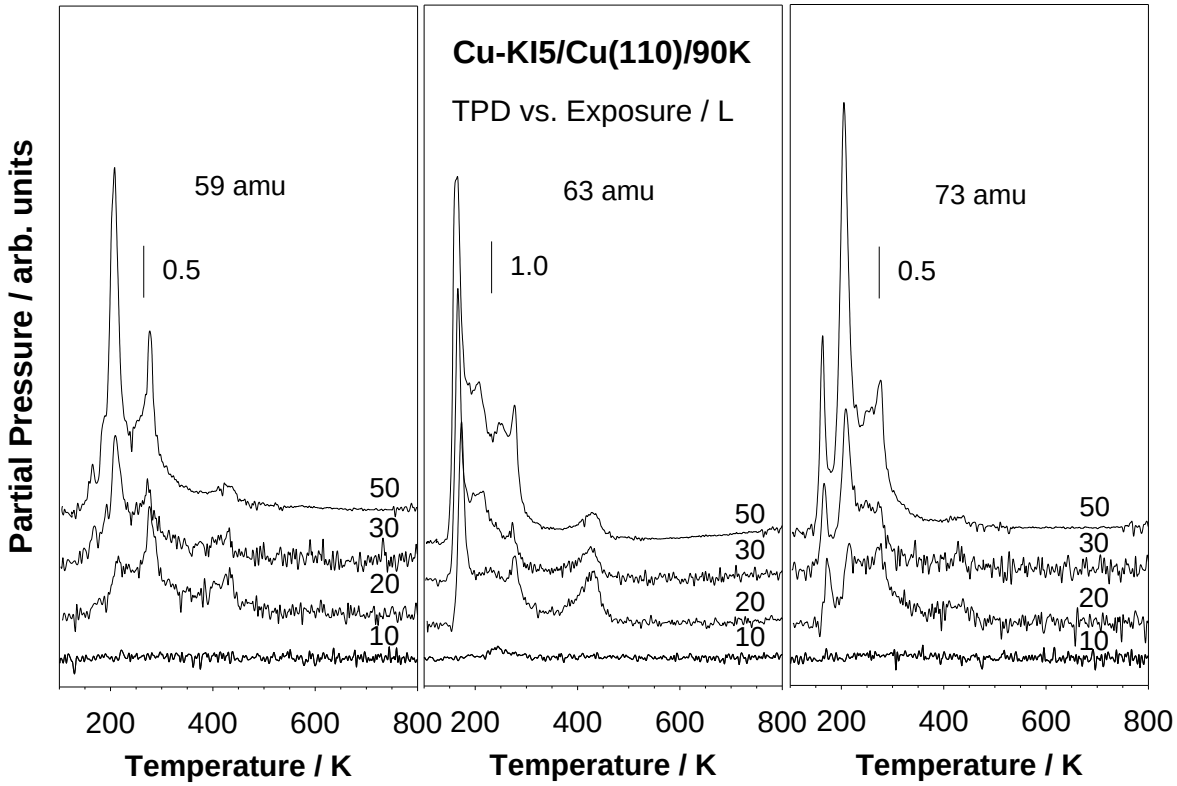

Figure 7.6 59, 63, 73 amu (left panel) and 96, 97, 98, 142, 143, 144, 239, 240, 241 amu (right panel) TPD from 50 L Cu-KI5 on clean Cu (110).

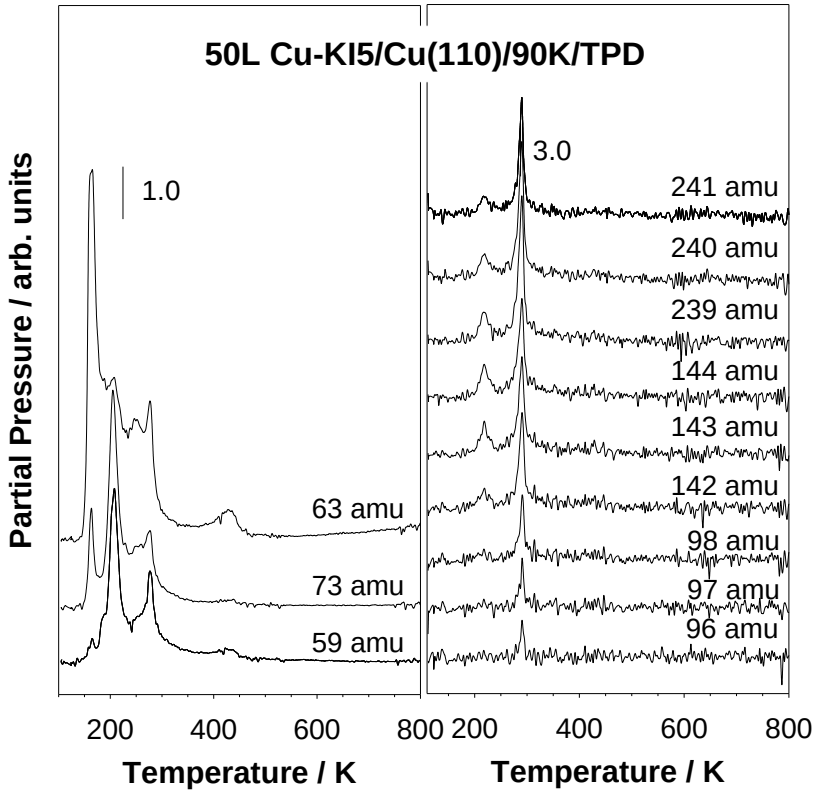

Figure 7.7 59, 63, 73 amu (left panel) and 96, 97, 98, 142, 143, 144, 239, 240, 241 amu (right panel) TPD from 50 L Cu-KI5 on clean Cu (110).

panel). Because the masses here are high, the signals are relatively weak, so all the signals are enlarge 50 times in this plot. All these traces display a peak at around 280 K. Since the mass of the intact molecule is 303 amu, and that of the ligand 240 amu, the peaks around 280 K seen here are likely from desorption of the ligand after the molecules loses the Cu atom. Evidence for this can be extracted from the XPS data, where the N 1s signal almost totally vanishes after annealing to 300 K. The TPD traces for the 140's and 240's amu groups also display another peak at 220 K, which may be attributed to molecular desorption. The 140's amu set also displays a small peak at 425 K, which may come from further decomposition of the ligand via scission of the N-C bond.

7.3. Summary

The adsorption and thermal activation of Cu-KI5 on Cu (110) single crystal surfaces was studied under ultrahigh vacuum conditions by using a combination of XPS and TPD. Cu-KI5 decomposes on Cu (110) around 400 K. Carbon, oxygen, and even silicon containing species retain on the surface though the annealing all the way to 800 K. No nitrogen containing species is observed on the surface above 400 K. The copper deposited with this molecule is not metallic copper. It is a combination of copper compounds with different oxidation states, which may include copper oxide.

From the TPD data, desorption peaks are seen at 280 and 425 K, which are attributed to desorption of the hydrogenated ligand and to further decomposition of that ligand, respectively.

7.4. References

[1] B. S. Lim, A. Rahtu, J. –S. Park, R. G. Gordon, *Inorganic Chemistry.* **2003**, *42,* 7951.

[2] Z. Li, S. T. Barry, R. G. Gordon, *Inorganic Chemistry*. **2005**, *44*, 1728.

[3] Z. Li, A. Rahtu, R. G. Gordon, *Journal of the Electrochemical Society*. **2006**, *153,* C787.

[4] S. Kim, D.-J. Choi, *Materials Research Society Symposium Proceedings*, **1998**, *516,* 281.

[5] A. Jain, T. T. Kodas, R. Jairath, M. J. Hampden-Smith, *Journal of Vacuum Science & Technology, B: Microelectronics and Nanometer Structures*, **1993**, *11*, 2107.

[6] J. A. T. Norman, M. Perez, S. E. Schulz, T. Waechtler, *Microelectronic Engineering*, 2008, 85, 2159.

[7] H. Song, J. A.T. Norman, Y. Shimogaki, *Microelectronic Engineering*, in press. **2009**

CHAPTER EIGHT

Thermal Reactivity of $Cu(acac)_2$ on Nickel and Copper Surfaces

8.1. Introduction

All the previous chapters focused on the chemistry of Cu(I) precursors on metal surfaces. Copper(I) species usually are unstable, and air and water sensitive. A more stable copper(II) precursor was investigated here to provide some comparable information to that recorded for the copper(I) species. The copper(II) precursor used here was copper(II) acetylacetonate, also called bis(2,4-pentanedionato)copper(II). The short name $Cu(acac)_2$ of this precursor will be used in the rest of this dissertation to save typing and space. The $Cu(acac)_2$ is commercial available, and its chemistry has been discussed somewhat already [1-5]. Since the precursor includes two (acac) ligands, the surface chemistry of Hacac was also studied.

In this chapter we report results from XPS and TPD studies on the adsorption and thermal activity of $Cu(acac)_2$ on (110) oriented nickel and copper surfaces. It is shown here that, $Cu(acac)_2$ decomposes on both surfaces at 300 K and produces Hacac, and possibly acetone. No CO or CO_2 was observed. Metallic copper is formed, and residual

carbon species are left on these surfaces. No other oxidation states of copper were identified at any temperature between 90 and 800 K: the Cu(II) precursor converts directly into Cu(0).

8.2. Results

8.2.1. Copper surface

8.2.1.1. XPS of $Cu(acac)_2$

Some preliminary experiments with $Cu(acac)_2$ were carried out on Cu (110) first. 100 L $Cu(acac)_2$ was dosed on clean Cu (110) surface at 90 K, and the surface annealed to various temperatures. At 90 K, the C 1s XPS displays two peaks at 285.2 eV and 287.2 eV respectively (Figure 8.1, left panel), for the two kinds of carbon atoms in the original molecule. The lower binding energy peak is assigned to the carbon in the CH_3- and –CH- moieties, the higher one to the carbon in the –CO- groups. The ratio of intensities is consistent with this interpretation, at around 3 to 2. Annealing at 250 K, leads to a peak intensity decrease and to a shift of both peaks down by about 0.3 eV, the intensity ratio, however, remains at around 3 to 2. It appears that some molecular desorption takes place in this temperature range. At higher temperatures, the size of both peaks decrease further and almost vanished by 500 K. Beyond that temperature, another peak develops at 284.3 eV, which remains even annealing to 800 K.

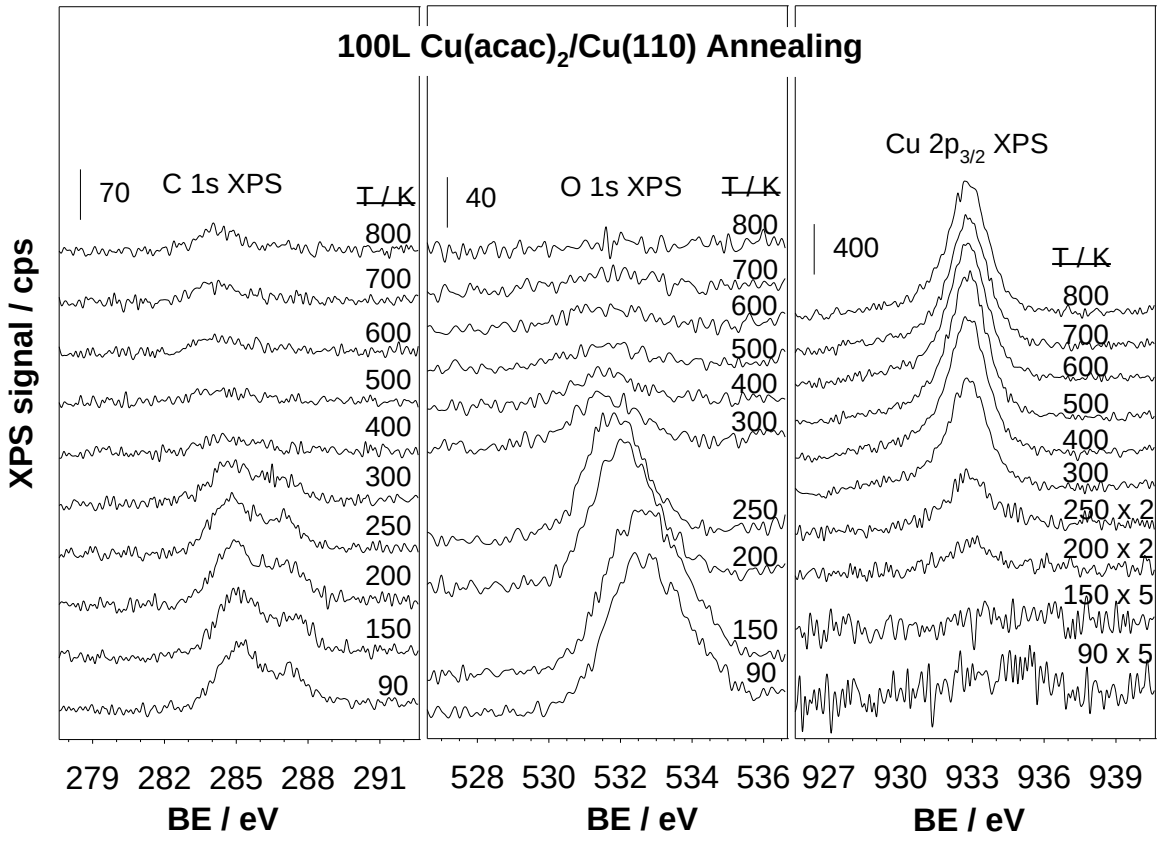

Figure 8.1 C 1s, O 1s and Cu $2p_{3/2}$ XPS from 100 L $Cu(acac)_2$ on clean Cu (110), dosed at 90 K and after annealing to the indicated temperatures.

At 90 K, the O 1s XPS displays a peak at 532.7 eV (Figure 8.1, center panel). At150 K, the peak intensity and binding energy remain same, but by 200 K, they decrease, the new binding energy is 532.0 eV. After annealing to 250 and 300 K, the peak intensity decreases further, and shifts to 531.8 and 531.4 eV, respectively. The O 1s XPS peak almost vanishes after annealing the surface at 800 K, with no copper oxide formation on the surface. That contradicts some previous reports, which claimed copper oxide formation during the $Cu(acac)_2$ decomposition.

The Cu $2p_{3/2}$ XPS is shown in Figure 8.1 (right panel). Since the substrate was Cu (110), it was difficult to see the changes in the Cu 2p signal. The signals at 90 and150 K were enlarged 5 times, and the signals at 200 and 250 K twice. At 90 K, a very weak Cu 2p peak is seen at about 935.3 eV, but the signal from the substrate (centered at 932.7 eV) grows and totally overwhelms the Cu(II) signal at higher temperatures. Finally, at 800 K, the copper peak is centered at 932.7 eV, in the range of metallic copper. This is consistent with the O 1s XPS: no oxide is formed on the surface.

8.2.1.2. TPD of $Cu(acac)_2$

For the TPDs, the signals for 2, 15, 39, 43, 85, and 100 amu were monitored first. For 10 L $Cu(acac)_2$ on Cu (110), peaks are seen at around 185, 295, 515, and 610 K (Figure 8.2,

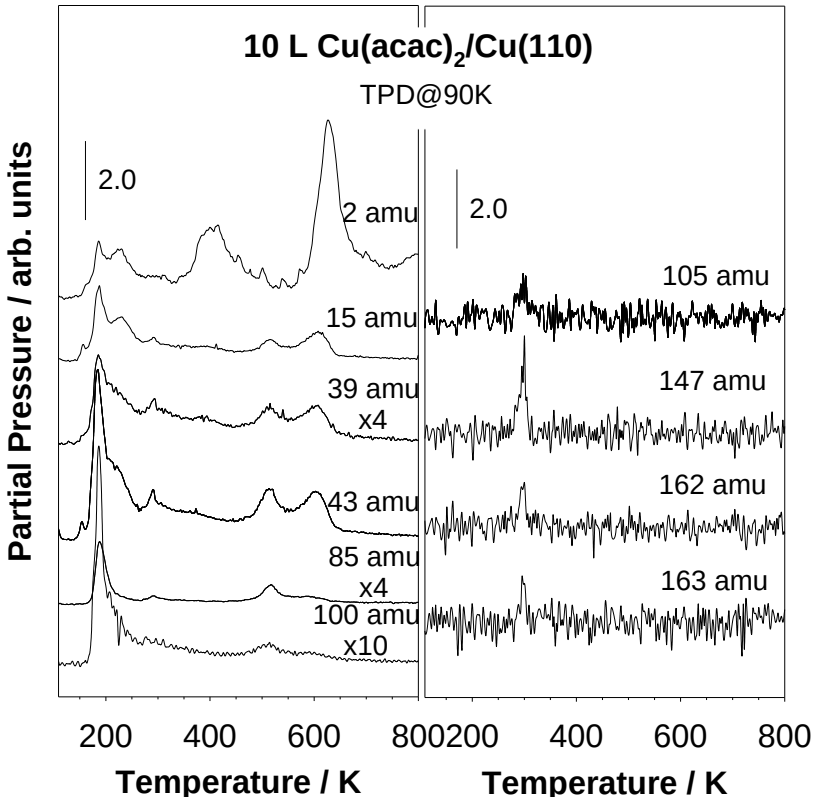

Figure 8.2 2, 15, 39, 43, 85 and 100 amu (left panel) and 105, 147, 162 and 163 amu (right panel) TPD from 10 L $Cu(acac)_2$ on clean Cu (110).

left panel). The two low-temperature peaks may come from molecular desorption, the two high-temperature peaks from decomposition products. Given the difference in ratios in the peaks at 515 and 610 K for 15, 39, 43, 85 and 100 amu, it is determined that at least two different products desorb at those two temperatures. Further TPD experiments are necessary to identify the products, but one of them may be Hacac, the hydrogenated ligand (Hacac) with a molecular signal 100 amu, which desorbs at 515 K. The 610 K, in contrast, must come from further decomposition of the acac ligand. Several high masses

such as105, 147, 162, and 163 amu were also monitored in a separate TPD experiment (Figure 8.2, right panel). Even though a higher sensitivity was used here, two to four orders of magnitude higher sensitivity than the others, the signals is still weak, and only one peak is seen around 295 K. We assign it to molecular desorption.

8.2.2. Nickel surface

8.2.2.1. XPS of $Cu(acac)_2$

Cu L_3VV AES, Cu $2p_{3/2}$, C 1s, O 1s and Ni $2p_{3/2}$ XPS data were acquired for 100 L $Cu(acac)_2$ on clean Ni (110). The Cu $2p_{3/2}$ XPS at 90 K display a peak at 935.3 eV (Figure 8.3, left panel), the same position as on Cu (110) surface. This is a value higher than that for Cu (I) $2p_{3/2}$, 934.0eV, and must therefore correspond to Cu (II) [6]. That

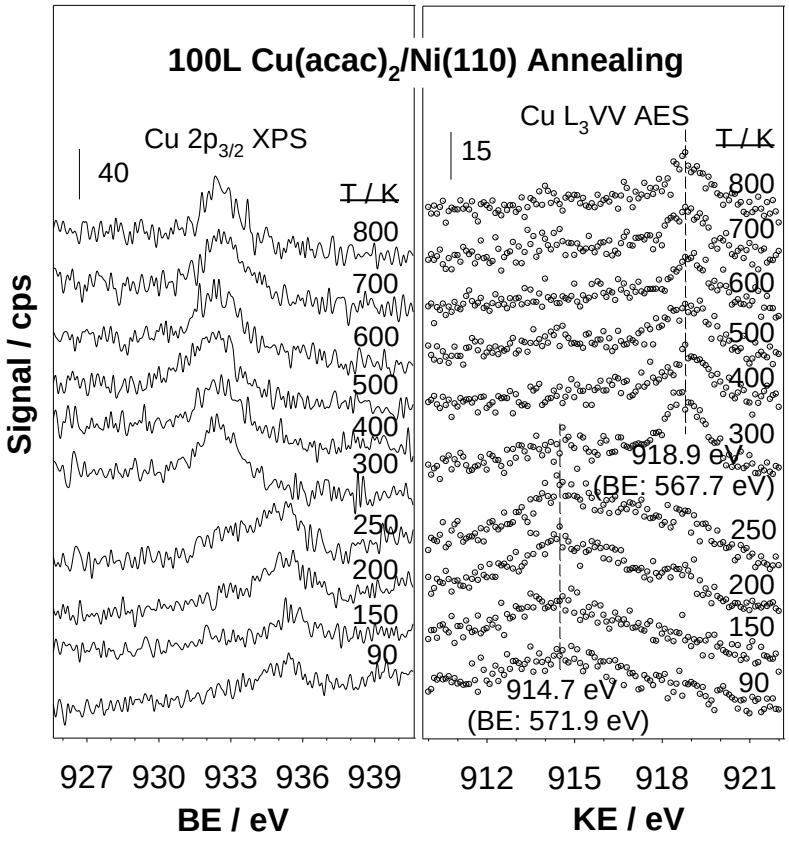

Figure 8.3 Cu $2p_{3/2}$ XPS and Cu LVV AES from 100 L $Cu(acac)_2$ on clean Ni (110), dosed at 90 K and after annealing to the indicated temperatures.

means that adsorbs on the Ni (110) surface is the intact Cu (II) species at 90 K. The peak intensity remains almost same up to 250 K, and so does the peak position. Annealing to 300 K cause the Cu $2p_{3/2}$ XPS peak to shift down to 932.5 eV, which is the typical binding energy of metallic Cu [6]. Further annealing to up to 800 K result in no further changes.

The Cu Auger peaks confirm the trends mentioned above (Figure 8.3, right panel). At 90 K, the Cu Auger peak has a kinetic energy of 914.7 eV, higher than that for Cu (I) (913.7eV) [7]. And annealing to 300 K, results in a shift to 918.9 eV, the kinetic energy of metallic Cu (as also seen with the Cu-acetamidinate precursor on Ni (110)).

The C 1s XPS is shown in Figure 8.4, left panel. At 90 K, it displays two peaks, at 285.2 and 287.2 eV, as on Cu (110). The peaks intensities and positions change little up to 250 K, but the intensity decreases dramatically and the position shifts down at 300 K. At 800 K, another peak grows at 284.3 eV, from carbon on the surface.

The O 1s XPS is shown in Figure 8.4, center panel. At 90 K, a peak is centered at 532.6 eV. Both the peak intensity and its binding energy decrease little at 250 K, but much more at 300 K; the new binding energy is 531.5 eV. The peak intensity continues to

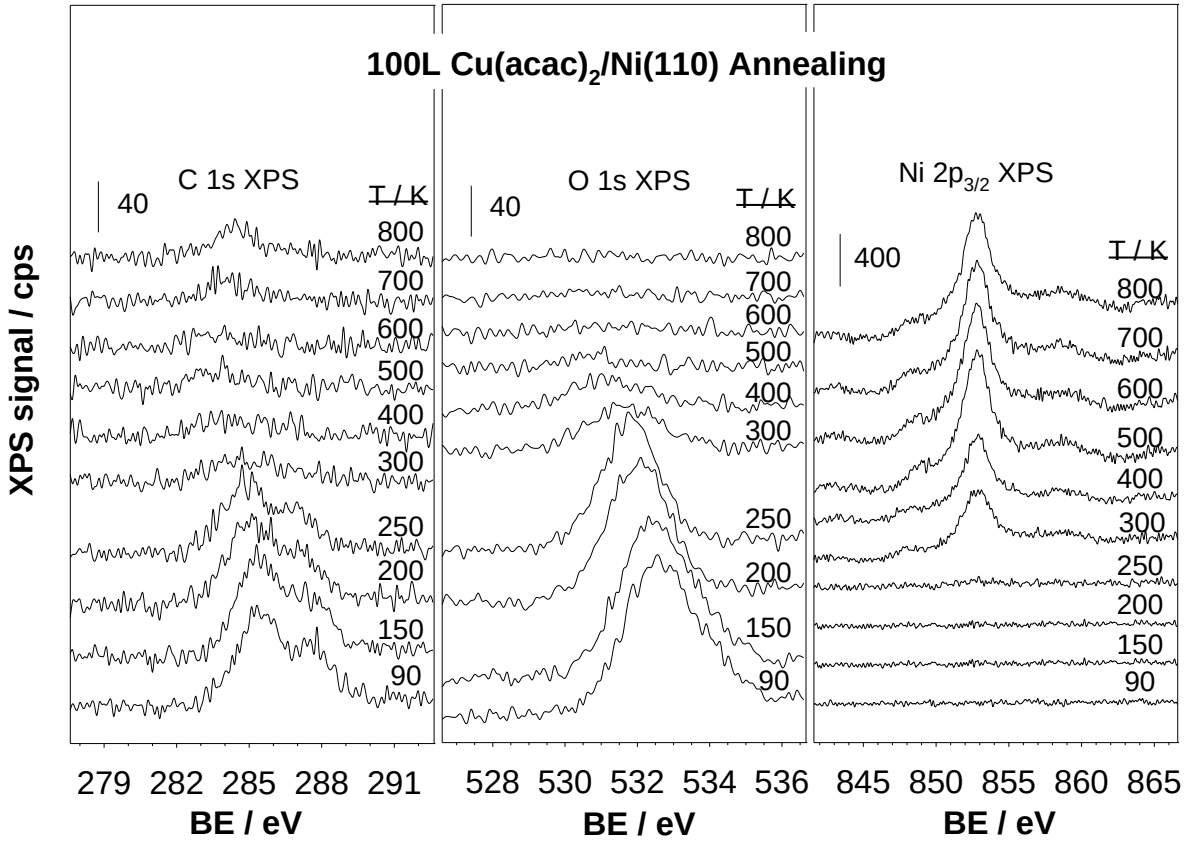

Figure 8.4 C 1s, O 1s and Ni $2p_{3/2}$ XPS form 100 L $Cu(acac)_2$ on clean Ni (110), dosed at 90 K and after annealing to the indicated temperatures.

decrease and shift to 531.1 eV at 500 K, and vanishes after annealing to 800 K. Again, no copper oxide forms on the surface.

The Ni $2p_{3/2}$ XPS is shown in Figure 8.4, right panel. At 90 K, no peaks are seen at lower temperatures, only at 300 K, a peak appears at 852.9 eV. The intensity stays same at 400 K, but increases at 500 K, after which it remains almost constant up to 800 K. This peak displays the same binding energy, 852.9 eV, at all temperatures. It is concluded that some desorption happens around 300 and 500 K; the Cu Auger and Cu $2p_{3/2}$, C 1s, O 1s, and Ni $2p_{3/2}$ XPS peaks from $Cu(acac)_2$ reveal the same information, that is: the main chemical conversion occurs between 250 to 300 K, and after 300 K the chemical bonds between the copper and oxygen atoms are broken. Metallic copper forms on the surface.

8.2.2.2. XPS of Hacac

XPS of Hacac were carried out to add to the knowledge about the surface chemistry of $Cu(acac)_2$. XPS data were acquired for 100 L of Hacac on Ni (110). Two C 1s XPS peaks are seen at 90 K, at 285.2 and 287.2 eV respectively (Figure 8.5, left panel), the same as with $Cu(acac)_2$ on Ni (110) surface. The intensities decreased starting at 200 K, and a new peak appears at 284.3 eV at 800 K. All this matches the data reported above for $Cu(acac)_2$.

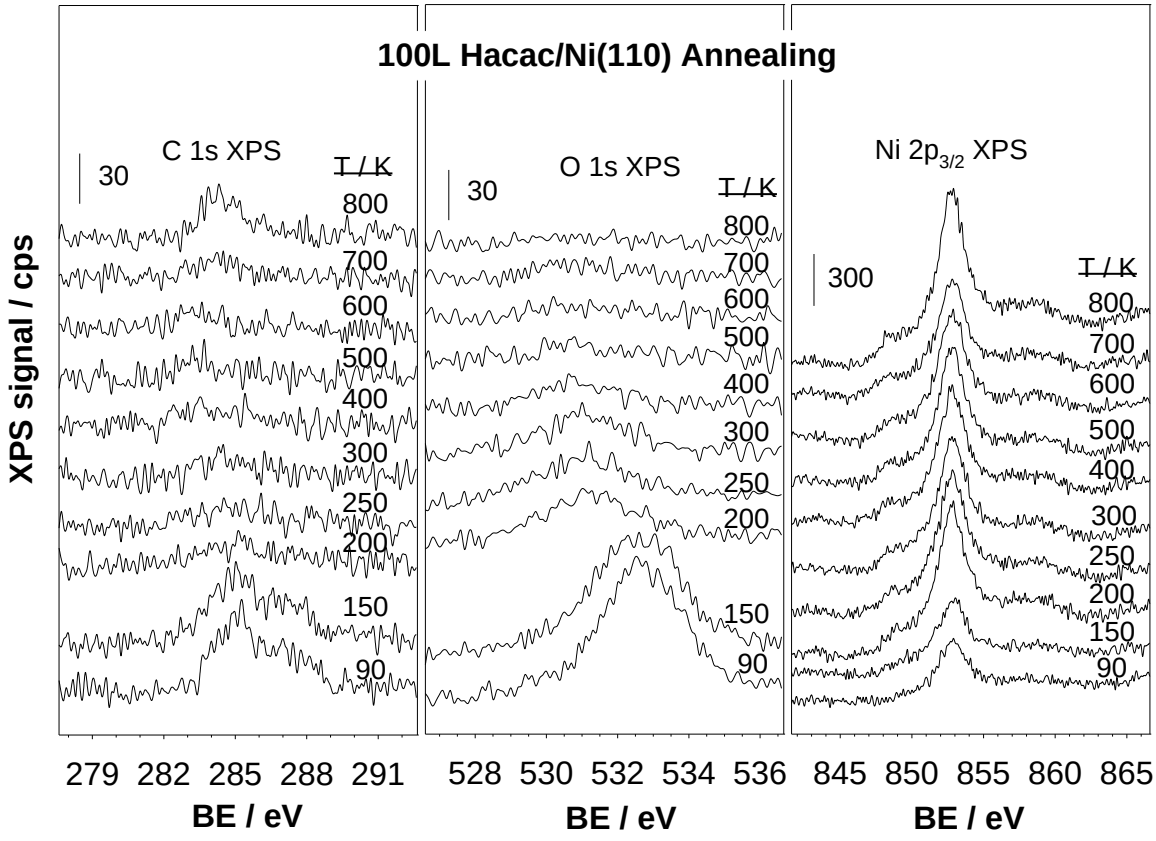

Figure 8.5 C 1s, O 1s and Ni $2p_{3/2}$ XPS form 100 L Hacac on clean Ni (110), dosed at 90 K and after annealing to the indicated temperatures.

The O 1s XPS shows a peak at 532.6 eV at 90 K (Figure 8.5, center panel), decreases in intensity and shift to lower binding energy (531.4 eV) at 200 K, and further shifts to 531.0 eV by 400 K. The peak totally disappears after annealing the surface at 800 K. The evolution of the Ni $2p_{3/2}$ XPS mirrors our previous report with the copper precursor

8.2.2.3. TPD

For $Cu(acac)_2$, TPD experiments were carried out for 58, 85 and 105 amu. The 105 amu represent $Cu(acac)_2$, and 85 amu Hacac, although some signal may also come from $Cu(acac)_2$. The 58 amu correspond to acetone, again, with some interfere from $Cu(acac)_2$ or Hacac. For 10 L $Cu(acac)_2$ on Ni (110), the 105 amu trace displays peaks at 170 and 195 K (Figure 8.6, left panel), from molecular desorption of $Cu(acac)_2$. The 85 amu signal displays three peaks, at 180 K, for Hacac, at ~200 K, from cracking from molecular desorption, and at 300 K, perhaps from Hacac or another product. The later peak matches the result form XPS, which changes dramatically after annealing to 300 K. The 58 amu TPD shows a very low temperature peak at 145 K, which may come from decomposition of $Cu(acac)_2$ during dosing, and a second feature at 300 K, as in the 85 amu data. We propose that the $Cu(acac)_2$ adsorbed on the Ni (110) surface, partially molecular desorbs at 198 K, the rest decomposing at 300 K to form Hacac. Since Hacac desorbed immediately after being produced (the desorption temperature of Hacac from Ni

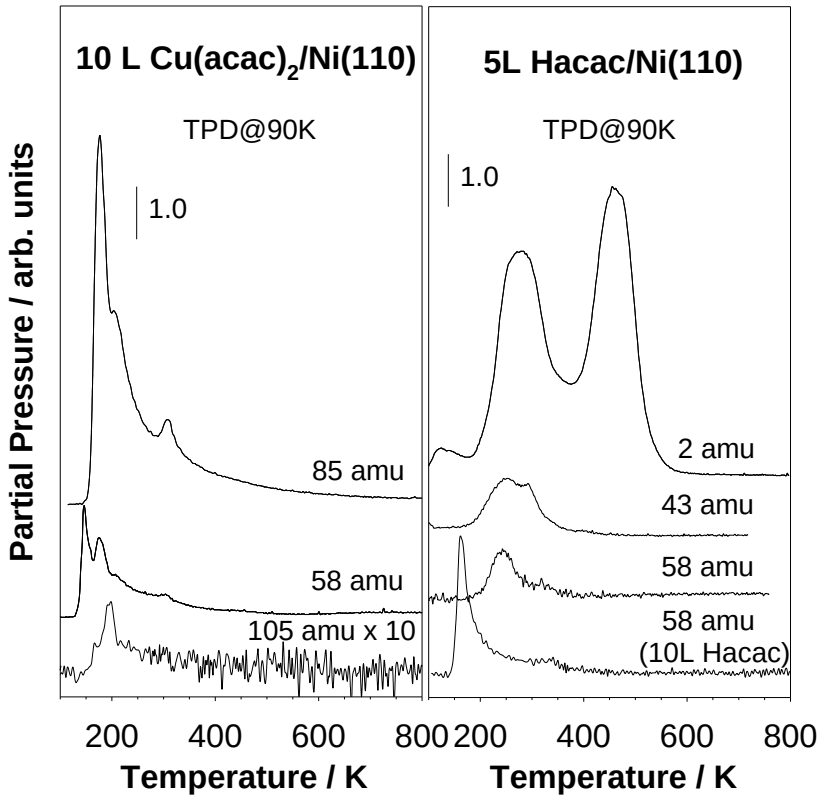

Figure 8.6 Left: 58, 85, 105 amu TPD from 10 L $Cu(acac)_2$ on clean Cu (110) and Right: 2, 43, 58 amu TPD from 5 L Hacac on clean Cu (110).

(110) is much lower), it does not remain on the surface to follow further decomposition. There may be a small amount of acetone formed, but too small a yield to be clearly observed.

For Hacac, TPD experiments were also carried out for 2, 43, 58 amu. For 5 L Hacac on Ni (110), both 43 and 58 amu display a low temperature peak at 245 K, and high temperature peaks at around 300 and 330 K. For 10 L, the 58 amu trace displays a sharp peak at 165 K, but no 245 K signal, the high temperature peak at 330 K still remains. The 2 amu TPD displays peaks at 280 and 460 K (Figure 8.6, right panel).

8.3. Discussion

It has been reported that in thermally activated deposition process on quartz and Al_2O_3 substrates using $Cu(acac)_2$, only discontinuous Cu films are obtained at temperatures T <550 K, and no Cu deposition is possible at T < 500 K [1]. This is different from our results, where, according to the XPS and Auger data, $Cu(acac)_2$ decomposes to form metallic copper at 300 K on Ni (110). This is a temperature 200 K lower than on quartz and Al_2O_3. The same results were obtained on Cu (110). For the ALD process, low temperatures are preferred so ALD may be feasible on metals but not on quartz or Al_2O_3. Our results are also different than those of Hiroshi Miura, who claims that $Cu(acac)_2$ does

not react on Ni or Al plates heated to up to 400 or 430 K, respectively [2]. Deposition of Cu was observed at 400~450 K on Ni Plate, more than 100 K high than on our Ni (110) and Cu (110) surfaces. One of the important information drawn from our results was $Cu(acac)_2$ decomposes at much lower temperatures than previously reported.

The main product from thermal decomposition of $Cu(acac)_2$ on Ni (110) is Hacac, which is observed at 300 K. Acetone may also form, since peaks are detected for 43 and 58 amu at around 140 K, but those may come from decomposition in the gas line during dosing instead of from the Ni (110) surface; note that the melting point of $Cu(acac)_2$ is 550 K and the vapor pressure is quite low, about 0.05 torr at 350 K. This later temperature is already 50 K higher than the decomposition temperature we obtained in our TPDs. In a report by Charles in 1958 [3], acetylacetone and acetone were reported from thermal decomposition of $Cu(acac)_2$. An inverse relationship exists between the acetylacetone and acetone concentrations that evolve from $Cu(acac)_2$ in the gas phase. This suggests that acetylacetone may form initially but then decomposes at higher temperatures to form acetone. It is possible that acetylacetone may be an intermediate in the production of acetone. The 43 amu TPD in Figure 8.2 (left panel) displays a peak at 610 K, which may be the desorption peak of acetone. It has also been claimed that the adsorbed ligands on Ni (110) can undergo a series of stepwise decomposition reactions with increasing

temperature, to eventually yield species like CO and CO_2 [4]. We did not identify any CO and CO_2 here at any temperature, but a decarbonylation reaction could be one source for the residual carbon found on the surfaces.

FT IR has also been used to investigate the kinetics of the thermal decomposition of $Cu(acac)_2$ and its reaction with water vapor on glass substrates under CVD conditions [5]. Copper (I) oxide was observed in those studies below 555 K, and metallic copper at higher temperatures. On our Ni (110) and Cu (110) surfaces, $Cu(acac)_2$ directly converts at 300 K from Cu(II) to metallic copper, without formation of any copper (I) or copper(II) oxide species.

In both C 1s and O 1s XPS data for Hacac on Ni (110), the initial binding energies were same as for $Cu(acac)_2$ on Ni (110) and Cu (110) surfaces; the main difference is that the binding of Hacac changes at 200 K while for $Cu(acac)_2$ that occurs at 300 K. It appears that Hacac is more active than $Cu(acac)_2$ on these surfaces.

8.4. Conclusions

The adsorption and thermal activation of $Cu(acac)_2$ on Ni (110) and Cu (110) single crystal surfaces was studied under ultrahigh vacuum conditions by XPS and TPD. The

only product identified from $Cu(acac)_2$ decomposition was Hacac. Acetone may also form, but the evidence is not conclusive. The $Cu(acac)_2$ conversion on both surfaces is relative mild: only small amounts of products are released. No CO or CO_2 was ever observed.

The $Cu(acac)_2$ decomposes at 300 K on both Ni (110) and Cu (110) surfaces. Metallic copper is left behind, and residual carbon species are also deposited on the surfaces. No other oxidation state for copper was identified anywhere from 90 to 800 K. The Cu(II) precursor directly converts into Cu(0).

8.5. References

[1] J. –Y. Zhang, H. Esrom, *Applied Surface Science*, **1992**, *54*, 465.

[2] H. Miura, K. Oki, H. Ochiai, H. Higuchi, M. Terasaka, T. Matsuda, *Bull. Chem. Soc. Jpn*., **1992**, *65*, 892.

[3] J. V. Hoene, R. G. Charles, W. M. Hickam, *J. Phys. Chem.* **1958**, *62*, 1098.

[4] M. Utriainen, M. Kröger-Laukkanen, L. –S. Johansson, L. Niinistö, *Applied Surface Science*, **2000**, *157*, 151

[5] C. R. Vestal, H. M. Sturgill, T. C. De Vore, *Proceedings - Electrochemical Society*, **2000**, *13*, 512

[6] C. D. Wagner, W. M. Riggs, L. E. Davis, J. F. Moulder, G. E. Muilenberg, G. E., *Handbook of X-Ray Photoelectron Spectroscopy*, Perkin-Elmer Corp.: Eden Prairie, MN, **1978.**

[7] D. Briggs, *Handbook of X-ray and Ultraviolet Photoelectron Spectroscopy*, Heyden: London, **1978**.

CHAPTER NINE

General Conclusions and Future work

9.1. General Conclusions

The work in this dissertation is part of a continuous effort in our group to understand the fundamental mechanisms of atomic layer deposition at a molecular level. Studies on Si (100) [1] as well as on some metal surfaces [2] have already been done in our group, and molecular insights have been provided for the reaction mechanisms of a few ALD processes on those surfaces. Our contribution is on the ALD of copper film, which are important for semiconductor industrial applications. Below, a brief discussion of several important points derived from my PhD study is listed.

Studies on the adsorption and thermal activation of copper(I)- *N*,*N'*-di-*sec*-butylacetamidinate on Ni (110) indicated two adsorption modes, molecular at low temperatures and dissociative above 300 K. The latter is activated, and leads to the reduction of the copper atoms directly from Cu(I) to a metallic copper state. Monolayer saturation is seen when the deposition is carried out at 350 K, but some additional decomposition and copper deposition is seen over time at temperatures as low as 400 K,

and almost a linear dependence of copper growth on exposure is observed by 460 K. 12 L exposures are sufficient to saturate the surface, but three saturation and annealing cycles are required to reach a monolayer coverage of copper on the surface, the equivalent of a film growth rate of ~ 0.75 Å/cycle. Two by- products from copper acetamidinate decomposition were identified, butene at 480 K, and ^{s}But–NH–C(CH_3)=NH at 300 K. Coadsorption of hydrogen does not result in any significant changes in this chemistry since the adsorbed hydrogen desorbs below these temperatures typically used in ALD processes [3].

The surface reactivity of copper acetamidinate on Cu (110) single crystal surfaces was similar with on Ni (110) surface, except that butene and ^{s}But–NH–C(CH_3)=NH desorb at higher temperatures, 560 and 480 K, respectively, as with small yields. On both nickel and copper surfaces, the copper acetamidinate precursor converts directly to metallic copper by itself, without the need of a second reducing precursor.

N,N'-di-*sec*-butylacetamidine was shown to be less reactive on both Ni (110) and Cu (110) relative the copper acetamidinate, with less amount of products released. Molecular desorption happened at around 223 K. Still the acetamidine does decompose on both surfaces and leave carbon species, the same as the copper acetamidinate. This may help

explain why the ALD of copper acetamidinate always introduces carbon impurities into the growing Cu film.

The adsorption and thermal activation of an alternate copper(I) precursor, Cu-KI5, was also tested on Cu (110). Decomposition was seen at around 400 K, and carbon, oxygen, and silicon containing species were determined to retain on the surface up to 800 K. No nitrogen is left behind above 400 K, however. Some hydrogenated ligand may be produced at 280 K. The deposited film was a mixture of Cu metal and CuO_x according to the binding energy and residual oxygen.

Finally, the adsorption and thermal activation of one copper (II) precursor, $Cu(acac)_2$, was studied on Ni (110) and Cu (110) single crystal surfaces. The one product clearly identified from $Cu(acac)_2$ decomposition is Hacac, but a small amount of acetone may be formed as well. The $Cu(acac)_2$ conversion on both surfaces was relatively weak, and small amounts of product are released. Also, no CO or CO_2 is observed. The $Cu(acac)_2$ decomposition on both surfaces occurs at 300 K, and metallic copper and some residual carbon species are left on those surfaces. Also in this case, only metallic copper is produced.

9.2. Future work

9.2.1. Studies on copper ALD

The studies on the Cu-KI5 precursor are incomplete, only the Cu (110) surface has been investigated so far. Future work should be carried out on Ni (110) for comparison, and a better identification of the final decomposition products from Cu-KI5 thermal activation should be pin down. The ligand used in Cu-KI5 is also available, and its study should help understand the reaction mechanism of the Cu-KI5. A second copper(I) precursor is also available, the so called CupraSelect^{TM} 2500, but has not been probed yet.

Moreover, the study of $Cu(acac)_2$ is not finished either. Its decomposition temperature on the nickel and copper surfaces were determined, but not all the products have been identified; more TPD work with $Cu(acac)_2$ and Hacac on both surfaces is necessary. Second copper(II) precursor, bis(2,2,6,6-tetramethyl-3,5-heptanedionato) copper (II), $Cu(TMHD)_2$, is available but has not been used yet.

One key result from our work is the detection of a smaller amidine. Studies on its chemistry are need. We are about to receive a sample of that compound from a collaborator for this.

9.2.2. Studies on ruthenium ALD

In recent years, ruthenium films have gained some significance as an alternative to copper as seed material. Since ruthenium and ruthenium oxides exhibit high chemical and thermal stabilities and relatively high work functions [4], they are expected to act as a barrier and seed layer for copper in the deposition of interconnects in microelectronics, capacitor electrode materials for memory devices, or gate metals for metal-oxide-semiconductor field effect transistors [5-7]. Several ruthenium precursors, including $Ru(^{t}BuNC(Me)N^{t}Bu)_3$, tris(di-*tert*-butylacetamidinato)-ruthenium(III); $Ru(^{i}PrNC(Me)N^{i}Pr)_2(CO)_2$, bis(diisopropylacetamidinato)ruthenium(II) dicarbonyl; $Ru(^{t}BuNC(Me)N^{t}Bu)_2(CO)_2$, bis(di-*tert*-butylacetamidinato)ruthenium(II) dicarbonyl; $Ru(^{i}PrNC(Me)N^{i}Pr)_3$, tris(diisopropylacetamidinato)-ruthenium(III); and $CpRuEt(CO)_2$, (cyclopentadienyl)-ethylruthenium dicarbonyl, have been proposed for ALD, and need surface chemistry characterization. The latter in particular has already been characterized by FTIR on hydrogen-terminated silicon [8]. SAFC, a chemical company, has developed a new series of Ru(0) oxidation state precursors, and has found that ALD growth using those with hydrogen is possible, the first demonstration of Ru ALD without the use of oxygen.

We could extend our work on copper to ruthenium. For instance, some TPDs of

$CpRuEt(CO)_2$ on metal surfaces could be carry out to identify various desorption products versus temperature. The sticking probability and saturation coverage may obtain from uptake curves using LEIS and XPS. The temperature window for ALD and the effect of reducing agents such as NH_3 or H_2 may be determined.

9.3. References

[1] B. –C. Kan, J. –H. Boo, I. Lee, F. Zaera, *J. Phys. Chem. A*, **2009**, *113*, 3946.

[2] H. Tiznado, M. Bouman, B. –C. Kang, I. Lee, F. Zaera, *J. Mol. Catal. A*, **2008**, *281*, 35.

[3] Z. Li, A. Rahtu, R. G. Gordon, *Journal of the Electrochemical Society*. **2006**, *153*, C787.

[4] T. Aaltonen, P. Al, M. Ritala, M. Leskel, *Chemical Vapor Deposition*, **2003**, *9*, 45.

[5] O.-K. Kwon, S.-H. Kwon, H.-S. Park, S.-W. Kang, *Journal of The Electrochemical Society*, **2004**, *151*, C753.

[6] O.-K. Kwon, J.-H. Kim, H.-S. Park, S.-W. Kang, *Journal of The Electrochemical Society*, **2004**, *151*, G109.

[7] S. Y. Kang, C. S. Hwang, H. J. Kim, *Journal of The Electrochemical Society*, **2005**, *152*, C15.

[8] S. K. Park, K. Roodenko, Y. J. Chabal, L. Wielunski, R. Kanjolia, J. Anthis, R. Odedra, N. Boag, *Mater. Res. Soc. Symp. Proc*. **2009**, *1156*, D04-02.